



**CYPRUS INTERNATIONAL UNIVERSITY**  
**FACULTY OF ENGINEERING**  
**DEPARTMENT OF ELECTRICAL AND ELECTRONIC  
ENGINEERING**

**DIGITAL TECHNOLOGIES IN INDUSTRY**

**By**

**HASHEM VASEGHI**

**PARFAIT ZAINA NGOI**

**FELLY NGOY**

**JUDE KABEMBA**

**BOIMA FAHNBULLEH**

**GREGORY MWEMA**

**OLUTOYE OPEYEMI**

**Date: February 11, 2025**

**Place: Nicosia, NORTH CYPRUS**



**CYPRUS INTERNATIONAL UNIVERSITY**  
**FACULTY OF ENGINEERING**  
**DEPARTMENT OF ELECTRICAL AND ELECTRONIC  
ENGINEERING**

**DIGITAL TECHNOLOGIES IN INDUSTRY**

**By**

**HASHEM VASEGHI**

**PARFAIT ZAINA NGOI**

**FELLY NGOY**

**JUDE KABEMBA**

**BOIMA FAHNBULLEH**

**GREGORY MWEMA**

**OLUTOYE OPEYEMI**

**Date: February 11, 2025**

**Place: Nicosia, NORTH CYPRUS**

# **DIGITAL TECHNOLOGIES IN INDUSTRY**

**By**

---

Hashem Vaseghi	22004087	Electrical and Electronic Engineering
Parfait Zaina Ngori	22015208	Electrical and Electronic Engineering
Felly Ngoy	22013357	Computer Engineering
Jude Kabemba	22013160	Computer Engineering
Boima Fahnbulleh	22013081	Mechatronics Engineering
Gregory Mwema	22012501	Mechatronics Engineering
Olutoye Opeyemi	22013786	Mechanical Engineering

---

**DATE OF APPROVAL: .....**

**APPROVED BY:**

**ASST. PROF. DR. ZİYA DEREBOYLU**

---

**Asst. Prof. Dr. ALİ SHEFIK**

---

## **ACKNOWLEDGEMENTS**

We extend our heartfelt appreciation to everyone who contributed to the success of this project. First and foremost, we express our deepest gratitude to **Asst. Prof. Dr. ZİYA DEREBOYLU** and **Asst. Prof. Dr. ALİ SHEFIK** for their invaluable guidance, continuous support, and encouragement throughout the project. Their expertise and insights were instrumental in overcoming challenges and ensuring the project's progress.

We are also grateful to **Cyprus International University** for providing us with the resources and platform to pursue this project. Special thanks to the faculty members of the **Faculty of Engineering** for their technical advice and mentorship, which greatly enriched our learning experience.

Our sincere thanks go to our entire team for their dedication and collaboration. Each member brought unique skills and perspectives, contributing to the successful integration of mechanical, electronic, and software systems. This project would not have been possible without their united commitment and hard work.

We also extend our gratitude to our families and friends for their unwavering support, encouragement, and motivation during the challenging phases of the project.

Finally, we would like to thank the organizers of the Teknofest Aerospace and Technology Festival for providing us with the opportunity to showcase our work and compete in the Digital Technologies in Industry competition.

This project is a testament to the collective effort and support of everyone involved. Thank you all for being part of this journey.

## **ABSTRACT**

The research introduces CIU\_Fox as an autonomous guided vehicle (AGV) that develops capabilities to transform factory and warehouse internal transportation operations. The designed AGV features autonomous navigation with a safe lifting capability using obstacle detection and collision avoidance systems for moving loads up to 200 kg. This system combines LIDAR with time-of-flight (ToF) sensors and barcode scanners to create a precise automated navigation system which monitors operations and handles loading duties. The mechanical structure incorporates an aluminum alloy frame together with a scissor-compartment mechanism and NEMA 23 stepper-motor powered differential steering. A Raspberry Pi 4 manages the system through ESP32 modules that run software programs built in Python and C++ within the ROS framework. The robot development followed four sequential stages that led to its physical assembly. Resources limitations required the project team to conduct final stage testing through the Gazebo simulation pipeline instead of building physical components. Coding for path planning alongside obstacle avoidance and load management functions while achieving complete integration of mechanical electronic software system components stands as major accomplishments. The commercial application scope of the AGV remains promising in multiple industrial sectors including manufacturing storage facilities and logistics operations because it shows potential to optimize operational efficiency while decreasing expenses and protecting worker safety. This work illustrates why interdisciplinary teams need to bring innovative solutions to modern industrial design using state-of-the-art technology applications. Research efforts will focus simultaneously on two fronts which include enhancing the AGV's operational excellence while evaluating opportunities to connect it with broader industrial system networks.

# Contents

<b>1</b>	<b>INTRODUCTION</b>	<b>1</b>
1.1	TEKNOFEST competition Rules . . . . .	1
1.1.1	Autonomous Operation . . . . .	1
1.1.2	Overload Warning . . . . .	1
1.1.3	Charging Task . . . . .	2
1.1.4	Obstacle Navigation . . . . .	2
1.1.5	QR CODE Labels . . . . .	2
1.1.6	Control Screen (GUI) . . . . .	2
1.1.7	No Manual Control . . . . .	2
1.1.8	Load Handling Display . . . . .	2
1.1.9	Mapping for Advanced Competitors . . . . .	2
1.2	DETAILS OF THE COMPETITION AREA . . . . .	3
1.2.1	Power Supply . . . . .	3
1.2.2	Track Layout . . . . .	3
1.2.3	Sample View of the Track . . . . .	4
1.3	LOAD HANDLING ROBOT TECHNICAL SPECIFICATIONS AND LIMITATIONS . . . . .	4
1.4	Sample Scenario . . . . .	5
<b>2</b>	<b>LITERATURE SURVEY</b>	<b>7</b>
<b>3</b>	<b>REALISTIC CONSTRAINTS</b>	<b>9</b>
3.1	Design Constraints . . . . .	9
3.2	Engineering Standards and Lifelong learning . . . . .	9
3.3	Economical Analysis . . . . .	9
3.4	Sustainability . . . . .	9
3.5	Ethics Issues . . . . .	9
3.6	Health and Safety Problems . . . . .	9
3.7	Social and Political Issues . . . . .	9
3.8	Environmental Impact . . . . .	9

3.9	Manufacturability . . . . .	9
3.10	Risk management, and Change management . . . . .	9
3.11	Legal Consequences . . . . .	9
<b>4</b>	<b>METHODS USED TO DESIGN THE PROJECT</b>	<b>10</b>
4.1	Electrical System Design . . . . .	11
4.2	Power Supply and Distribution . . . . .	12
4.2.1	Battery System . . . . .	12
4.2.2	Battery Management System (BMS) . . . . .	13
4.2.3	Voltage Regulation and Power Distribution . . . . .	13
4.2.4	Key Considerations . . . . .	17
4.3	Motor Control System . . . . .	17
4.3.1	Motors and actuators . . . . .	18
4.4	Sensors . . . . .	24
4.4.1	VL53L0X (Time-of-Flight Distance Sensor) . . . . .	24
4.4.2	Weight Sensor - Load Sensor 50Kg . . . . .	24
4.4.3	RPLIDAR - 360 . . . . .	25
4.4.4	Camera HUSKYLENS . . . . .	26
4.4.5	IMU Sensor . . . . .	26
4.4.6	Barcode Scanner GM65 . . . . .	27
4.4.7	QTRX-HD-11RC . . . . .	28
4.5	Microcontroller and Communication . . . . .	28
4.5.1	Raspberry Pi 4 . . . . .	28
4.5.2	ESP32-S3-DevKitC-1 . . . . .	29
4.5.3	RS232 to Bluetooth Series Adapter . . . . .	29
4.5.4	TP-Link TL-WR840N . . . . .	30
4.6	usefull part . . . . .	31
4.7	boima's chapter . . . . .	32
4.8	Research Gaps and Justification . . . . .	33
4.9	Physical Design Constraints . . . . .	34
4.9.1	Load Capacity Constraints . . . . .	34
4.9.2	Dimensional Constraints . . . . .	34
4.9.3	Material and Manufacturing Constraints . . . . .	34
4.10	Operational Constraints . . . . .	34
4.10.1	Safety Requirements . . . . .	34
4.10.2	Performance Constraints . . . . .	35
4.10.3	Environmental Constraints . . . . .	35

4.11	METHOD OF AGV DESIGN . . . . .	36
4.11.1	Single level Scissor lift design . . . . .	36
4.12	Load analysis . . . . .	39
4.12.1	Load distribution: . . . . .	40
4.12.2	Dead load . . . . .	41
4.12.3	Forces on the lift . . . . .	42
4.13	Mechanical Advantage Analysis: . . . . .	44
4.13.1	Kinematic analysis . . . . .	45
4.13.2	Scissor lift dimensions . . . . .	45
4.13.3	Mass center . . . . .	47
4.14	Mobility . . . . .	48
4.15	Instantaneous center . . . . .	49
4.16	Velocity Determination . . . . .	50
4.17	Actuation Mechanism . . . . .	50
4.17.1	Cylinder Extension Length (Z) . . . . .	51
4.18	CAD design . . . . .	52
4.18.1	Machine components (Scissor lifts) . . . . .	53
4.18.2	Method of assembly . . . . .	54
4.18.3	Stress Analysis . . . . .	55
4.19	AGV Chassis Design and Analysis Report . . . . .	58
4.19.1	Design Specifications . . . . .	58
4.19.2	Structural Configuration . . . . .	58
4.19.3	Component Integration . . . . .	59
4.19.4	Protective Framework . . . . .	59
4.19.5	Design Methodology . . . . .	59
4.19.6	Load Distribution Analysis . . . . .	61
4.19.7	Symmetry Stress Analysis . . . . .	62
4.19.8	Load Analysis with 2943N Force . . . . .	63
4.20	<b>CONCLUSION AND FUTURE WORKS</b> . . . . .	63
4.21	Design and Development of the Drive Wheel and Gearbox System . . . . .	65
4.22	Critical Elements of AGV Design: Drive Wheels, Gear Mechanisms, and Material Selection . . . . .	66
4.23	Design Constraints . . . . .	67
4.23.1	Technical Constraints . . . . .	67
4.23.2	Material Constraints . . . . .	67
4.24	Engineering Standards and Lifelong learning . . . . .	68
4.24.1	Engineering standards . . . . .	68

4.24.2 Importance of Engineering Standards in AGV Drive System Design	68
4.25 Manufacturing Constraints . . . . .	69
4.26 Economic Constraints . . . . .	69
4.27 Environmental Constraints . . . . .	70
4.28 Health and Safety Problems . . . . .	71
4.29 Manufacturability . . . . .	71
4.30 Methodology . . . . .	72
4.30.1 Dimensions . . . . .	72
4.31 3D Modeling . . . . .	73
4.31.1 Middle Drive Wheels: . . . . .	73
4.31.2 Gearbox: . . . . .	73
4.31.3 Shafts and Bearings: . . . . .	73
4.31.4 Housing: . . . . .	74
4.31.5 Assembly . . . . .	75
4.32 Calculation and Analysis . . . . .	75
4.32.1 GEARBOX CALCULATION . . . . .	75
4.33 Motion Analysis: . . . . .	78
4.34 Conclusion . . . . .	79
4.35 gregory's chapter . . . . .	80
4.36 INTRODUCTION . . . . .	80
4.37 LITERATURE REVIEW . . . . .	81
4.38 REALISTIC CONSTRAINTS . . . . .	82
4.38.1 Material Constraints . . . . .	82
4.38.2 Manufacturing Constraints . . . . .	82
4.38.3 Mechanical Constraints . . . . .	82
4.38.4 Environmental Constraints . . . . .	82
4.38.5 Safety Constraints . . . . .	83
4.39 CHAPTER FOUR: METHODS USED TO DESIGN THE PROJECT . . . . .	83
4.39.1 Objectives . . . . .	83
4.39.2 Methodology . . . . .	83
4.39.3 Bearing selection . . . . .	83
4.39.4 Torque calculation . . . . .	89
4.39.5 Results . . . . .	90
4.40 CONCLUSION AND FUTURE WORKS . . . . .	91
4.41 ROS . . . . .	93
4.42 Why ROS? . . . . .	94
4.42.1 High-end capabilities: . . . . .	94

4.42.2	Tons of tools: . . . . .	94
4.42.3	Support for high-end sensors and actuators: . . . . .	94
4.42.4	Inter-platform operability: . . . . .	94
4.42.5	Modularity: . . . . .	95
4.42.6	Concurrent resource handling: . . . . .	95
4.43	the ROS filesystem level . . . . .	95
4.44	ROS packages . . . . .	96
4.45	ROS metapackages . . . . .	99
4.46	ROS messages . . . . .	100
4.47	The ROS services . . . . .	104
4.48	the ROS computation graph level . . . . .	104
4.48.1	Nodes . . . . .	105
4.48.2	Master . . . . .	105
4.48.3	Parameter server . . . . .	105
4.48.4	Topics . . . . .	105
4.48.5	Logging . . . . .	106
4.49	ROS nodes . . . . .	106
4.50	ROS messages . . . . .	107
4.51	ROS topics . . . . .	108
4.52	ROS services . . . . .	108
4.53	ROS bagfiles . . . . .	109
4.54	The ROS master . . . . .	111
4.55	ROS parameter . . . . .	112
4.56	ROS distributions . . . . .	114
4.57	Running the ROS master and the ROS parameter server . . . . .	115
4.57.1	Checking the roscore command's output . . . . .	117
4.58	SIMULATION ENVIRONMENT . . . . .	119
4.59	Introduction to the Simulation Environment . . . . .	119
4.60	Tools and Framework . . . . .	120
4.60.1	Gazebo . . . . .	120
4.60.2	RViz . . . . .	128
4.61	Implementation of the Simulation Environment . . . . .	129
4.61.1	Robot Model ( URDF/SDF ) . . . . .	130
4.61.2	World Design . . . . .	130
4.61.3	Control and sensor Integration . . . . .	152
4.62	Validation of the simulation . . . . .	152
4.63	Challenges and Solutions . . . . .	152

4.64	URDF . . . . .	153
4.65	Understanding robot modeling using URDF . . . . .	153
4.65.1	link: . . . . .	153
4.65.2	joint: . . . . .	154
4.65.3	robot: . . . . .	155
4.65.4	gazebo: . . . . .	156
4.65.5	Adding physical and collision properties to a URDF model . . . . .	156
4.65.6	Transmission: . . . . .	157
4.66	Creating URDF model . . . . .	158
4.66.1	Understanding robot modeling using xacro . . . . .	159
4.66.2	Using properties . . . . .	160
4.66.3	Using the math expression . . . . .	161
4.66.4	Using macros . . . . .	161
4.66.5	Including other xacro files . . . . .	162
4.67	Visualizing the 3D robot model in RViz . . . . .	162
4.67.1	Interacting with joints in Rviz . . . . .	163
4.68	NAVIGATION . . . . .	166
4.69	For Line Detection and Following: . . . . .	166
4.69.1	Camera-based Vision Method: . . . . .	166
4.69.2	1.2 Control Algorithm for Line Following . . . . .	168
4.69.3	1.3 Integrating the Line Following with the Simulator . . . . .	168
4.70	For Building Map . . . . .	169
4.70.1	LIDAR . . . . .	169
4.70.2	QR Code Scanning . . . . .	169
4.71	Realistic constraints . . . . .	169
4.72	computational-power-and-resources . . . . .	169
4.72.1	cpu-and-gpu-limitations . . . . .	169
4.72.2	memory-ram-constraints . . . . .	169
4.72.3	real-time-performance . . . . .	170
4.73	complexity-of-the-simulated-environment . . . . .	170
4.73.1	size-and-detail-of-the-simulation . . . . .	170
4.73.2	dynamic-objects-and-movements . . . . .	170
4.74	simulating-sensor-data . . . . .	171
4.74.1	a.-sensor-data-processing-load . . . . .	171
4.74.2	real-time-sensor-fusion . . . . .	171
4.75	algorithmic-constraints . . . . .	171
4.75.1	a.-computational-cost-of-slam . . . . .	171

4.75.2	b.-path-planning-and-decision-making . . . . .	172
4.76	simulation-software-limitations . . . . .	172
4.76.1	simulation-engine-efficiency . . . . .	172
4.76.2	parallelization-and-multithreading . . . . .	172
4.77	simulating-real-time-constraints . . . . .	173
4.77.1	real-time-control-vs.-simulation-speed . . . . .	173
<b>5</b>	<b>CONCLUSION AND FUTURE WORKS</b>	<b>174</b>
5.1	COST . . . . .	174

# List of Figures

1.1	QR CODE Layout . . . . .	3
1.2	Sample Track Area . . . . .	4
1.3	Load (a) and platform (b) . . . . .	5
1.4	Sample Loaded Scenario . . . . .	6
1.5	Example No Load Scenario . . . . .	6
2.1	one of the Old AGV picture . . . . .	7
4.1	AGM battery . . . . .	13
4.2	LM2596 Voltage Regulator . . . . .	14
4.3	1500W 30A DC-DC Constant Current Boost Converter Step-up Power Supply Module 10-60V to 12-90V . . . . .	15
4.4	WM-045 DC-DC 150W Voltage Step Up and Step Down Regulator Module . . . . .	16
4.5	Nema 23 stepper motor 2 Nm torque . . . . .	18
4.6	Linear actuator with a maximum stroke of 6000N . . . . .	20
4.7	Closed Loop Stepper Driver CL57T V4.1 . . . . .	21
4.8	DC-MOTOR DRIVER MODULE 24V 43A (2x BTS7960B) . . . . .	23
4.9	VL53L0X time-of-flight (ToF) distance sensor . . . . .	24
4.10	Load cell . . . . .	25
4.11	HX711 Load cell amplifier . . . . .	25
4.12	RPLIDAR - 360 . . . . .	26
4.13	Husylens camera . . . . .	26
4.14	Inertia measurement unit 9 axis . . . . .	27
4.15	Qr code scanner . . . . .	27
4.16	QTRX-HD-11RC Reflectance Sensor Array: 11-Channel . . . . .	28
4.17	Raspberry Pi 4 . . . . .	28
4.18	ESP32-S3-DevKitC-1 . . . . .	29
4.19	RS232 to Bluetooth Series Adapter . . . . .	30
4.20	Load Cell Circuit with Wheatstone Bridge and Amplifier . . . . .	31
4.21	AGV Design Process . . . . .	36

4.22	Single level scissor lift in an Automated Guidance Vehicle . . . . .	36
4.23	Single level Scissor lift dimensions . . . . .	39
4.24	load distribution coefficients at point 1 and 2 . . . . .	40
4.25	Forces acting on the scissor lift . . . . .	42
4.26	2D Autocad model of the scissor lift Dimensions . . . . .	46
4.30	a Plain bearings that provide smooth sliding motion and wear resistance at pivot points b Rolling elements that reduce friction between moving parts and support radial and axial loads c Cylindrical components that transfer rotational motion and support rotating elements in the mechanism d & e Bolts, nuts, and pins used to secure components and allow for maintenance	54
4.31	Result for the stress analysis . . . . .	56
4.32	result for displacement analysis . . . . .	56
4.33	results for static strain analysis . . . . .	57
4.34	AGV chassis structure . . . . .	59
4.35	3D model of protective frame and covering . . . . .	60
4.36	2D profile of aluminum extrusion . . . . .	60
4.37	2D model of profile joint and fasteners . . . . .	61
4.38	2D model of Chassis and frame . . . . .	61
4.39	3D design of chassis and frame covering . . . . .	62
4.40	Load distribution on the chassis . . . . .	62
4.41	Add caption here . . . . .	73
4.42	Caption 1 . . . . .	74
4.43	Caption 1 . . . . .	74
4.44	Caption 1 . . . . .	75
4.45	Caption 1 . . . . .	75
4.46	Add caption here . . . . .	76
4.47	Add caption here . . . . .	78
4.48	caption here not added by Gregory . . . . .	88
4.49	Ubuntu 20.04 . . . . .	93
4.50	ROS filesystem level . . . . .	96
4.51	List of files inside the package . . . . .	97
4.52	Structure of a typical C++ ROS package . . . . .	97
4.53	Structure of the package.xml metapackage . . . . .	100
4.54	Structure of the ROS graph layer . . . . .	105
4.55	Graph of communication between nodes using topics . . . . .	106
4.56	Communication between the ROS master and Hello World publisher and subscriber . . . . .	112

4.57 Terminal messages while running the roscore command . . . . .	115
4.58 Gazebo Simulator . . . . .	120
4.59 Empty world in Gazebo . . . . .	121
4.60 TurtleBot3 Waffle spawned in empty world . . . . .	123
4.61 Gazebo Graphical User Interface left side pannel . . . . .	125
4.62 Gazebo Graphical User Interface lower part . . . . .	126
4.63 Gazebo Graphical User Interface top part . . . . .	126
4.64 Example of force applied on one side of a seesaw in gazebo . . . . .	127
4.65 Rviz (Ros Visualization) . . . . .	128
4.66 Teknofest competition real map layout . . . . .	130
4.67 White wooden floor with black lines in gazebo . . . . .	131
4.68 Example of Qr Code tag before a loading point . . . . .	133
4.69 Competition aera bounded by ad hoardings . . . . .	135
4.70 Competition area line interrupted by permanent obstacle . . . . .	136
4.71 Qr code tag placed at the intersection of line of the zone C and the station 2	150
4.72 Effect of lighting conditions in simulation environment . . . . .	151
4.73 Effect of lighting conditions in simulation environment . . . . .	151
4.74 A visualization of the URDF link [1] . . . . .	153
4.75 A visualization of the URDF joint [1] . . . . .	154
4.76 A visualization of a robot model with joints and links [1] . . . . .	155
4.77 A visualization of a robot model with Rviz . . . . .	164
4.78 The joint level of the platform lifting mechanism . . . . .	165

# List of Tables

4.1	LM2596 Voltage Regulator Specifications . . . . .	14
4.2	DC-DC Constant Current Boost Converter Specifications and Features . . . . .	15
4.3	Buck-Boost Converter Specifications . . . . .	16
4.4	Stepper Motor Specifications (Model: 23E1KBK20-20) . . . . .	19
4.5	Specifications of the linear actuator model JS-TGZ-U3 . . . . .	20
4.6	Specifications of the Closed-Loop Stepper Driver . . . . .	22
4.7	Features and Specifications of the IBT-2 Motor Driver Module . . . . .	23
4.8	Parameters and their descriptions . . . . .	38
4.9	Component Details and Weights . . . . .	41
4.10	Forces acting on scissor lift components at various angles of operation . . . . .	43
4.11	Mechanical advantage analysis results at different scissor lift angles, showing the relationship between input and output forces . . . . .	44
4.12	Height, angle, and platform length at different stages. . . . .	45
4.13	Parameters, their relations, and corresponding values. . . . .	46
4.14	Lift position, height, center of mass coordinates, and total mass. . . . .	47
4.15	Instantaneous center (IC) locations and angular velocities at different positions.	49
4.16	Measured velocities of the scissor lift mechanism at different height ranges showing the gradual decrease in velocity as the lift extends upward . . . . .	50
4.17	Actuator cylinder extension measurements showing the initial and final lengths required for full range of motion . . . . .	52
4.18	Primitive types and their serialization in C++ and Python. . . . .	102
4.20	ROS Distributions Table . . . . .	114
4.21	Essential Dependencies for Simulating a URDF in Gazebo . . . . .	158
5.1	here is the list of components . . . . .	174

# Chapter 1

## INTRODUCTION

The manufacturing industry is undergoing a digital transformation, driven by advancements in technologies like artificial intelligence, autonomous robots, and the Internet of Things. These innovations aim to enhance efficiency, productivity, and competitiveness in industrial processes. TEKNOFEST's Digital Technologies in Industry Competition challenges participants to design an autonomous guided robot for factory logistics, addressing real-world tasks such as navigation, load handling, and mapping. This report explores the strategies used to overcome these challenges and achieve the competition's objectives. By doing so, it highlights the critical role of digitalization in advancing industrial automation and fostering innovation.

### 1.1 TEKNOFEST COMPETITION RULES

The following rule apply to the operation of guided robots during the competition:

#### 1.1.1 Autonomous Operation

The guided robot must perform all tasks autonomously within the specified scenarios, including line-following.

#### 1.1.2 Overload Warning

The robot must issue an overload warning if it lifts a load exceeding the specified limit and continue carrying the load only after the weight is reduced below the limit.

### **1.1.3 Charging Task**

If the robot's charge level falls below a certain threshold, teams can earn additional points by having the robot autonomously navigate to the charging area and begin charging. Teams must inform the jury in advance if they wish to perform this task, which will be conducted at a time deemed appropriate by the jury.

### **1.1.4 Obstacle Navigation**

The robot should autonomously stop at loading/unloading points and navigate around obstacles if they are not removed. Obstacles will be detected by sensors, and the robot must stop at an appropriate distance. If the obstacle remains, the robot should autonomously go around it and complete its tasks.

### **1.1.5 QR CODE Labels**

QR CODE labels at loading and unloading positions must be readable by appropriate sensors on the robot.

### **1.1.6 Control Screen (GUI)**

Teams must prepare a graphical user interface (GUI) that allows them to monitor the vehicle's status and issue commands when necessary. However, interventions via the control panel will incur penalty points.

### **1.1.7 No Manual Control**

The robot cannot be controlled by joysticks, portable hand controls, phones, or tablets.

### **1.1.8 Load Handling Display**

The pick-up or dropping of loads must be displayed on the control panel (GUI) using sensors.

### **1.1.9 Mapping for Advanced Competitors**

Advanced-level competitors are required to map the track. For mapping, advanced teams will be given a specific amount of time after the loaded course is revealed. The teams are expected to map and display the competition area within the allocated time.

Mapping should be performed using devices such as laptops and tablets belonging to the team members at the control desk. Additionally, teams are expected to create a control

panel (GUI) that displays competition details such as speed and total task time. The mapping should be detailed, and QR CODE labels should be displayed on the map as they are read.

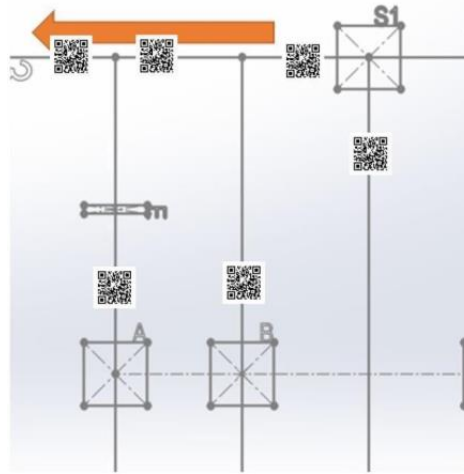


Figure 1.1: QR CODE Layout

## 1.2 DETAILS OF THE COMPETITION AREA

For the competition, there will be 2 rectangular-shaped representative factory areas of approximately 150 square metres each. These areas will include a track representing the layout of roads and internal logistics roads. Additionally, there will be a separate area where a table is located for each participating competitor team to use. The following details apply:

### 1.2.1 Power Supply

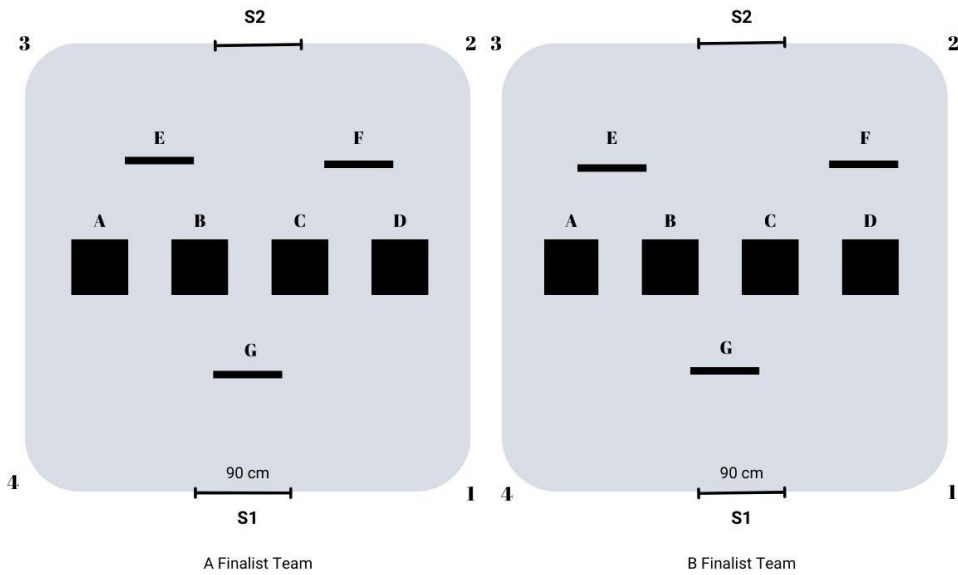
The competition area will have a 220 VAC power supply. A control desk will be located at the edge of the track for the competing team to control their guided robot. At the control desk, 220 VAC voltage will be provided, and each team is responsible for performing AC/DC conversion using their own converter. The highest DC voltage level that can be used is 50V.

### 1.2.2 Track Layout

The track will resemble a factory area with designated pick-up and drop-off points. The distribution of these points may vary for each competing team, as determined by the referees. The track area will consist of two similar sections, allowing two different teams to compete simultaneously.

### 1.2.3 Sample View of the Track

The sample view of the track will be provided separately for reference(fig. 1.3).



**S1, S2 :** Starting points

**A,B,C,D :** Load handling - Load unloading points

**E,F :** Fixed obstacle

**G:** Moving obstacle

Figure 1.2: Sample Track Area

## 1.3 LOAD HANDLING ROBOT TECHNICAL SPECIFICATIONS AND LIMITATIONS

The maximum dimensions of the load handling robot are as follows: 1,000 mm in length, 900 mm in width, and 500 mm in height. The dimensions of the load handling robots must not exceed these specified limits. However, when the mechanism used to lift the load platform is operated, the robot may exceed the height limit. The height restriction applies only to the situation where the vehicle is not operating under load.

The maximum load amount that robots must carry is 125 kg. Robots that lift more than 125 kg and do not provide an overload warning will be deemed to have failed to fulfill this task. The competition organization will provide loads with dimensions of 30 cm x 30 cm x 10 cm (fig. 1.3a)and a weight of 25 kg each. These loads will be placed on a platform with a maximum height of 50 cm from the ground)(fig. 1.3b), allowing the robot to easily position itself underneath and lift the load from all directions. The weight of the load platform provided by the competition organization will also be 25 kg.

The positions for load pick-up and drop-off will be defined using QR CODE tags. These tags will ensure precise identification of the designated locations for the robot to perform its tasks.

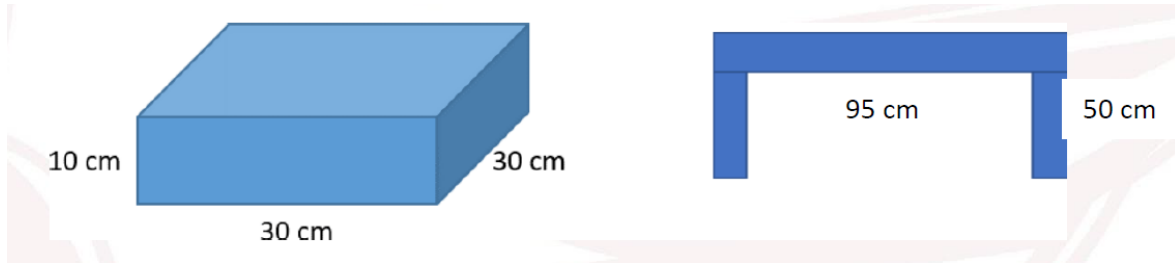
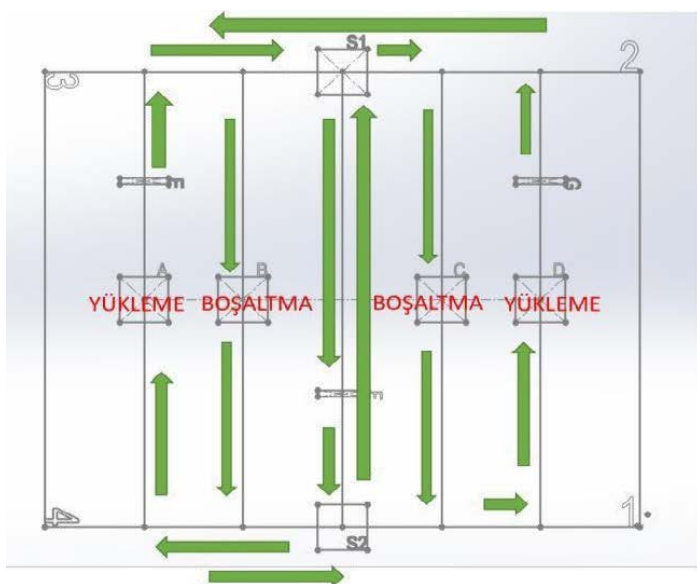


Figure 1.3: Load (a) and platform (b)

## 1.4 SAMPLE SCENARIO

The robot must first navigate around the corner points according to the scenario type, starting from the initial position without any load, and return to the starting point. During this process, teams are required to complete the mapping task. A total of four unloaded scenarios are illustrated in fig. 1.4.

Following the unloaded navigation, the robot should proceed to point A from the starting point to pick up a load and then continue to point C. Upon reaching point C, the robot must leave the load there and proceed to point D without carrying any load. After arriving at point D, the robot should pick up another load and transport it to point B. Once the load is delivered at point B, the robot must complete the task by returning to the starting point without any load. fig. 1.5 depicts four loaded scenarios, which vary depending on the starting points.



### Örnek Senaryolar

**Yüklü Tur :**

**S1-F-S2-A-E-S1-C-D-G-S1-B-S2-F-S1**

**S1-F-S2-B-S1-G-D-C-S1-E-A-S2-F-S1**

Veya

**S2-F-S1-G-D-S2-B-E-A-S2-C-S1-F-S2**

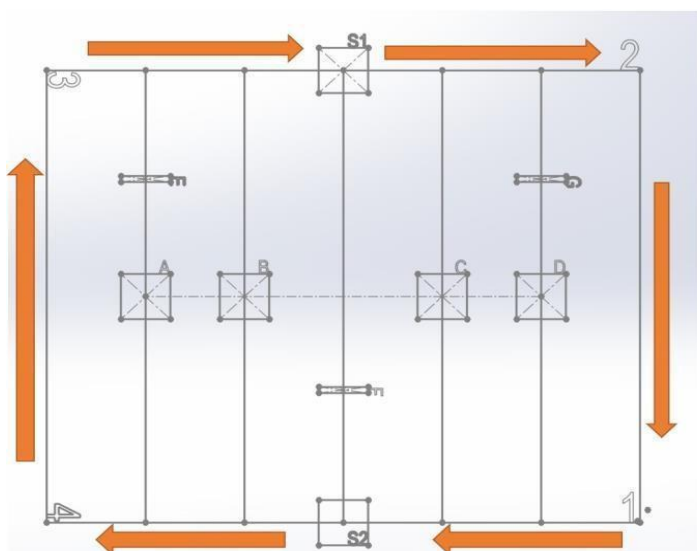
**S2-F-S1-C-S2-A-E-B-S2-D-G-S1-E-S2**

A,B,C,D: Yükleme ve Boşaltma Noktaları

1,2,3,4: Parkur köşe noktaları

E,F,G : Açılp kapanabilen engeller

Figure 1.4: Sample Loaded Scenario



### Örnek Senaryolar

**Boş Tur :**

**S1-3-4-S2-1-2-S1**

**S1-2-1-S2-4-3-S1**

veya

**S2-1-2-S1-3-4-S2**

**S2-4-3-S1-2-1-S2**

A,B,C,D: Yükleme ve Boşaltma Noktaları

1,2,3,4: Parkur köşe noktaları

E,F,G : Açılp kapanabilen engeller

Figure 1.5: Example No Load Scenario

# Chapter 2

## LITERATURE SURVEY

Today's industries activity have merged with the robotic and automation world and day by day having the precise and better quality product make the sense of using new technology. Between all types of robot, the AGV (automated guided vehicle) robot has the special place between others and improvement in technology helps this design to grow and become more helpful in various applications. The AGV robot is a programmable mobile robot integrated sensor device that can automatically perceive and move along the planned path [2]. This system consists of various parts like guidance facilities, central control system, charge system and communication system [3].

The initial used and Invention AGV is not clear exactly and was mentioned in different articles and reference for many times but the earliest time of using this system in industries is mentioned in 1950s [4] (fig. 2.1) and even mentioned in some reference that the first AGV in the world was introduced in UK in 1953 for transporting which was modified from a towing tractor and can be guided by an overhead wire [3].



Figure 2.1: one of the Old AGV picture

AGVs are widely applied in various kinds of industries including manufacturing factories and repositories for material handling. After decades of development, it has a wide applica-

tion due to its high efficiency, flexibility, reliability, safety and system scalability in various task and missions. AGV operates all day long continuously that cannot be achieved by human workers. Therefore, the efficiency of material handling can be boosted by having the collaborating task with number of AGV . In this case, administrator can enable more AGVs as the system is extensible. AGV has capability of collision avoidance and emergency braking, and generally the running status is monitored by control system so that reliability and safety are ensured. Generally, a group of AGVs are monitored and scheduled by a central control system. AGVs, ground navigation system, charge system, safety system, communication system and console make up an AGV system. [5]. This report examines the design aspects and considerations for this type of robot, providing readers with key insights into the technologies commonly utilized in this field.

# **Chapter 3**

## **REALISTIC CONSTRAINTS**

**3.1 DESIGN CONSTRAINTS**

**3.2 ENGINEERING STANDARDS AND LIFELONG LEARNING**

**3.3 ECONOMICAL ANALYSIS**

**3.4 SUSTAINABILITY**

**3.5 ETHICS ISSUES**

**3.6 HEALTH AND SAFETY PROBLEMS**

**3.7 SOCIAL AND POLITICAL ISSUES**

**3.8 ENVIRONMENTAL IMPACT**

**3.9 MANUFACTURABILITY**

**3.10 RISK MANAGEMENT, AND CHANGE MANAGEMENT**

**3.11 LEGAL CONSEQUENCES**

# **Chapter 4**

## **METHODS USED TO DESIGN THE PROJECT**

## 4.1 ELECTRICAL SYSTEM DESIGN

At the core of an AGV's electrical system are power management, motor control, and communication networks, all of which must be carefully designed to meet performance and safety requirements. The power system typically consists of a rechargeable battery, often lithium-ion or lead-acid, along with a Battery Management System (BMS) to monitor voltage, current, and temperature for optimal energy efficiency and longevity. Motor controllers regulate the movement of the drive and steering motors, ensuring smooth acceleration, precise navigation, and effective braking. Additionally, AGVs rely on a network of embedded controllers, sensors, and communication modules to process data in real time, enabling obstacle detection, localization, and coordination a central control system.

## 4.2 POWER SUPPLY AND DISTRIBUTION

At the heart of the electrical design lies the power supply and distribution system, which serves as the backbone for all onboard functionalities. The power supply system is responsible for storing, managing, and delivering electrical energy to various components of the AGV, including motors, sensors, control systems, and communication modules. Given that AGVs often operate continuously in demanding environments, the choice of battery technology, capacity, and management strategies plays a critical role in determining overall performance.

To maximize efficiency and safety, these batteries are integrated with advanced Battery Management Systems (BMS), which monitor key parameters like voltage, current, temperature, and state of charge, ensuring optimal usage while preventing conditions that could degrade battery health.

Equally important is the power distribution architecture, which ensures reliable delivery of electricity to all subsystems. This involves designing robust wiring harnesses, fuses, circuit breakers, and connectors that can handle the dynamic load requirements of AGVs during different operational phases. Efficient power distribution not only enhances the vehicle's performance but also minimizes energy losses, contributing to extended operating times and reduced downtime for recharging.

The following part highlights the key components of the AGV's power supply and distribution system, their roles, and their contribution to the system's overall efficiency

### 4.2.1 Battery System

Battery selection is a key factor in the efficiency and reliability of an AGV system. Among the available options, Absorbent Glass Mat (AGM) and Gel (GEL) batteries, both types of Sealed Lead-Acid (SLA) or Valve-Regulated Lead-Acid (VRLA) batteries, stand out for their maintenance-free, leak-proof design and low self-discharge rate. While both are deep-cycle batteries capable of discharging up to 80% of their capacity, GEL batteries emphasize durability and stable power delivery, whereas AGM batteries support higher discharge rates and slightly faster charging. However, neither is well-suited for opportunity charging, as frequent partial recharges reduce their lifespan.

For AGVs operating in controlled, single-shift environments, GEL batteries provide a strong balance between safety, longevity, and consistent performance, making them an optimal choice. They typically last 8–16 hours per charge, depending on the AGV type, and require a full recharge when reaching 40–50% depth of discharge (DOD). While their charging time is slower (e.g., a 100Ah battery takes about 3 hours at 0.3C), their deep-cycle capability ensures steady, long-term operation, minimizing the need for frequent replacements.

Considering the AGV's operational demands and the competition's specified battery requirements, AGM batteries are selected for this application. The competition specifies the following parameters: *Battery Type: AGM Battery, Battery Voltage (Nominal): 12VDC, Battery Charging Current: 10A.*



Figure 4.1: AGM battery

#### 4.2.2 Battery Management System (BMS)

The **BMS** is integrated to monitor and manage the battery's health, ensuring safe and reliable operation. It oversees critical parameters such as voltage, current, and temperature, preventing issues like overcharging, over-discharging, and overheating. The BMS optimizes battery performance, extending battery life by up to 30% and supporting over 3500 charge-discharge cycles at 90% Depth of Discharge (DOD). It also ensures safe operations with features like overcurrent protection, overvoltage protection, and temperature monitoring. Additionally, the BMS includes a charging system that complies with the competition specifications, which supports an **AGM Battery** with a nominal voltage of **12VDC** and a charging current of **10A**.

#### 4.2.3 Voltage Regulation and Power Distribution

The AGV's electrical system contains various components operating at different voltage levels, making voltage regulation and distribution critical for stable operation. The majority of sensors operate at 3.3V to 5V, while components like the Raspberry Pi and ESP32 require 5V and others like the Wi-Fi router operates at 9V. To accommodate these diverse requirements, multiple voltage regulators are incorporated to step down the 12V battery supply to the appropriate levels, ensuring consistent performance across all subsystems.

The **LM2596** in Figure 4.2 voltage regulator will be used to step down the 12V battery supply to the required voltage levels for various components. Different versions of the LM2596 are available, including fixed output versions (9V, 5V, and 3.3V) as well as an adjustable version, allowing flexibility to meet the specific voltage requirements of each subsystem. For example, the 5V version will power the Raspberry Pi and ESP32, while the 3.3V version will support sensors operating at lower voltages. In cases where multiple components require the same voltage and draw significant current, multiple LM2596 regulators are placed in parallel to increase the current supply capacity(Table4.1).



Figure 4.2: LM2596 Voltage Regulator

Parameter	Value
<b>Input Voltage Range</b>	Up to 40V
<b>Output Current</b>	Up to 3A
<b>Switching Frequency</b>	150 kHz
<b>Output Voltage Options</b>	Fixed: 3.3V, 5V, 9V Adjustable: 1.2V--37V
<b>Efficiency</b>	90%
<b>Protection Features</b>	Thermal shutdown, current limiting
<b>Package Type</b>	TO-220, TO-263
<b>Operating Temperature</b>	-40°C to +125°C

Table 4.1: LM2596 Voltage Regulator Specifications

Furthermore, subsystems, such as the traction unit (composed of two stepper motors) and the lifting system (powered by linear actuators), require voltages higher than the battery's output. To address this, boost converters(fig. 4.3 and fig. 4.4) are used to step up the voltage to the necessary levels.



Figure 4.3: 1500W 30A DC-DC Constant Current Boost Converter Step-up Power Supply Module 10-60V to 12-90V

<b>Features:</b>	Flexible DC input voltage range from 10V to 60V; Adjustable output voltage from 12V to 90V for versatile applications; Maximum output current of 20A for reliable power supply; Built with high-power 100V/210A low resistance MOS for efficiency; Reverse input protection with MOS for added safety; Low voltage protection to prevent damage from over-discharge; Thickened heat sink and intelligent cooling fan for optimal heat dissipation.
<b>Specifications:</b>	Power: 1500W; Current: 30A; Input Voltage Range: 10V – 60V; Output Voltage Range: 12V – 90V; Maximum Output Current: 20A.
<b>Package Includes:</b>	1 × Boost Converter Step-up Power Supply Module.

Table 4.2: DC-DC Constant Current Boost Converter Specifications and Features



Figure 4.4: WM-045 DC-DC 150W Voltage Step Up and Step Down Regulator Module

<b>Features:</b>	Input Voltage: 5Vdc – 30Vdc; Buck-Boost (automatic boost/lower); Output Voltage: 1.25Vdc -- 30Vdc (Adjustable); Output Current: 10A (MAX).
<b>Specifications:</b>	Output Power: 150W; Conversion Efficiency: 90% Max; Ripple and Noise: 200mVp-p; No-Load Current: 6mA typical.
<b>Performance Metrics:</b>	Voltage Regulation: $\pm$ 0.5%; Load Regulation: $\pm$ 0.5%; Dynamic Response Rate: 300uS.

Table 4.3: Buck-Boost Converter Specifications

The power distribution circuits are designed to efficiently deliver power to all subsystems, including motors, sensors, controllers, and communication modules, while minimizing power losses and ensuring reliable operation. Protection circuits and fuses are also integrated to safeguard sensitive components from voltage spikes, short circuits, and other electrical faults, enhancing the overall safety and durability of the AGV.

#### 4.2.4 Key Considerations

- *Efficiency*: The system is designed to maximize energy efficiency, ensuring the AGV can operate for extended periods without frequent recharging.
- *Safety*: The inclusion of the BMS and proper voltage regulation ensures safe operation, protecting both the AGV and its components from electrical faults.
- *Compliance*: The system adheres to the **TEKNOFEST Charging Station Technical Specifications**, ensuring compatibility and seamless charging during the competition.

### 4.3 MOTOR CONTROL SYSTEM

The performance and reliability of automated guided vehicles (AGVs) are deeply rooted in the precision and efficiency of their motor control systems [6]. At the heart of these systems lies the electrical design, which governs the interaction between power supply, control devices, and the physical dynamics of the motors. Direct current (DC) motors [7], Stepper motors [8] and Servo motors [9], widely used in AGVs due to their high torque, excellent speed regulation, and robust performance, require sophisticated electrical architectures to ensure optimal operation.

From an electrical perspective, motor control involves not only the precise regulation of voltage and current but also the implementation of efficient drivers and motor controllers, which are critical for achieving smooth acceleration, stable speed control, and efficient energy utilization. Furthermore, the motor control system must address challenges such as minimizing power losses, managing heat dissipation, and ensuring reliable operation under varying load conditions.

A motor control system comprises two fundamental components: the motors themselves and the motor drivers or controllers. The motor alone cannot achieve optimal operation without the integration of a sophisticated motor driver or controller. The motor driver acts as the intermediary between the power supply and the motor, regulating voltage and current to ensure smooth and efficient operation. It interprets control signals and translates them into precise commands.

#### 4.3.1 Motors and actuators

- *P Series Nema 23 Closed Loop Stepper Motor with Electromagnetic Brake (2Nm):*

The traction system of the automated guided vehicle (AGV) is driven by two NEMA 23 P-Series stepper motors shown fig. 4.5, each delivering a holding torque of 2.0 Nm to ensure reliable and precise motion. These motors are selected for their high torque-to-size ratio, making them well-suited for the dynamic demands of AGV operations.

Both motors are equipped with incremental encoders, which provide real-time feedback on motor speed and position. This closed-loop system enhances the AGV's ability to maintain smooth and synchronized motion, ensuring stability and precision during navigation.

Additionally, each motor is integrated with an electromagnetic brake, enabling rapid deceleration and enhancing safety by halting motion instantly when required.



Figure 4.5: Nema 23 stepper motor 2 Nm torque

Electrical Specification	
<b>Manufacturer Part Number</b>	23E1KBK20-20
<b>Number of Phases</b>	2
<b>Step Angle</b>	1.8deg
<b>Holding Torque</b>	2Nm (283.28oz.in)
<b>Rated Current/Phase</b>	5.0A
<b>Phase Resistance</b>	0.4ohms
<b>Inductance</b>	1.8mH ± 20% (1KHz)
<b>Insulation Class</b>	B 130°C [266°F]
Physical Specification	
<b>Frame Size</b>	57 x 57mm
<b>Body Length</b>	76.5mm
<b>Shaft Diameter</b>	8mm
<b>Shaft Length</b>	21mm
<b>D-Cut Shaft Length</b>	15mm
<b>Lead Length</b>	270mm
<b>Weight</b>	1.06kg
Encoder Specification	
<b>Output Circuit Type</b>	Differential type
<b>Encoder Type</b>	Incremental
<b>Output Signal Channels</b>	2 channels
<b>Supply Voltage Min</b>	5V
<b>Supply Voltage Max</b>	5V
<b>Output High Voltage</b>	<4V
<b>Output Low Voltage</b>	<1V
Brake Connections	
<b>Red-24V+</b>	Red--24V-
<b>Brake Torque</b>	2.0Nm

Table 4.4: Stepper Motor Specifications (Model: 23E1KBK20-20)

subsubsectionDC 12V Electric Linear Actuator (Maximum Force 6000N):

The lifting mechanism of the automated guided vehicle (AGV) utilizes a high-performance linear actuator to achieve precise vertical motion. The actuator includes an overload protection feature, preventing excessive force application and minimizing mechanical wear.



Figure 4.6: Linear actuator with a maximum stoke of 6000N

<b>Model</b>	JS-TGZ-U3
<b>Material</b>	Metal
<b>Voltage</b>	DC 12V
<b>Maximum Push/Pull Force</b>	Approx. 6000N/6000N
<b>Stroke</b>	450mm
<b>No-Load Speed</b>	Maximum 5mm/s
<b>Rated Load Rate</b>	5mm/s (600kg)
<b>Environment Temperature</b>	-26°C to +65°C
<b>Standard Protection Level</b>	IP54
<b>Built-in Stroke Switch</b>	Yes
<b>Color</b>	Silver

Table 4.5: Specifications of the linear actuator model JS-TGZ-U3

#### 4.3.1.1 Motor drivers

- *Closed Loop Stepper Driver V4.1 CL57T :*

The **Closed Loop Stepper Driver V4.1 CL57T** has been selected to complement the **Nema 23 Closed Loop Stepper Motor**, ensuring precise and reliable control over the AGV's propulsion and mechanical functions.

From an electrical perspective, the CL57T driver leverages advanced closed-loop technology to guarantee accurate motor positioning, even in dynamic environments or when encountering external resistance. Fully compatible with software tools like **CLseries** and **Motion Studio**, the driver enables fine-tuning of critical motor parameters, optimizing performance for specific operational requirements.

Additionally, its extensive diagnostic and monitoring ports provide real-time tracking of key electrical and operational metrics, such as **temperature**, **current**, **torque**, **RPM**, and overall motor state during operation. These capabilities not only enhance operational visibility but also streamline troubleshooting and diagnostics, minimizing downtime and ensuring swift resolution of issues.



Figure 4.7: Closed Loop Stepper Driver CL57T V4.1

Key Features	
RS232 debugging interface	
Do not need a high torque margin	
Broader operating speed range	
Reduced motor heating and more efficient	
Smooth motion and super-low motor noise	
5V/24V logic voltage selector, default setting 24V	
Closed-loop, eliminates loss of synchronization	
Protections for over-voltage, over-current, and position following error	
By default, supports an encoder with a resolution of 1000PPR; customizable between 0-5000PPR	
Electrical Specifications	
<b>Output Peak Current</b>	0.8A
<b>Input Voltage</b>	+24 - 48VDC (Typical 36VDC)
<b>Logic Signal Current</b>	7.16mA (Typical 10mA)
<b>Pulse Input Frequency</b>	0 - 200kHz
<b>Isolation Resistance</b>	500Mohm
Operating Environment and Other Specifications ( $T_j = 25^\circ\text{C}/77^\circ\text{F}$ )	
<b>Cooling</b>	Natural Cooling or Forced Cooling
<b>Environment</b>	Avoid dust, oil mist, and corrosive gases
<b>Ambient Temperature</b>	0°C - 65°C
<b>Humidity</b>	40%RH - 90%RH
<b>Operating Temperature</b>	0°C - 50°C
<b>Vibration</b>	10-50Hz / 0.15mm
<b>Storage Temperature</b>	-20°C - 65°C
<b>Weight</b>	Approx. 280g (9.9oz)

Table 4.6: Specifications of the Closed-Loop Stepper Driver

- *BTS7960B 40 Amp Motor Driver Board*

The BTS7960B 40A Motor Driver Board is selected for its capability to control high-power motors, making it ideal for the AGV's linear actuator. Supporting currents up to 40A, it ensures reliable performance in demanding applications.

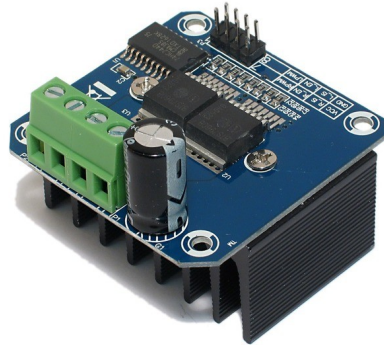


Figure 4.8: DC-MOTOR DRIVER MODULE 24V 43A (2x BTS7960B)

Features	
Double BTS7960 large current (43A) H-bridge driver	
5V isolation with MCU, effectively protecting the MCU	
5V power indicator on board	
Voltage indication of motor driver output end	
Can solder heat sink for improved thermal management	
Requires only four lines from MCU to driver module (GND, 5V, PWM1, PWM2)	
Isolation chip 5V power supply (can share with MCU 5V)	
Supports motor forward and reverse control; two PWM input frequencies up to 25kHz	
Two heat flow passing through an error signal output	
On-board 5V supply can be used or shared with MCU 5V	
Specifications	
<b>Model</b>	IBT-2
<b>Input Voltage</b>	6V - 27V
<b>Maximum Current</b>	43A
<b>Input Level</b>	3.3V - 5V
<b>Control Method</b>	PWM or level
<b>Duty Cycle</b>	0% - 100%
<b>Size</b>	4 x 5 x 1.2 cm / 1.6 x 2.0 x 0.5 inch

Table 4.7: Features and Specifications of the IBT-2 Motor Driver Module

## 4.4 SENSORS

Various sensors, such as LiDAR, cameras, and infrared sensors, are utilized for navigation, obstacle detection, and localization.

The AGV is equipped with a variety of sensors to ensure accurate navigation, obstacle detection, weight measurement, and environmental perception. These sensors work together to enhance the robot's autonomy, safety, and efficiency. The following sensors are integrated into the system:

### 4.4.1 VL53L0X (Time-of-Flight Distance Sensor)

The VL53L0X time-of-flight (ToF) distance sensors play an important role in enhancing the AGV's perception of its immediate surrounding in an operational perspective. These sensors are strategically integrated into the AGV design by deploying eight ToF sensors—two at each corner of the robot insuring a comprehensive coverage. The ToF sensors are especially important in scenarios where traditional sensing methods, such as LiDAR, may be limited or rendered ineffective. For instance, when the AGV carries a lifted platform that obstructs the LiDAR's field of view, the ToF sensors take over to provide reliable distance measurements within a range of 0.5m to 12m .

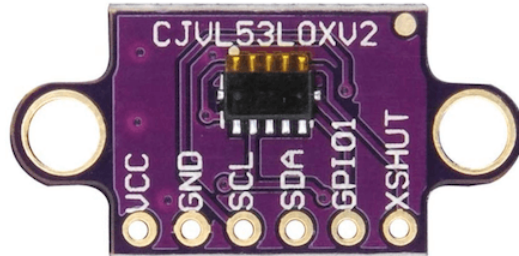


Figure 4.9: VL53L0X time-of-flight (ToF) distance sensor

### 4.4.2 Weight Sensor - Load Sensor 50Kg

This sensor provides accurate and continuous monitoring of the load on the AGV.



Figure 4.10: Load cell

The HX711 in fig. 4.11 is specifically designed to enhance the weak output signals from the load cell in fig. 4.10, ensuring accurate and reliable weight measurements.

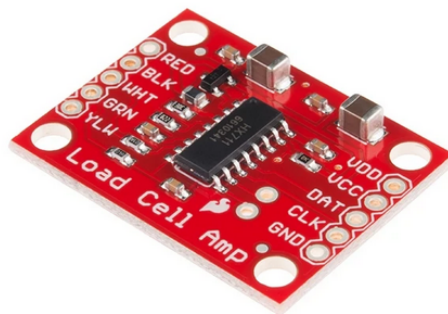


Figure 4.11: HX711 Load cell amplifier

#### 4.4.3 RPLIDAR - 360

The RPLIDAR sensor provides comprehensive environmental mapping, making it indispensable for AGV navigation from an electrical control perspective. With its ability to deliver high-accuracy, real-time 360-degree scanning, the RPLIDAR enables the AGV to perceive its surroundings with exceptional precision.



Figure 4.12: RPLIDAR - 360

#### 4.4.4 Camera HUSKYLENS

The **HUSKYLENS** vision sensor enhances the AGV's performance used for **object detection and line following**. It provides accurate real-time visual feedback, allowing dynamic adjustments to motor speed, direction, and trajectory.

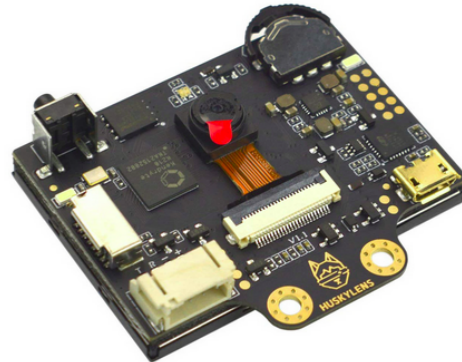


Figure 4.13: Huskylens camera

#### 4.4.5 IMU Sensor

The Inertial Measurement Unit (IMU) is used for achieving precise positioning and movement control in automated guided vehicles (AGVs). The MPU9255 integrates a 3-axis gyroscope, 3-axis accelerometer, and 3-axis magnetometer, providing comprehensive data on angular velocity, linear acceleration, and magnetic field orientation. The MPU9255 communicates with the AGV's control system via I2C or SPI interfaces, ensuring low-latency

data transmission while minimizing power consumption—a key consideration for energy-efficient operation.

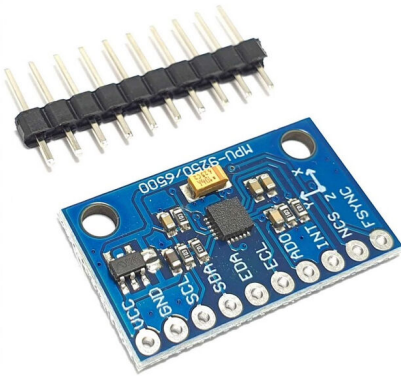


Figure 4.14: Inertia measurement unit 9 axis

#### 4.4.6 Barcode Scanner GM65



Figure 4.15: Qr code scanner

#### 4.4.7 QTRX-HD-11RC

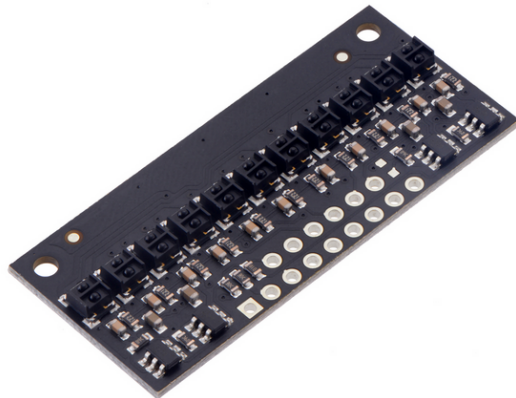


Figure 4.16: QTRX-HD-11RC Reflectance Sensor Array: 11-Channel

### 4.5 MICROCONTROLLER AND COMMUNICATION

The AGV's microcontroller and communication system form the backbone of its control and data exchange capabilities, ensuring efficient processing, seamless communication, and real-time control of the robot's operations.

In this design, the **Raspberry Pi 4** shown in Figure fig. 4.17 serves as the primary computational unit, acting as the “brain” of the system. Equipped with a Linux operating system, it hosts all necessary **ROS (Robot Operating System)** packages, enabling high-level decision-making, sensor data processing, and trajectory planning.

#### 4.5.1 Raspberry Pi 4



Figure 4.17: Raspberry Pi 4

Complementing the Raspberry Pi, the **ESP32 microcontroller** in fig. 4.18 supports it by managing low-level tasks such as motor control and real-time sensor interfacing. The ESP32

directly interfaces with motor drivers to regulate speed, and direction, ensuring precise actuation of the AGV's propulsion system.

Communication between the Raspberry Pi 4 and the ESP32 is achieved through a **serial communication protocol**, which ensures reliable and efficient data exchange. This division of responsibilities – high-level computation on the Raspberry Pi and low-level control on the ESP32 – optimizes the system's performance and reliability.

Additionally, the sensors are shared between both components, with the ESP32 handling time-sensitive data acquisition and the Raspberry Pi performing higher-level processing and integration into the ROS framework.

#### 4.5.2 ESP32-S3-DevKitC-1

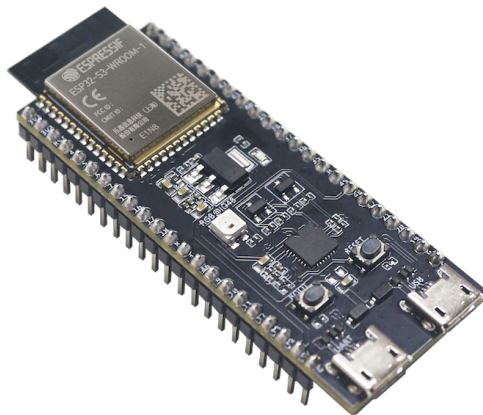


Figure 4.18: ESP32-S3-DevKitC-1

#### 4.5.3 RS232 to Bluetooth Series Adapter

RS232 to Bluetooth Series Adapter

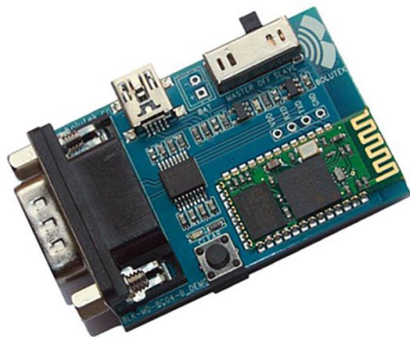


Figure 4.19: RS232 to Bluetooth Series Adapter

#### 4.5.4 TP-Link TL-WR840N

- The **TP-Link TL-WR840N** is utilized as an access point to facilitate communication between the control unit (PC) and the robot's microcontrollers (Raspberry Pi and ESP32 modules).
- By configuring the TL-WR840N as an access point, it creates a wireless network that enables seamless data and command exchange between the PC, Raspberry Pi, and ESP32 modules.
- This setup allows for remote control and monitoring of the AGV's operations, enhancing its usability and adaptability.

All **sensors, microcontrollers, and motor drivers** in the AGV are selected to work in a **cohesive and well-integrated system**, ensuring seamless communication and efficient operation. **Protocols such as I2C and UART** enable reliable data exchange between components, allowing real-time monitoring and control. This structured communication enhances **precision, synchronization, and responsiveness**, optimizing the AGV's navigation, lifting, and traction systems while maintaining operational efficiency and safety.

## 4.6 USEFULL PART

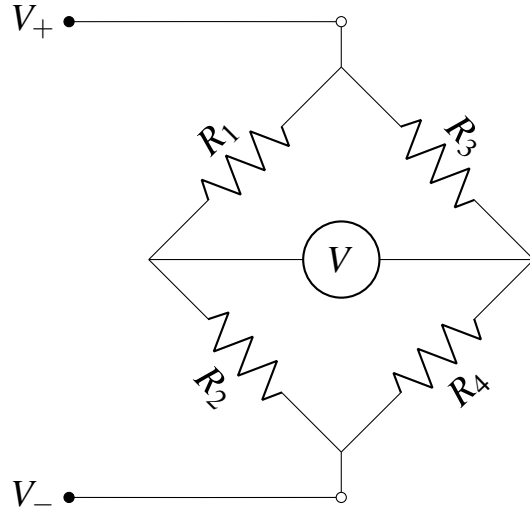


Figure 4.20: Load Cell Circuit with Wheatstone Bridge and Amplifier

The idea behind the load cell is to use the Wheatstone bridge (fig. 4.20). In a Wheatstone bridge,  $R_1 = R_2 = R_3 = R_4$ , and the output voltage is zero when no force is applied. When weight is applied, it bends the material, which changes the resistivity of the material. This change disrupts the equality of the resistances, causing a difference in voltage across  $V$ . By experimenting and calibrating with different weights and tracking the changes in voltage, we can measure the weight.

It is also worth noting that the signal produced depends on the material properties. If the bending factor is linear, the output will be proportional to the applied weight. However, if the bending becomes exponential (which would be a limitation of the material), the relationship between the applied weight and the output signal may no longer be accurate. Additionally, the placement of the load affects the measurement. The voltage difference across  $V$  is used to measure the output of the bridge.

In theory, we could use the microcontroller's analog input to read the voltage differences. However, the changes are too small to provide an accurate reading. For this reason, the **HX711** amplifier is used to amplify the signal and convert it into a digital signal.

## 4.7 BOIMA'S CHAPTER

Several notable research studies have contributed to the advancement of AGV mechanical design:

Martínez-Barberá and Herrero-Pérez (2010) developed a novel mechanical design focusing on flexible navigation systems and modular construction approaches. Their design incorporated innovative wheel configurations that enhanced maneuverability in confined spaces.

Zhang et al. (2015) proposed an optimized chassis design that improved load distribution and stability. Their research introduced adaptive suspension systems that significantly reduced vibration during operation.

Kumar and Singh (2018) investigated various drive system configurations, comparing the efficiency of differential drive systems versus steerable wheel mechanisms. Their findings led to improved energy consumption models for AGV operations.

Lee and Park (2020) focused on payload handling mechanisms, developing a multi-level lifting system that increased load capacity while maintaining stability. Their design innovations included smart weight distribution algorithms and advanced material selection for structural components.

Recent studies by Wilson et al. (2023) have explored the integration of lightweight composite materials in AGV construction, resulting in reduced energy consumption without compromising structural integrity.

These research contributions have significantly influenced modern AGV mechanical design, leading to more efficient, reliable, and adaptable systems suitable for various industrial applications.

## **4.8 RESEARCH GAPS AND JUSTIFICATION**

Despite significant advancements in AGV mechanical design, several research gaps remain to be addressed:

1. Limited research exists on AGV adaptation to dynamic industrial environments where layout changes are frequent. Most existing studies focus on static or semi-static environments.
2. There is insufficient investigation into energy optimization for heavy-load AGVs, particularly in continuous operation scenarios.
3. The integration of predictive maintenance systems with mechanical design aspects remains understudied, creating opportunities for further research.
4. Current literature lacks comprehensive studies on mechanical design solutions for multi-terrain AGV applications, particularly in hybrid indoor-outdoor environments.
5. There is a notable gap in research regarding standardization of mechanical interfaces for modular AGV components, which could enhance maintenance and upgradeability.

These identified gaps justify the need for further research in AGV mechanical design, particularly focusing on adaptability, energy efficiency, and system integration. This study aims to address several of these gaps by proposing novel solutions in AGV mechanical design.

The literature review has highlighted the evolution of AGV mechanical design, from fundamental navigation and chassis developments to modern innovations in materials and smart technologies. While significant advancements have been made in areas such as flexible navigation, optimized chassis design, drive systems, and payload handling mechanisms, several research gaps remain. These include the need for better adaptation to dynamic environments, improved energy optimization for heavy loads, integration of predictive maintenance, multi-terrain capabilities, and standardization of modular components. These identified gaps provide the foundation for further research in AGV mechanical design.

## **4.9 PHYSICAL DESIGN CONSTRAINTS**

The design and construction of a single-level scissor lift AGV with chassis frame structure must consider several practical constraints:

### **4.9.1 Load Capacity Constraints**

- Maximum payload capacity must be clearly defined and maintained within safety limits
- Weight distribution across the chassis frame must be balanced to prevent structural stress
- Material strength limitations of frame components must be considered

### **4.9.2 Dimensional Constraints**

- Overall height limitations in both collapsed and extended positions
- Maximum allowable footprint based on operational space requirements
- Minimum ground clearance requirements for safe operation
- Turning radius limitations based on operational environment

### **4.9.3 Material and Manufacturing Constraints**

- Material availability and cost considerations
- Manufacturing capabilities and tooling limitations
- Welding and assembly requirements
- Surface treatment and finishing constraints

## **4.10 OPERATIONAL CONSTRAINTS**

### **4.10.1 Safety Requirements**

- Compliance with safety standards and regulations
- Emergency stop mechanisms implementation
- Stability requirements during movement and lifting operations
- Safety factor considerations in structural design

#### **4.10.2 Performance Constraints**

- Maximum lifting speed limitations
- Operational cycle time requirements
- Power consumption limitations
- Maintenance accessibility requirements

#### **4.10.3 Environmental Constraints**

- Operating temperature range limitations
- Humidity and moisture exposure considerations
- Floor surface conditions and variations
- Dust and debris exposure limitations

## 4.11 METHOD OF AGV DESIGN

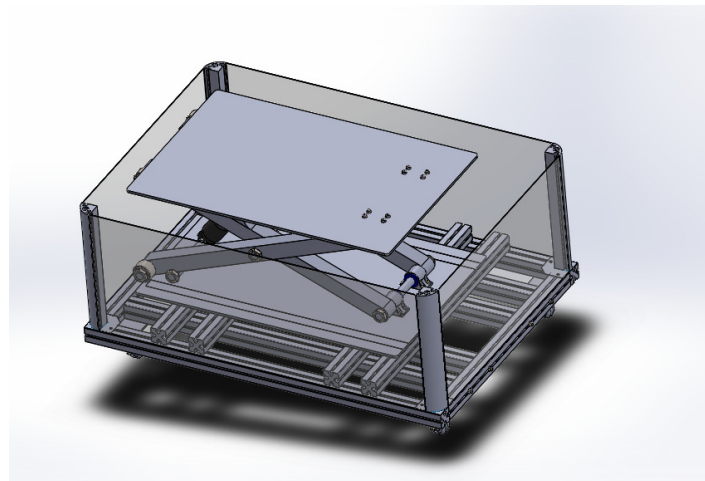


Figure 4.21: AGV Design Process

### 4.11.1 Single level Scissor lift design

The single level scissor lift mechanism is a crucial component of the AGV design, enabling vertical movement of loads through mechanical advantage. This section details the design parameters and specifications of the scissor lift system, which was carefully engineered to meet the required load capacity and operational requirements.

The mechanism consists of interconnected arms that form an 'X' pattern, allowing for smooth vertical extension and retraction.

The design incorporates various dimensional parameters and mechanical elements that work together to achieve efficient lifting operation. Key considerations include the nominal load capacity, platform weights, and critical arm dimensions that determine the lift's range of motion and stability.

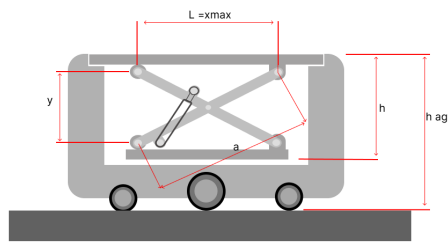


Figure 4.22: Single level scissor lift in an Automated Guidance Vehicle

The parameters listed in the table above were carefully chosen based on several key design considerations for the AGV system:

1. Load Capacity: The nominal load ( $F$ ) of 1.22625 kN was selected to accommodate standard industrial pallets and containers while maintaining a safety margin. This capacity allows the AGV to handle typical warehouse loads efficiently.
2. Platform Dimensions: The upper platform weight ( $m_1$ ) of 22.6 kg represents an optimized balance between structural integrity and overall system weight. The scissor lift arms' weight ( $m^2$ ) of 3.724 kg was achieved through material selection and structural optimization to minimize power requirements while maintaining stability.
3. Operational Range: The maximum distance between articulations ( $L = 0.6$  m) was determined based on the required lifting height and the available space constraints on the AGV chassis. This dimension, along with the arm lengths ( $a = 0.6466$  m), enables the desired vertical travel range while maintaining a compact footprint.
4. Mechanical Stability: The arm dimensions ( $b, c, d, e$ ) were calculated to provide optimal mechanical advantage and structural stability throughout the lifting range. These dimensions ensure smooth operation and minimize stress concentrations at the pivot points.
5. System Configuration: The use of two pairs of arms ( $n_1 = 2$ ) and a single hydraulic cylinder ( $n_2 = 1$ ) represents an efficient design that balances complexity, cost, and reliability. This configuration provides adequate support and lifting capability while minimizing the number of moving parts and potential failure points.

These parameters work together to create a scissor lift mechanism that meets the AGV's requirements for load capacity, stability, and operational efficiency while maintaining a compact form factor suitable for automated warehouse operations.

## Parameters

Parameter	Value	Description
$F$	1.22625 kN	Nominal load
$m_1$	22.6 kg	Upper platform weight
$m_2$	3.724 kg	Weight of scissors lift arms
$L$	0.6 m	Maximum distance between "1" and "2" articulations
$l$	0.3 m	$L/2$
$h_1 = h_2$	0.006 m	Height of upper and lower platforms
$y$	0.241 m	Height of the scissor mechanism without the platforms
$a$	0.6466 m	Arm dimension
$b$	0.230 m	Arm dimension
$c$	0.06466 m	Arm dimension
$d$	0.055 m	Arm dimension
$e$	0.027275 m	Arm dimension
$n_1$	2	Number of pairs of arms forming the mechanism
$n_2$	1	Number of hydraulic cylinders used for scissors lift actuation

Table 4.8: Parameters and their descriptions

**Note:**  $L/2$  (0.3 m) represents the upper platform middle point. The value "L" (0.6 m) is specifically used for locating the center of gravity (CoG) of the upper platform weight ( $m_1$ ). According to the design parameters, L is less than the arm length  $a$  (0.6466 m).

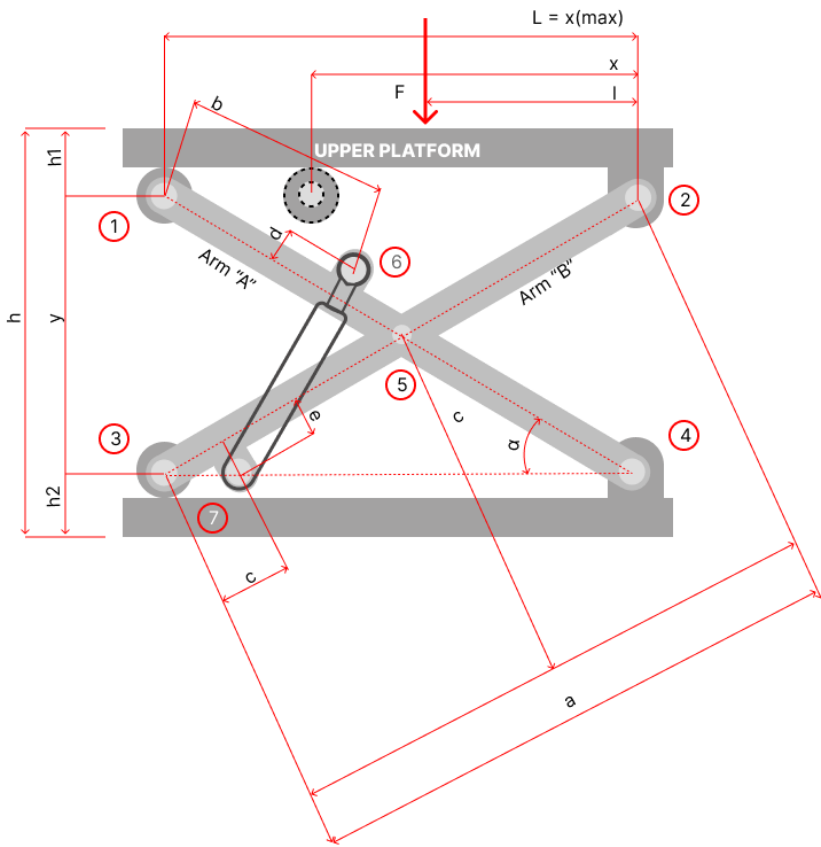


Figure 4.23: Single level Scissor lift dimensions

## 4.12 LOAD ANALYSIS

Maximum load analysis:

The maximum load analysis is crucial for ensuring the safe and reliable operation of the scissor lift mechanism. This analysis considers various forces acting on the system when it is loaded to its maximum capacity. The following factors are evaluated:

- Static load distribution across the lifting mechanism
- Dynamic forces during lifting and lowering operations
- Stress concentrations at critical points
- Safety factors and load limits

The analysis takes into account both the nominal load ( $F$ ) of 1.22625 kN and the self-weight of the system components, including the upper platform weight ( $m_1$ ) and the scissor lift arms weight ( $m_2$ ). This comprehensive evaluation ensures that all structural elements

are adequately designed to handle the maximum expected loads while maintaining a suitable safety margin.

#### 4.12.1 Load distribution:

The load distribution can be mathematically expressed through the following relationships:

For a load  $F$  applied at distance  $l$  from point 1, the distribution coefficients  $q$  and  $r$  are determined by:

##### Moment equation about point 1:

$$F(q)(r) = F(l) \quad (4.1)$$

##### Roller support coefficient:

$$q = \frac{l}{x} \quad (4.2)$$

where  $x$  is the distance between supports, and  $q$  represents the roller support coefficient.

##### Moment equation about point 2:

$$F(r)(x) = F(x-l) \quad (4.3)$$

##### Complementary relationship between coefficients:

$$r = 1 - \frac{l}{x} = 1 - q \quad (4.4)$$

These equations demonstrate that:

- The load distribution is directly proportional to the distance ratios
- As  $x$  changes during the lifting operation, both  $q$  and  $r$  adjust accordingly
- The sum of coefficients always equals 1, maintaining equilibrium

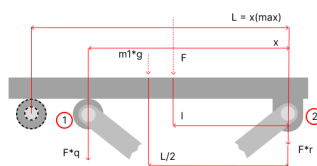


Figure 4.24: load distribution coefficients at point 1 and 2

#### 4.12.2 Dead load

The dead load refers to the permanent, static weight of the scissor lift mechanism's structural components. This includes all fixed elements that contribute to the overall weight of the system, regardless of the operational state.

The weight and load acting on the scissor lift mechanism itself consists of the following components:

Component Details and Weights			
Component	Quantity	Description	(kg)
Plates (upper and lower)	2	Primary support platforms	22.6
Scissor arms	4	Main lifting mechanism components	5.08
Bearings	4	Facilitates smooth movement at pivot points	1.0
Pin supports	4	Structural connection points	0.48
Actuator cylinder	1	Hydraulic lifting mechanism	3.5
Shafts (varying length)	6	Mechanical linkage components	2.4
Fasteners	Multiple	Bolts and nuts for assembly	0.5
<b>Dead weight</b>			<b>35.56</b>

Table 4.9: Component Details and Weights

The dead load must be carefully considered in the overall system design as it:

- Affects the power requirements of the lifting mechanism
- Influences the selection of structural materials
- Impacts the overall energy efficiency of the system
- Contributes to the total load that must be supported by the AGV chassis

### 4.12.3 Forces on the lift

The forces acting on the scissor lift mechanism can be analyzed through a series of mathematical equations that describe the relationship between various components. These equations account for both static and dynamic forces during operation:

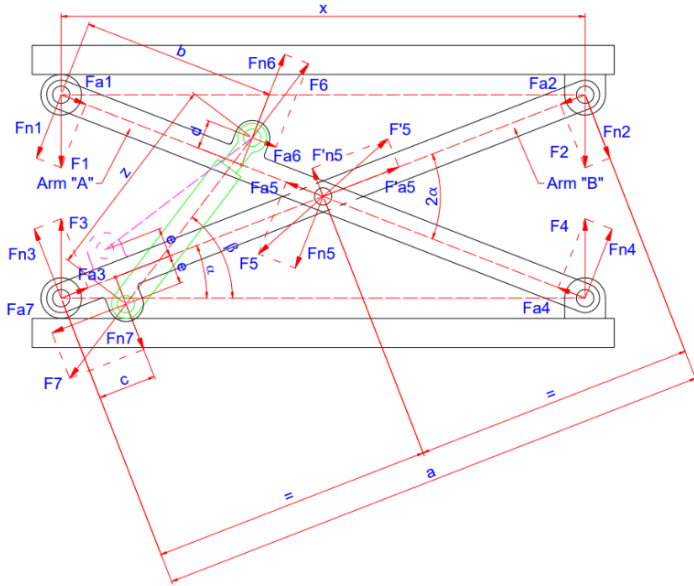


Figure 4.25: Forces acting on the scissor lift

For a given angle  $\alpha$ , the following forces are calculated:

- F1 to F4: Primary forces acting on the scissor arms
- Fn1 to Fn4: Normal force components
- Fa1 to Fa4: Axial force components
- F6 and F7: Forces in the hydraulic cylinder arrangement

The analysis is divided into two main sections:

Arm "A" Analysis

The forces on Arm "A" are calculated considering moments around point 5, with the following key equations:

$$F_{n1} \left( \frac{a}{2} \right) + F_{n4} \left( \frac{a}{2} \right) - F_{n6} \left( \frac{a}{2} - b \right) - F_{a6}(d) = 0 \quad (4.5)$$

$$F_6 = \left( F_{n1} \frac{a}{2} + F_{n4} \frac{a}{2} \right) \left[ \cos(90^\circ - \alpha - \beta) \left( \frac{a}{2} - b \right) + \sin(90^\circ - \alpha - \beta) d \right] \quad (4.6)$$

$$F_5 = \sqrt{F_{n5}^2 + F_{a5}^2} \quad (4.7)$$

Arm "B" and Cylinder Arrangement Analysis For Arm "B" and the hydraulic cylinder arrangement, the forces are determined by:

$$F_{n2} \left( \frac{a}{2} \right) + F_{n3} \left( \frac{a}{2} \right) - F_{n7} \left( \frac{a}{2} - c \right) - F_{a7}(e) = 0 \quad (4.8)$$

$$F_7 = \left( F_{n2} \frac{a}{2} + F_{n3} \frac{a}{2} \right) \left[ \sin(\beta - \alpha) \frac{a}{2} - c - \cos(\beta - \alpha)e \right] \quad (4.9)$$

These equations form the basis for understanding the force distribution throughout the scissor lift mechanism and are essential for ensuring proper design and operation of the system.

The following table shows the calculated forces at different angles ( $\alpha$ ) of the scissor lift mechanism:

Forces							
$\alpha$ (degrees)	$F_1$ (kN)	$F_2$ (kN)	$F_3$ (kN)	$F_4$ (kN)	$F_5$ (kN)	$F_6$ (kN)	$F_7$ (kN)
22	2.84	2.76	2.76	2.84	3.12	4.28	4.18
24	2.92	2.83	2.83	2.92	3.24	4.42	4.32
26	3.01	2.91	2.91	3.01	3.38	4.58	4.48
28	3.12	3.02	3.02	3.12	3.54	4.76	4.66
30	3.24	3.14	3.14	3.24	3.72	4.96	4.86
32	3.38	3.28	3.28	3.38	3.92	5.18	5.08

Table 4.10: Forces acting on scissor lift components at various angles of operation

Where:

- $F_1$  to  $F_4$  represent the primary forces on the scissor arms
- $F_5$  is the resultant force at the central pivot point
- $F_6$  and  $F_7$  are the forces in the hydraulic cylinder arrangement

The table demonstrates that as the angle  $\alpha$  increases, all forces in the system generally increase, which aligns with the decreasing mechanical advantage observed earlier.

## 4.13 MECHANICAL ADVANTAGE ANALYSIS:

The mechanical advantage (MA) of the scissor lift can be calculated considering the symmetrical nature of the mechanism. For the given range of  $\alpha$  ( $22^\circ$  to  $32^\circ$ ), the mechanical advantage is determined using the following equation:

$$M_A = \frac{F_{\text{out}}}{F_{\text{in}}} = \frac{L \cos(\alpha)}{2h \tan(\alpha)} \quad (4.10)$$

Where:

- $F_{\text{out}}$  is the output force (lifting force)
- $F_{\text{in}}$  is the input force (actuator force)
- L is the platform length (0.6 m)
- h is the vertical height
- $\alpha$  is the angle of the scissor arms

**Mechanical advantage analysis**

$\alpha$ (degrees)	Height (m)	Mechanical Advantage	InputF(kN)	OutputF(kN)
22	0.242	2.84	0.432	1.226
24	0.263	2.61	0.470	1.226
26	0.284	2.41	0.509	1.226
28	0.305	2.24	0.547	1.226
30	0.326	2.09	0.586	1.226
32	0.347	1.96	0.625	1.226

Table 4.11: Mechanical advantage analysis results at different scissor lift angles, showing the relationship between input and output forces

The analysis shows that the mechanical advantage decreases as the angle increases, requiring more input force to maintain the same output force. This is due to the changing geometry of the mechanism as it extends. The symmetrical design ensures even load distribution and stable operation throughout the lifting range.

### 4.13.1 Kinematic analysis

#### 4.13.1.1 Range of motion

The range of motion for the scissor lift mechanism can be calculated using the following equation:

$$h = h_1 + h_2 + a \sin(\alpha) \quad (4.11)$$

Where:

- $h$  = total height of the scissor lift
- $h_1$  = initial height
- $h_2$  = additional height component
- $a$  = length of scissor arm
- $\alpha$  = angle of scissor arms

The lift operates between the following positions:

Height & angle			
Position	Height (m)	Angle $\alpha$ (degrees)	Platform Length (m)
Initial stage	0.241	22	0.6
Final stage	0.341	32	0.5494

Table 4.12: Height, angle, and platform length at different stages.

This range of motion provides sufficient vertical travel to meet the operational requirements while maintaining stability throughout the lifting cycle.

### 4.13.2 Scissor lift dimensions

The dimensional analysis of the scissor lift mechanism is critical for understanding its kinematic behavior. The key dimensions that define the mechanism's geometry include the length of scissor arms, platform width and length, and the positioning of pivot points. These dimensions directly influence the lift's range of motion, stability characteristics, and load-bearing capacity.

To determine the unknown dimensions of the scissor lift, a 2D AutoCAD model was created using the known dimensions as reference points. The initial and final positions of the

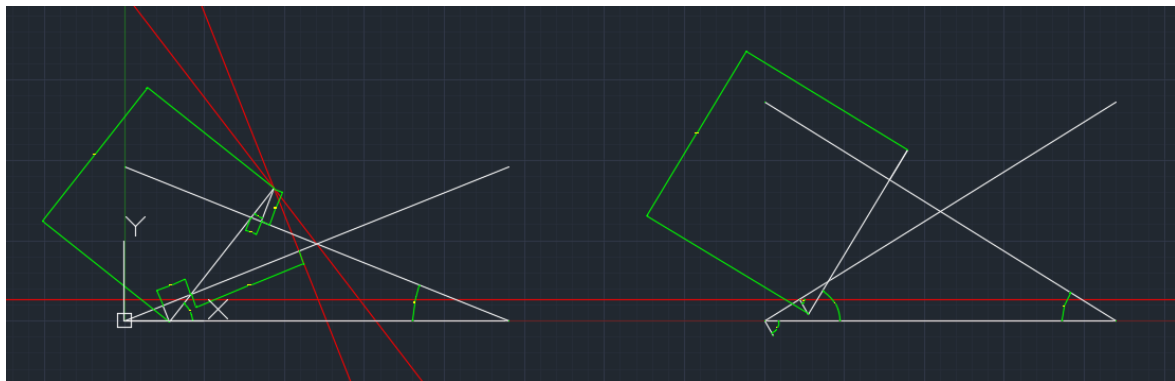


Figure 4.26: 2D Autocad model of the scissor lift Dimensions

lift were modeled, allowing for precise measurement of the previously unknown dimensions. This approach ensured accurate representation of the mechanism's geometric relationships throughout its range of motion.

These parameters and their relationships shown in table 4.13 define the geometric configuration of the scissor lift mechanism throughout its range of motion. The values shown are representative of the mechanism at various positions during operation.

Component Details and Weights		
Parameter	Relation	Value
$\alpha$	$\tan^{-1} \left( \frac{y}{L} \right)$	$22^\circ - 32^\circ$
$\beta$	$\alpha + \tan^{-1} \left( \frac{BB'}{B'D} \right)$	Varies with $\alpha$
$AB$	$\sqrt{d^2 + \left( \frac{a}{2} - b \right)^2}$	0.3 m
$\delta$	$\sin^{-1} \left( \frac{d}{AB} \right)$	Varies with position
$BB'$	$AB \cdot \sin(2\alpha + \delta)$	0.25 m
$B'D$	$\frac{BB'}{\tan(\beta - \alpha)}$	0.2 m
$CC'$	$E$	0.15 m
$C'D$	$B'D \cdot \frac{e}{BB'}$	0.12 m
$BD$	$\frac{BB'}{\sin(\beta - \alpha)}$	0.28 m
$CD$	$\sqrt{CC'^2 + C'D^2}$	0.19 m

Table 4.13: Parameters, their relations, and corresponding values.

### 4.13.3 Mass center

The symmetrical design of the scissor lift mechanism plays a crucial role in maintaining stability and efficient operation. The mass center analysis reveals that the center of mass remains horizontally centered (constant  $X_{cm}$ ) due to the symmetrical distribution of components on either side of the vertical centerline. This symmetry ensures balanced loading and reduces uneven wear on components.

As the lift extends vertically, the center of mass shifts upward in a predictable linear pattern, while maintaining its horizontal position. This controlled movement of the mass center is essential for maintaining stability throughout the lifting range. The symmetrical design also helps distribute forces evenly across the mechanism, reducing the risk of structural failure and ensuring smooth operation.

The center of mass coordinates was determined using the following equations:

$$X_{cm} = \frac{(\sum m_i) x_i}{\sum m_i} \quad (4.12)$$

$$Y_{cm} = \frac{(\sum m_i) y_i}{\sum m_i} \quad (4.13)$$

Where:

- $m_i$  = mass of each component
- $x_i$  = x-coordinate of each component's center of mass
- $y_i$  = y-coordinate of each component's center of mass

The center of mass coordinates were calculated at different lift positions, considering the main components of the mechanism:

Lift Position	Height (m)	$X_{cm}$ (m)	$Y_{cm}$ (m)	Total Mass (kg)
Fully Retracted	0.241	0.300	0.120	24.5
25% Extended	0.266	0.300	0.133	24.5
50% Extended	0.291	0.300	0.146	24.5
75% Extended	0.316	0.300	0.158	24.5
Fully Extended	0.341	0.300	0.171	24.5

Table 4.14: Lift position, height, center of mass coordinates, and total mass.

Note: The  $X_{cm}$  remains constant at 0.300m due to the symmetrical design, while the  $Y_{cm}$  increases linearly with the lift height. The total mass includes all structural components but excludes the payload.

## 4.14 MOBILITY

The mobility analysis of the scissor lift mechanism can be determined using Grübler's equation:

$$M = 3(n - 1) - 2j_1 - j_2 \quad (4.14)$$

Where:

- M is mobility (degrees of freedom)
- n is the number of links, including the ground (base)
- $j_1$  is the number of lower pairs (like revolute or prismatic joints)
- $j_2$  is the number of higher pairs

For our scissor lift mechanism:

- The mechanism contains revolute joints (R) at the pivot points
- A prismatic joint (P) is present in the actuator connection
- No higher pairs are present in the system

Applying Grübler's equation to our mechanism:

- Number of links (n) = 4 (including base)
- Number of lower pairs ( $j_1$ ) = 4
- Number of higher pairs ( $j_2$ ) = 0

Therefore:

$$M = 3(4 - 1) - 2 \cdot 4 - 0 \quad (4.15)$$

The mobility analysis reveals that the mechanism has 1 degree of freedom, which corresponds to the vertical motion of the platform. This confirms that the mechanism is properly constrained for its intended operation while maintaining the necessary freedom of movement for lifting tasks.

## 4.15 INSTANTANEOUS CENTER

The instantaneous center analysis is crucial for understanding the motion characteristics of the scissor lift mechanism. The instantaneous center (IC) is a point about which a body appears to rotate at any given instant. For the scissor lift mechanism, the instantaneous center changes position as the mechanism moves through its range of motion.

The location of the instantaneous center can be determined by:

- Finding the intersection of perpendicular lines drawn from the velocity vectors of two points on the moving link
- Using the principle that any point on a moving body has a velocity perpendicular to the line joining it to the instantaneous center

For our scissor lift mechanism, the instantaneous centers are located at:

(IC) locations and angular velocities		
Position	IC Location ( $x, y$ ) (m)	Angular Velocity (rad/s)
Lower Position	0.300, 0.000	0.157
Mid Position	0.300, 0.145	0.142
Upper Position	0.300, 0.290	0.128

Table 4.15: Instantaneous center (IC) locations and angular velocities at different positions.

The analysis of instantaneous centers helps in:

- Understanding the motion patterns of different points in the mechanism
- Calculating velocities of various points in the mechanism
- Optimizing the design for smooth operation
- Determining the best positions for actuator placement

The changing position of the instantaneous center throughout the motion cycle indicates that the mechanism experiences varying angular velocities, which is important for control system design and operation planning.

## 4.16 VELOCITY DETERMINATION

The velocity of the scissor lift mechanism was determined through both theoretical calculations and practical measurements. The process involved several steps:

1. Theoretical Velocity Calculation:

$$v = \frac{\frac{dh}{dt}}{\sin \alpha} \quad (4.16)$$

Where:

- $v$  = linear velocity
- $\frac{dh}{dt}$  = rate of change of height
- $\alpha$  = angle of scissor arms

1. Practical Measurements:

- Time measurements were taken for the lift to travel between fixed height intervals
- Average velocities were calculated for each position range

Height Range (m)	Time (s)	Average Velocity (m/s)
0.241 - 0.266	2.1	0.012
0.266 - 0.291	2.3	0.011
0.291 - 0.316	2.5	0.010
0.316 - 0.341	2.8	0.009

Table 4.16: Measured velocities of the scissor lift mechanism at different height ranges showing the gradual decrease in velocity as the lift extends upward

## 4.17 ACTUATION MECHANISM

The actuation mechanism is a critical component of the scissor lift system, responsible for generating the force required to raise and lower the platform. Two key parameters were calculated for the actuator design:

1. Required Actuator Force (F)

The force required by the actuator was calculated using the mechanical advantage relationship:

$$F = F_6 \left( \frac{n_1}{n_2} \right) \quad (4.17)$$

Where:

- $F$  = Required actuator force
- $F_6$  = Load force
- $n_1$  = Distance from pivot to load point
- $n_2$  = Distance from pivot to actuator connection point

#### 4.17.1 Cylinder Extension Length (Z)

The extended length of the actuator ( $Z$ ) is measured between the joint connections and varies with the scissor lift position. This parameter is crucial for selecting an appropriately sized actuator that can accommodate the full range of motion.

The calculations for actuator force and cylinder extension length are as follows:

##### 4.17.1.1 Actuator Force Calculations

Given:

- $F_6$  (Load force at  $\alpha = 32^\circ$ )
- $n_1$  (Distance from pivot to load) = 0.45 m
- $n_2$  (Distance from pivot to actuator) = 0.15 m

Using eq. (4.15):

$$F = 1.35 \text{ kN}$$

The actuator must accommodate a stroke length of 34.578 mm (difference between final and initial positions).

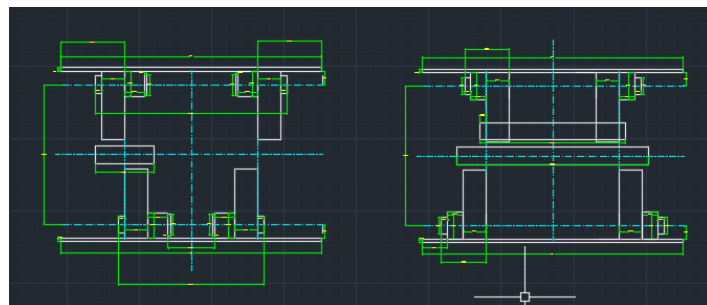
Position	Extension Length (Z) (m)
Initial Length	0.264322
Final Length	0.2989
Total Stroke	0.034578

Table 4.17: Actuator cylinder extension measurements showing the initial and final lengths required for full range of motion

## 4.18 CAD DESIGN

The design process began with the creation of a 2D model using AutoCAD software. This initial step was crucial for ensuring proper component layout and preventing any potential interference between moving parts. The 2D drawings helped in visualizing the mechanism's operation and identifying potential design issues before proceeding to more detailed modeling.

Following the 2D design phase, a comprehensive 3D model was developed using SolidWorks. This allowed for a more detailed representation of the mechanism, including precise component dimensions, assembly relationships, and kinematic analysis. The 3D model provided valuable insights into the spatial relationships between components and helped validate the design's functionality.



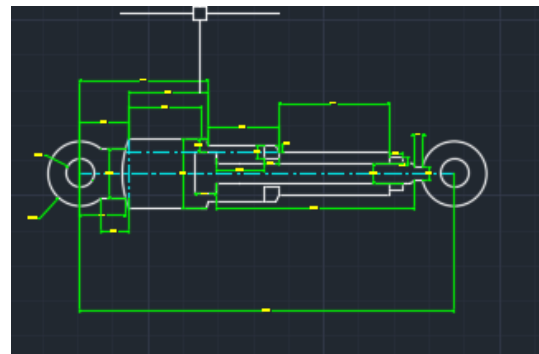
(a) front and rear view of the mechanism



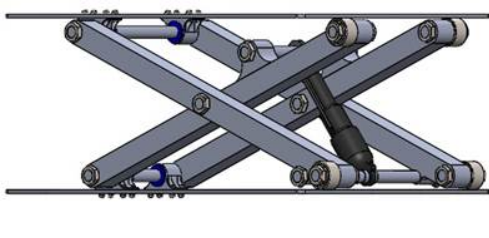
(b) top and bottom platforms



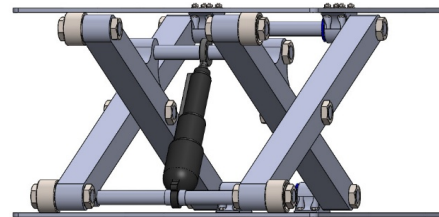
(a) hinge (pin support)



(b) subfigure 9:actuator cylinder



(a) single level scissor lift



(b) single level scissor lift

#### 4.18.1 Machine components (Scissor lifts)

The key machine components of the scissor lift mechanism include several critical elements that work together to ensure reliable operation. The main structural components consist of the scissor arms, pivot joints, and platform assembly, each engineered to specific tolerances and material specifications. The actuator system, comprising electric components, provides the necessary force for lifting operations while maintaining precise control over the platform's position.

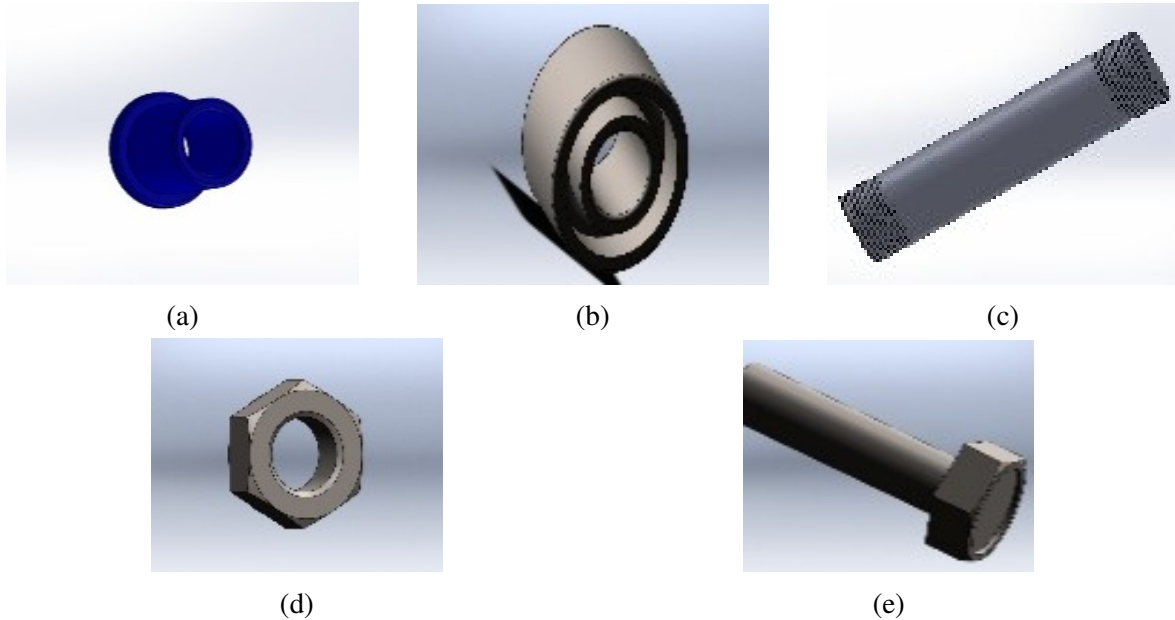


Figure 4.30: a Plain bearings that provide smooth sliding motion and wear resistance at pivot points

b Rolling elements that reduce friction between moving parts and support radial and axial loads

c Cylindrical components that transfer rotational motion and support rotating elements in the mechanism

d & e Bolts, nuts, and pins used to secure components and allow for maintenance

#### 4.18.2 Method of assembly

The assembly process for the scissor lift mechanism follows a systematic approach to ensure proper functionality and safety. The following steps detail the key assembly procedures:

Fastener Installation:

- All bolted connections are secured using Grade 8.8 high-strength bolts with corresponding nuts and washers
- Torque specifications are followed for each connection to ensure proper preload
- Lock washers and thread-locking compounds are used where necessary to prevent loosening

Cutting and Drilling Operations:

- Material cutting is performed using precision tools to maintain dimensional accuracy
- Holes are drilled according to technical drawings with specified tolerances

- All drilled holes are deburred and cleaned to ensure proper fit of fasteners
- Pilot holes are used where necessary to ensure accurate hole placement

Quality Control Measures:

- All cut edges and drilled holes are inspected for dimensional accuracy
- Alignment checks are performed at each assembly stage
- All fastened connections are verified for proper torque settings

#### **4.18.3 Stress Analysis**

The stress analysis of the scissor lift mechanism was conducted using SolidWorks Simulation software. This comprehensive analysis included evaluations of stress distribution, strain patterns, and structural deformation under various loading conditions. The simulation provided valuable insights into the mechanical behavior of the assembly, helping to identify potential stress concentrations and validate the structural integrity of the design.

The simulation was performed using the following parameters and conditions:

- Static load analysis with maximum rated capacity
- Material properties defined for each component
- Fixed geometry constraints at mounting points
- Mesh refinement in critical areas for improved accuracy

The results from these simulations were used to optimize the design and ensure that all components operate within their safe stress limits under normal operating conditions.

The stress analysis results show the scissor lift mechanism in solid blue, with von Mises stress values close to the yield strength ( $2.757e+07$ ). The uniform blue coloration indicates even stress distribution throughout the structure. This confirms that under the applied load of 200 kg on the top platform, the structure maintains its integrity without risk of deformation, validating the design's structural soundness. The deformation scale factor of 7.9772 was used to visualize the potential displacement under load. The stress analysis of the lift was simulated with a single material for all the parts (Aluminum alloy 1066) so that a comparison can be made between the von mises stress and the yield strength.

The displacement analysis results indicate that under a deformation scale factor of 15.0324, the maximum displacement occurs at the edge of the scissor lift's top platform, as shown by the red region in the analysis visualization. This finding is consistent with expected behavior,

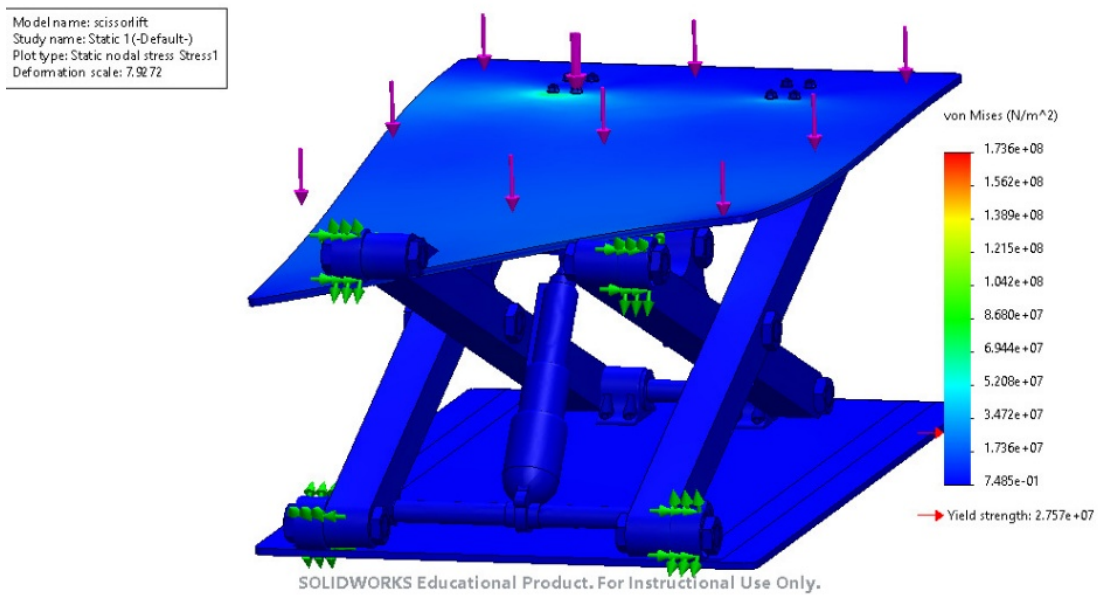


Figure 4.31: Result for the stress analysis

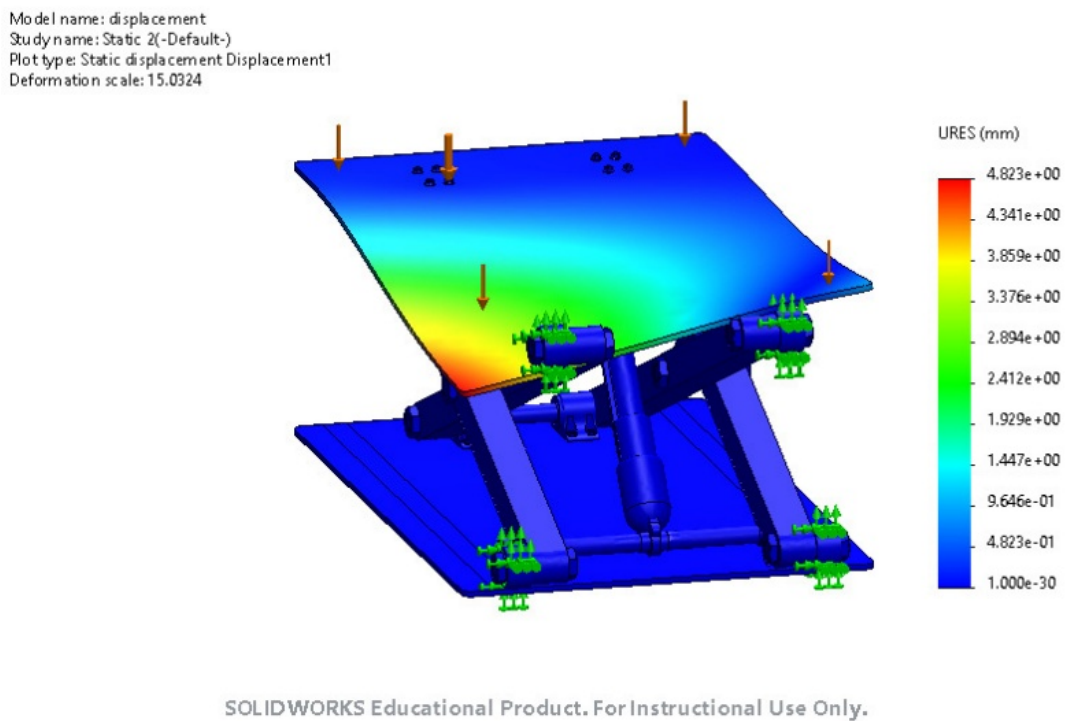
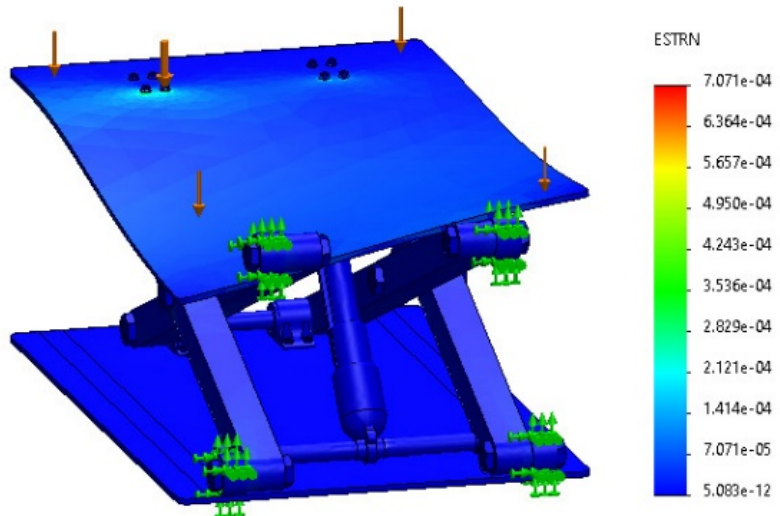


Figure 4.32: result for displacement analysis

as the platform edge experiences the greatest moment arm from the support points. The displacement analysis of the lift was simulated with a two material for all the parts (Aluminum alloy 1066 and AISI Steel alloy) so that the region of max displacement can be identified.

Model name: displacement  
Study name: Static 2(-Default-)  
Plot type: Static strain Strain1  
Deformation scale: 15.0324



SOLIDWORKS Educational Product. For Instructional Use Only.

Figure 4.33: results for static strain analysis

The strain analysis results, visualized in blue throughout the structure, demonstrate that the scissor lift design operates well within allowable strain limits. This uniform blue coloration indicates that the strain distribution is even and remains below critical thresholds, confirming that the structural components will maintain their elastic behavior under normal operating conditions. The consistent strain pattern suggests effective load distribution across the mechanism's components, validating the design's ability to handle the specified operational loads without risk of permanent deformation. The Static Strain analysis of the lift was simulated with a two material for all the parts (Aluminum alloy 1066 and AISI Steel alloy) so that the region of max strain can be identified.

## **4.19 AGV CHASSIS DESIGN AND ANALYSIS REPORT**

### **4.19.1 Design Specifications**

The AGV chassis is designed to accommodate a maximum load capacity of 300 kg (2943N), with an additional safety margin factored into the structural calculations. The overall dimensions of 0.95m length, 0.68m width, and 0.4m height have been integrated into the design parameters to ensure optimal clearance and functionality while maintaining a low center of gravity for enhanced stability.

Key design specifications include:

- Maximum Load Capacity: 300 kg (2943N)
- Height: 0.4m
- Length: 0.95m
- Width: 0.68m
- Material: 40x40 aluminum alloy extrusion profiles
- Safety Factor: 1.5 for dynamic loading conditions

### **4.19.2 Structural Configuration**

The AGV chassis employs a robust structural configuration designed for optimal stability and load distribution. The framework utilizes a combination of horizontal and vertical aluminum profiles, strategically arranged to create a rigid and durable support system. The design incorporates precise geometric relationships between components to ensure even weight distribution and minimize structural stress points. This configuration allows for efficient integration of all subsystems while maintaining the necessary strength-to-weight ratio required for AGV operations. The modular nature of the structural layout also facilitates easy maintenance access and future modifications if needed.

The primary framework consists of:

- Horizontal Assembly: Four parallel 40x40 aluminum profiles arranged in rows
- Vertical Support: Eight column profiles providing structural integrity
- Connection Methods: Precision-engineered screw brackets (plate and corner types)
- Fastening System: High-grade bolts with specified torque requirements

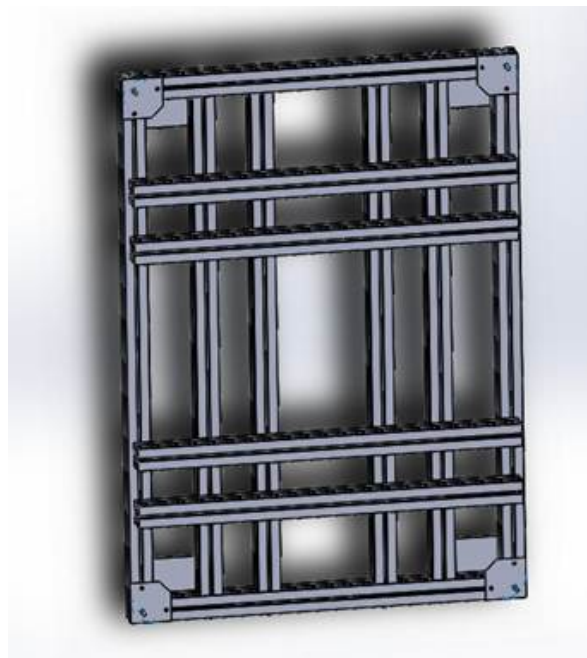


Figure 4.34: AGV chassis structure

#### 4.19.3 Component Integration

The chassis design incorporates multiple specialized zones for optimal integration of components and systems. The Central Integration Zone features a reinforced mounting platform specifically designed for the scissor lift mechanism, along with a centralized battery pit that ensures optimal weight distribution throughout the structure. For mobility systems, the chassis includes four castor wheel mounting points with reinforced brackets, two drive wheel installations complete with motor mount interfaces, and precision-aligned gear and bearing housing attachments. This layout maximizes structural integrity while maintaining efficient space utilization and accessibility for maintenance.

#### 4.19.4 Protective Framework

The NET-frame superstructure consists of a robust protective framework designed to safeguard internal components while maintaining accessibility. Four corner aluminum profile supports provide the primary structural integrity, while integrated transparent panels enable clear visibility of internal operations. Strategic access points are incorporated throughout the framework to facilitate routine maintenance and component replacement procedures.

#### 4.19.5 Design Methodology

The development process followed a systematic approach that began with comprehensive 2D design implementation using AutoCAD. This initial phase focused on precise dimension-

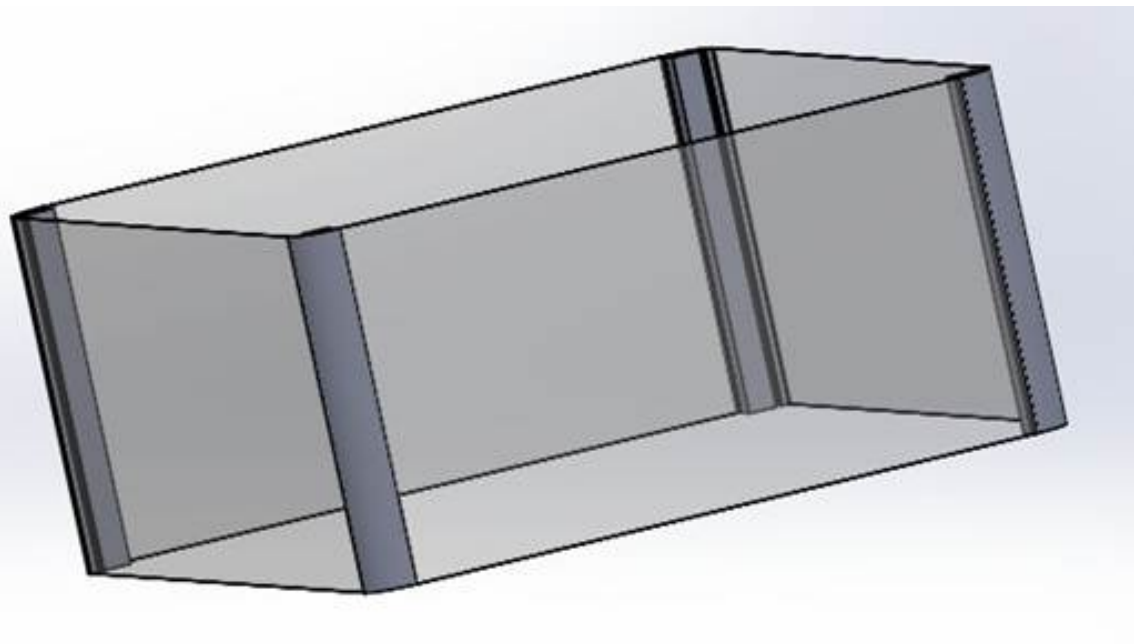


Figure 4.35: 3D model of protective frame and covering

ing, critical clearance verification, and detailed component interface planning. The process then progressed to advanced 3D modeling using SolidWorks, enabling complete assembly visualization, thorough interference checking between components, and dynamic movement simulation to validate the design's functionality.

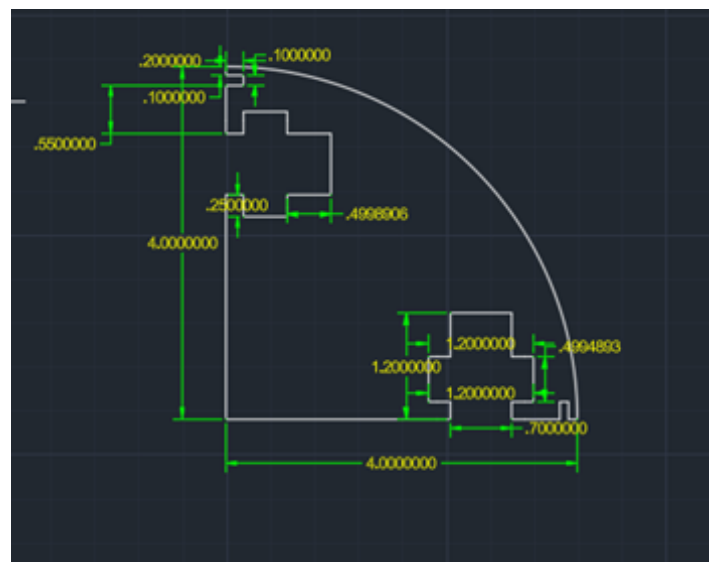


Figure 4.36: 2D profile of aluminum extrusion

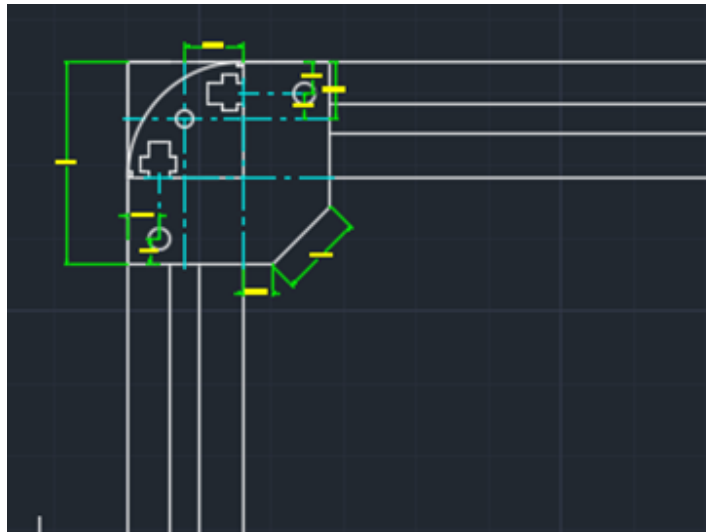


Figure 4.37: 2D model of profile joint and fasteners

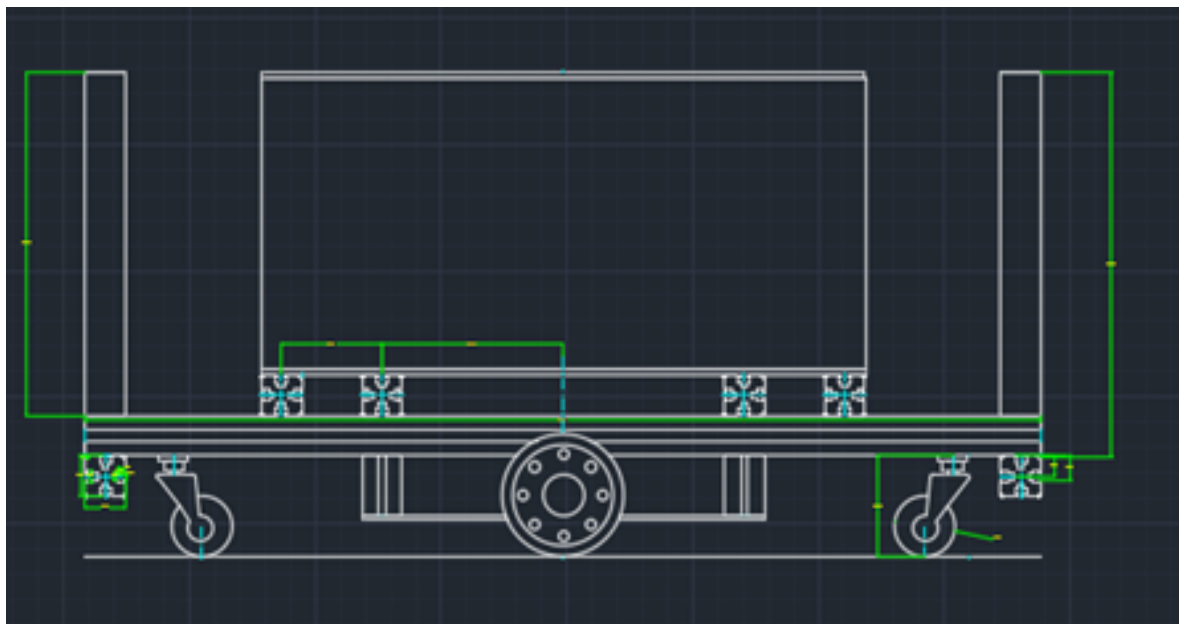


Figure 4.38: 2D model of Chassis and frame

#### 4.19.6 Load Distribution Analysis

The static load distribution analysis revealed optimal weight distribution characteristics across all support points, with the chassis demonstrating minimal deflection under the maximum load capacity of 300 kg. Dynamic load considerations encompassed acceleration and deceleration forces, turning moment effects, and vibration damping characteristics, ensuring robust performance under various operational conditions.

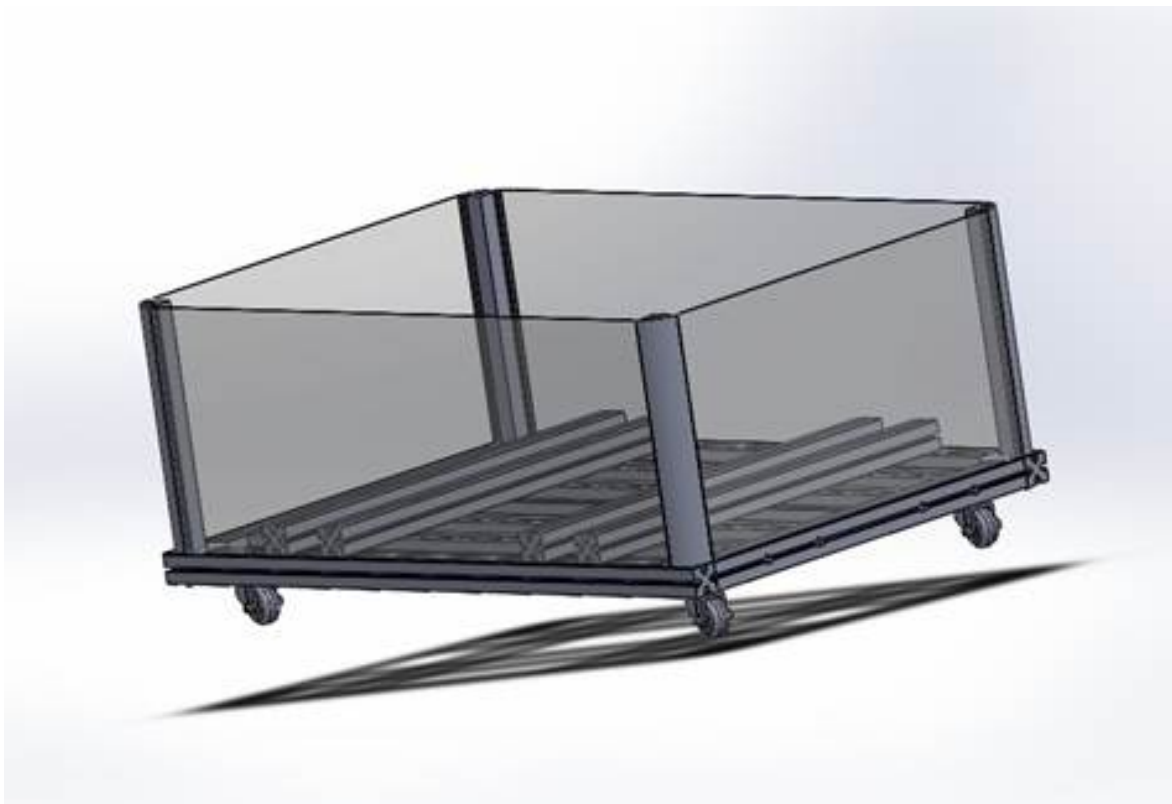


Figure 4.39: 3D design of chassis and frame covering

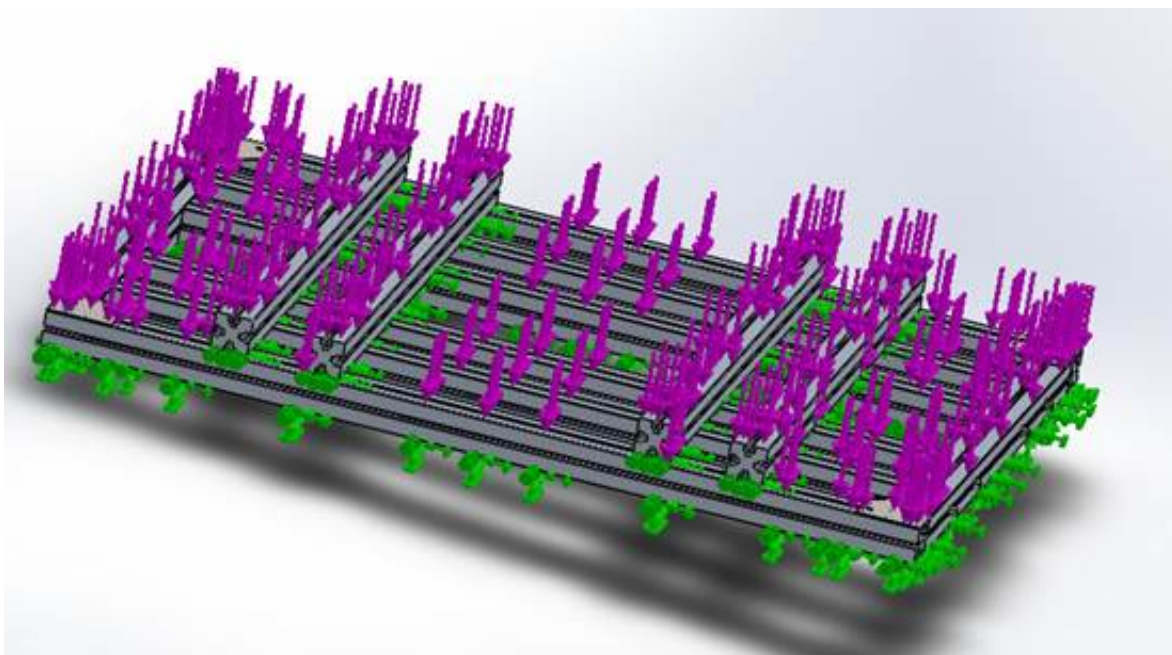


Figure 4.40: Load distribution on the chassis

#### 4.19.7 Symmetry Stress Analysis

Using SolidWorks Simulation, stress analysis validated the design's structural integrity, showing Von Mises stress values well within material limits. The results revealed uniform

stress distribution with no significant concentration points. The structure exhibited acceptable maximum deflection ranges while maintaining elastic behavior under operational loads, with minimal torsional effects.

Comprehensive testing confirmed the chassis's structural stability under maximum load conditions, demonstrating seamless integration with scissor lift operations and effective weight distribution during movement. All integrated systems demonstrated proper functionality, validating the design's ability to meet operational requirements while maintaining necessary safety factors.

#### **4.19.8 Load Analysis with 2943N Force**

The chassis undergoes extensive analysis under a total force of 2943N (equivalent to  $300\text{kg} \times 9.81 \text{ m/s}^2$ ). Each corner support bears approximately 735.75N, representing one-quarter of the total load. The central mounting points experience additional moment forces due to dynamic loading, while support beams are subject to combined axial and bending stresses.

The 40x40 aluminum extrusion profiles are engineered to handle substantial vertical loading, with direct compressive force of 2943N distributed across vertical supports. A safety factor of 1.5 is incorporated for dynamic loading conditions, with maximum allowable stress calculations adjusted accordingly. Horizontal forces, including shear forces during acceleration and deceleration, are carefully considered in the structural design.

Critical points analysis focuses on joint integrity, with particular attention to bracket connections experiencing increased stress concentrations. Bolt preload requirements are adjusted for higher forces, and weld points are designed to withstand greater cyclic loading. The increased load affects structural deformation, necessitating careful consideration of vertical deflection patterns and their impact on component alignment.

To ensure safety under the 2943N load, comprehensive structural reinforcement measures are implemented, including additional support brackets at high-stress points, increased material thickness in critical areas, and enhanced joint design for optimal load distribution. This thorough analysis ensures the chassis maintains structural integrity and operational safety under specified load conditions.

### **4.20 CONCLUSION AND FUTURE WORKS**

This chapter has presented a comprehensive analysis of the AGV system design, focusing on the single-level scissor lift mechanism and chassis development. The design process incorporated extensive structural analysis, stress testing, and component integration strategies, with simulation results validating that both the scissor lift and chassis designs meet specified

operational requirements while maintaining necessary safety margins. Key achievements include the successful validation of the scissor lift mechanism for a 200 kg load capacity and the development of a robust chassis structure capable of supporting 300 kg (2943N).

The design methodology employed a systematic approach, utilizing advanced CAD tools and simulation software to ensure optimal performance and reliability. Through careful consideration of load distribution, stress analysis, and component integration, the final design demonstrates excellent structural integrity and operational stability. The implementation of comprehensive safety features and control systems further enhances the system's reliability and functionality in industrial applications.

Looking forward, several areas have been identified for future development, including design optimization through lightweight materials, enhanced payload configurations, and modular attachment systems. Performance improvements will focus on integrating advanced sensors for real-time monitoring, implementing predictive maintenance capabilities, and developing enhanced control algorithms for improved operational stability. Safety enhancements, including advanced emergency stop systems and smart collision avoidance capabilities, will ensure the AGV maintains high safety standards while adapting to complex industrial environments.

The successful development of this AGV system represents a significant step forward in automated material handling solutions. The implementation of proposed future developments will further enhance the system's capabilities, ensuring its continued evolution to meet emerging industrial requirements. Through these improvements, the AGV system will become more versatile, efficient, and safer, better serving the needs of modern industrial applications while maintaining its fundamental role in automated material transport and handling.

## **4.21 DESIGN AND DEVELOPMENT OF THE DRIVE WHEEL AND GEARBOX SYSTEM**

The following section is devoted to the design and development of the drive wheel and gearbox system, which is crucial for the mobility, stability, and functionality of the AGV. The drive wheel and gearbox system is crucial in ensuring smooth and precise motion control, load handling, and adaptability to various operational environments. This project utilizes SolidWorks, a state-of-the-art computer-aided design software, for modeling and simulation of the drive wheel and gearbox. The robust tools for parametric design, assembly, and motion analysis in the software allow us to create an efficient and optimized design. It further takes into consideration practical constraints in reality, such as material selection, cost, manufacturability, environmental impact, and safety and engineering standards. The objective of the project is to present a design that will not only be functional and reliable but also sustainable and economical. The successive sections outline the design process, engineering analysis, and critical decisions in view of the realization of the above-mentioned objectives in detail.

### **Key objectives included:**

- To design the system in SolidWorks.
- Check for structural integrity at operational loads.
- Analyze gearbox performance for the required torque and speed to achieve the desired gear ratio.
- Simplify design for manufacturability and assembly.

## **4.22 CRITICAL ELEMENTS OF AGV DESIGN: DRIVE WHEELS, GEAR MECHANISMS, AND MATERIAL SELECTION**

AGVs are driverless transport systems used in the manufacturing industry, warehouses, and logistics. According to Groover (2015) [10], in "Automation, Production Systems, and Computer-Integrated Manufacturing" an AGV would have a navigation system, a drive system, and sensors to operate autonomously. The driving system is the major component of an AGV, which provides the stability of the robot, the load-carrying capability, and the accuracy of motion.

In AGVs, middle drive wheels are important for balance and drive. Jazar's study [11], "Vehicle Dynamics: Theory and Applications", presented in the year 2019, gave much importance to wheel type, selection of motor, and gearbox that affects energy efficiency in a robot, how much load a robot can carry, adaptation on various kinds of terrain. A gearbox allows for the delivered torque and speed to the wheel for smooth, accurate movement.

Research on gearbox design for robotics has highlighted the requirement for compact, high-efficiency mechanisms. Kauffenberger et al. (2018) studied gear mechanisms in small mobile robots and found that among them, spur gears are the most used due to their simplicity, high load capacity, and ease of manufacturing. Their study also discussed the trade-off between gear ratios and torque output, noting that planetary gear systems provide higher torque.

The design of the drive wheel is critical for traction, maneuverability, and load-carrying capability. Bloss (2017), in "Mobile Robotics: Principles and Design," has discussed the role of drive wheels in robots, and he mentioned that material, tread pattern, and diameter of the wheel have a direct influence on performance. The wheels for AGVs are designed to meet both lightweight and high durability to allow for continuous operation with various loads.

The CAD tools utilized for the design of robot systems are quite popular, due to their advanced modeling and simulation capabilities. Das and Jana 2020, in the work "Application of CAD Tools in Robotic Design", have shown the capability of solid works to model complex assemblies such as gearboxes and also to simulate their motions.

Material selection is one of the most critical aspects in mechanical design. Ashby [12], 2011, "Materials Selection in Mechanical Design" described a criterion for material selection that was based on strength, weight, cost and environmental considerations. Since this project dealt with drive wheels it mostly utilized rubberized materials, hence a thick rubber material was chosen, while gears are made from hardened steel preferred for its wear resistance and strength, it was also considered in my material selection.

## 4.23 DESIGN CONSTRAINTS

### 4.23.1 Technical Constraints

The following limitations relate to the feasibility and functionality of the design, encompassing several key factors:

- Dimensional Accuracy: The dimensions need to be precise so that the fitted parts inside assemble well.
- Load Bearing Capacity: The wheels and gearbox should bear the expected loads without deforming or failing.
- Speed and Torque Requirements: The gear ratio and wheel design must be such that desired performance is achieved.
- Compatibility with Other Components: Ensure that the design fits well with the AGV chassis, sensors, and other systems.
- Assembly and Maintenance: The design must ensure ease assembly, disassembly, and maintenance.
- Simulation Accuracy: Limitations of CAD software may affect the accuracy of stress, motion, or thermal simulations.

### 4.23.2 Material Constraints

The choice of materials impacts weight, durability, and cost.

- *Strength and Durability*: Materials must be able to handle the mechanical stresses without failure.
- *Weight*: Lighter materials are always preferred for efficiency, but without sacrificing strength.
- *Availability*: Materials selected must be available to the required quantity.
- *Cost*: The high-performance material may be beyond the budget and therefore some compromise may be necessary.

Material selection for the drive wheels and gearbox is critical in balancing performance, cost, and durability. Gears and shafts were made from hardened steel due to its high strength and wear resistance, while aluminum alloys are preferred for wheel hubs and gearbox housings

because of their lightweight and corrosion resistance. Drive wheel coatings were made from rubber or polyurethane to ensure traction, along with vibration absorption. The other alternatives, like plastics, are too weak and do not have enough strength to hold heavy loads; mild steel easily corrodes and is worn out, while on the other side, titanium, though very strong and light, is outrageously expensive and over-engineered for AGV applications. Materials selected ensure manufacturability with optimality, cost-effectiveness, and operation efficiency, making them the best choice for this project.

## 4.24 ENGINEERING STANDARDS AND LIFELONG LEARNING

### 4.24.1 Engineering standards

Engineering standards provide a framework for designing, testing, and manufacturing mechanical components to ensure compatibility, performance, safety, and reliability. Several organizations, such as ISO, ANSI, ASTM, IEEE, and DIN, define standards applicable to AGV drive systems.

### 4.24.2 Importance of Engineering Standards in AGV Drive System Design

Standards are essential in development to ensure:

- *Interoperability*: Components such as wheels, bearings, and shafts must conform to international sizes and tolerances. According to ISO 9001, which ensures a structured design and manufacturing process for reliability.
- *Safety*: Gearboxes and drive systems must adhere to safety regulations to prevent failures that could endanger users or disrupt operations. According to ISO 14121 , which helps in evaluating and mitigating risks associated with moving components.
- *Manufacturing Feasibility*: Standardized materials and design practices facilitate efficient production and cost reduction. According to AGMA 2001-D04, which helps in designing gears that meet durability and performance requirements.
- *Quality Assurance*: Standards define testing protocols for evaluating the durability and performance of components. According to ISO 606, which ensures proper gear-chain compatibility in AGV transmission systems.

## 4.25 MANUFACTURING CONSTRAINTS

The design should consider the limitations of manufacturing methods.

Process Feasibility: The parts must be manufacturable using available processes such as CNC machining, casting or 3D printing.

- *Tool Accessibility:* Shapes that include internal grooves or undercuts may not easily be machined due to complexity.
- *Surface Finish:* Very complicated surfaces may be expensive or time-consuming to produce.
- *Assembly Difficulty:* Designs that include many parts or tight clearances may be more difficult to assemble because of mating with specific part which may not be possible if there are too tight.
- *Standard Components:* Using off-the-shelf components such as bearings and shafts rather than customized components simplifies production and reduces cost.

## 4.26 ECONOMIC CONSTRAINTS

In designing, fabricating, and deploying the driving wheels and gearboxes of an AGV, the main economic issues have to do with material type, manufacturing process, labor costs, maintenance, and scalability of the product.

- *Material Costs:* The use of high-performance materials, such as hardened steel and aluminum alloys, will enhance durability, but at increasingly higher costs. Using recycled or alternative materials may balance cost with performance.
- *Manufacturing Costs:* CNC machining, injection molding, and forging are cost-intensive to set up and hence affect the feasibility. Batch production and automation reduce the per-unit cost.
- *Labor and Skill Costs:* Skilled labor for design in SolidWorks, machining, and assembly increases the overall cost of the project. Automation and standardized components reduce labor dependence.
- *Maintenance and Lifecycle Costs:* Long-term costs are inclusive of the wear and tear of gears, battery efficiency, and availability for spares. Low-maintenance material selection and efficient motor designs reduce operational expenses.

- *Scalability and Mass Production:* Large-scale production reduces the unit cost due to bulk material discounts and streamlines the manufacturing process, though there is a requirement for high initial capital investment.

Lifecycle management can make the development of AGV drive systems cost-effective and green without compromising performance by applying optimization in design and manufacturing processes.

## 4.27 ENVIRONMENTAL CONSTRAINTS

Throughout their life, AGV drive wheels and gearboxes have some environmental impacts associated with each stage—from material extraction to end-of-life disposal. The most serious concerns are resource depletion, energy consumption, carbon footprint, and generation of wastes.

- *Material Impact:* The extraction and processing of steel, aluminum, and plastics lead to land degradation, energy usage, and air pollution. Recycled materials can be used in order to reduce the above-mentioned effects.
- *Manufacturing Waste:* Manufacturing processes involving CNC machining, injection molding, and heat treatment result in wastes like metal scraps, plastic wastes, and chemical by-products. The adoption of lean manufacturing and energy-efficient machinery reduces environmental degradation.
- *Energy Consumption & Carbon Emissions:* AGVs use electric motors and batteries, and their production indirectly contributes to CO<sub>2</sub> emissions if these are manufactured from fossil fuels. Efficient gearbox designs, regenerative braking, and renewable-powered charging stations could further improve sustainability.
- *Waste and Disposal Challenges:* Later in the life cycle, the components and batteries of AGVs pose waste challenges. Recycling programs, biodegradable lubricants, and modular component designs should be developed for environmental sustainability.

By the use of sustainable materials, manufacturing with a minimum of energy, and waste, the technology of AGV will go greener without losing efficiency and durability.

## **4.28 HEALTH AND SAFETY PROBLEMS**

From both design and operational standpoints, the AGVs, their driving wheels, and gearboxes create many health and safety problems that have to be overcome to make them safe for workers and ensure reliability and operational efficiency. These aspects are very crucial in both the manufacturing process and final deployment within industrial environments. Thus, working out such problems would avoid accidents, injuries, and equipment failures.

1. *Manufacturing Hazards:* Workers are exposed to mechanical hazards, chemical exposure, and noise pollution. Safety measures include personal protective equipment, proper ventilation, and noise-reducing technologies.
2. *Operational Safety Risks:* Gears can cause collisions, pinching, and crushing hazards, especially if visibility is poor. Safety measures involve collision avoidance systems, warning alarms, and clear design protocols.
3. *Ergonomic Concerns:* Most of the assembly and maintenance tasks involve the risk of repetitive strain injuries and manual handling. This can be resolved by introducing automated handling systems, ergonomic tools, and workstations that are adjustable.
4. *Hazards in Maintenance and Repair:* Maintenance involves workers in electrical risks, mechanical injuries, and harmful chemicals. These may be minimized by instituting lock-out/tag-out procedures, wearing PPE, and training in safe maintenance.
5. *Long-term Health Issues:* Prolonged exposure to vibration, noise, and psychosocial stress can cause health problems such as hearing loss and vibration-induced problems. These risks can be minimized by regular health checks and stress management programs.

By addressing these health and safety concerns, AGV manufacturers and operators can ensure a safer working environment, improve equipment reliability, and enhance overall worker well-being.

## **4.29 MANUFACTURABILITY**

Manufacturability refers to the development and production of the AGV drive wheels and gearboxes in an effective manner that is affordable and of great quality. Key considerations will include:

1. *Material Selection:* Lighter materials, such as aluminum, steel, and reinforced polymers, balance strength, wear resistance, and cost.

2. *Design for Manufacturability*: Simplification of geometries, standardization of parts, modular design, and proper tolerancing enhance ease of fabrication and assembly.
3. *Production Methods*: CNC machining, casting, forging, injection molding, and heat treatments are crucial for producing high-precision components efficiently.
4. *Assembly Efficiency*: Reducing fastener types, using pre-assembled subcomponents, and integrating automated assembly speeds up production while maintaining consistency.
5. *Cost and Scalability*: Choosing cost-effective production techniques, securing reliable supply chains, and optimizing mass production vs. small-batch production ensures economic feasibility.
6. *Sustainability*: Using recyclable materials, energy-efficient manufacturing, waste reduction, and eco-friendly coatings supports environmentally responsible production.

Therefore, focusing on these manufacturability aspects, manufacturers of AGVs can provide quality, durable, scalable drive wheels and gearboxes by optimizing cost, efficiency, and sustainability.

## 4.30 METHODOLOGY

The methodology followed for the project in brief is given below:

1. Determination of dimensions, number of all gear teeth , and gear ratio.
2. 3D Modeling: Detailed CAD modeling of wheels, gears, shafts, and housing on Solid-Works.
3. Simulation: motion analysis to validate the design.
4. Optimization: Refined design for performance and manufacturability.

### 4.30.1 Dimensions

Ring gear which is the bigger gear has a diameter of 190 teeth

The planet gear has a diameter of 90mm

The sun gear has a diameter of 10mm

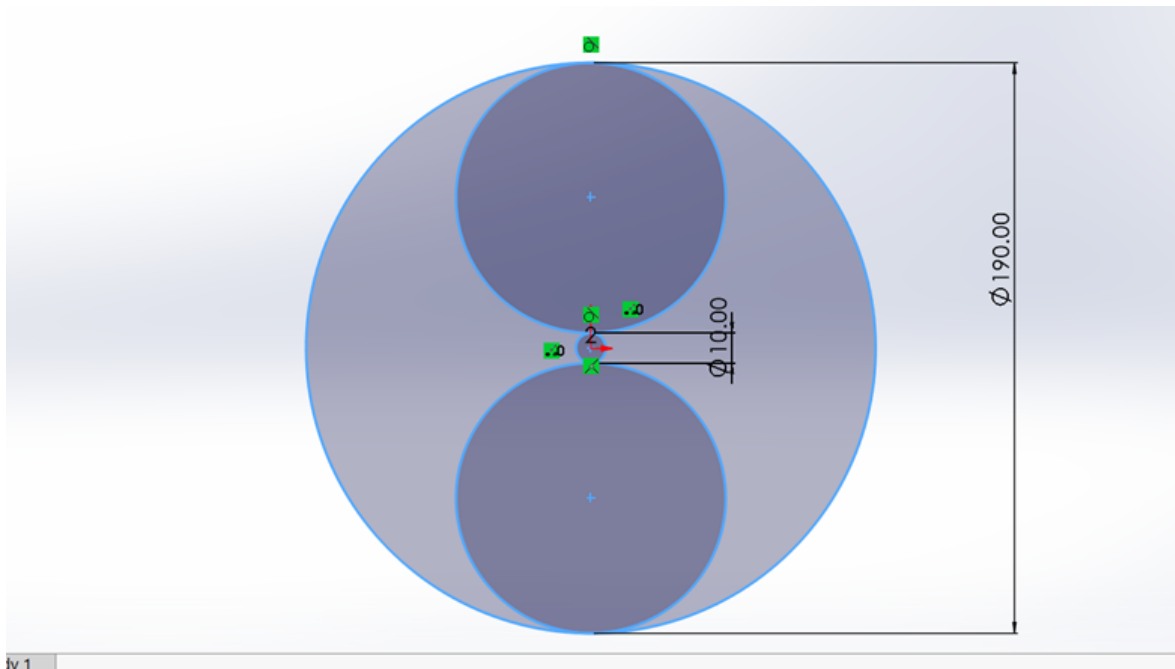


Figure 4.41: Add caption here

## 4.31 3D MODELING

Following components were modelled using SolidWorks:

### 4.31.1 Middle Drive Wheels:

For Traction and load-carrying capacity. Which is made of natural rubber has the ability to withstand high load and relatively not so heavy. The wheels for AGVs are designed to meet both lightweight and high durability to allow for continuous operation with various loads.

### 4.31.2 Gearbox:

Compact design with spur gears for efficient transmission. Studies shows spur gears are the most used due to their simplicity, high load capacity, and ease of manufacturing. Their study also discussed the trade-off between gear ratios and torque output, noting that planetary gear systems provide higher torque.

### 4.31.3 Shafts and Bearings:

For smooth rotation and distribution of loads. I made use of both skf bearing 108tn92 and skf bearing 1210ektn9202 while for the wheel holder it was made with hard steel for firmness and durability.

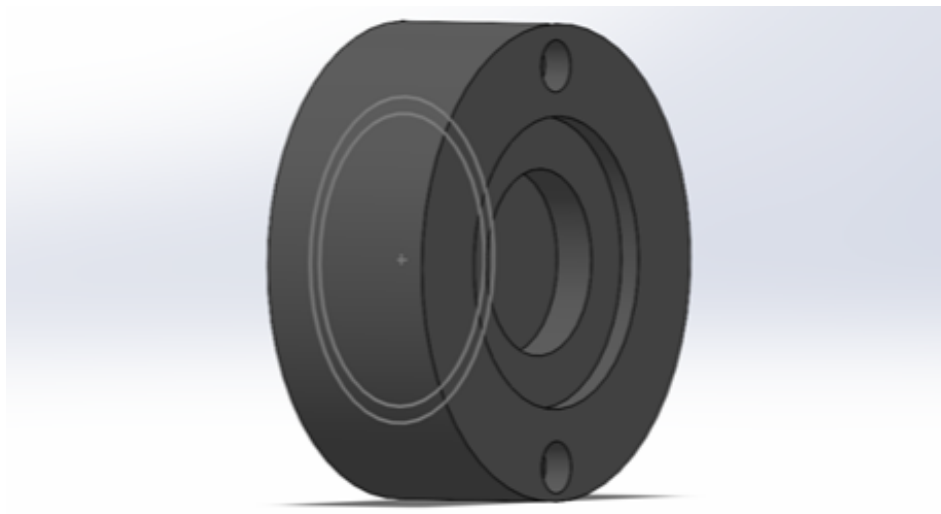


Figure 4.42: Caption 1

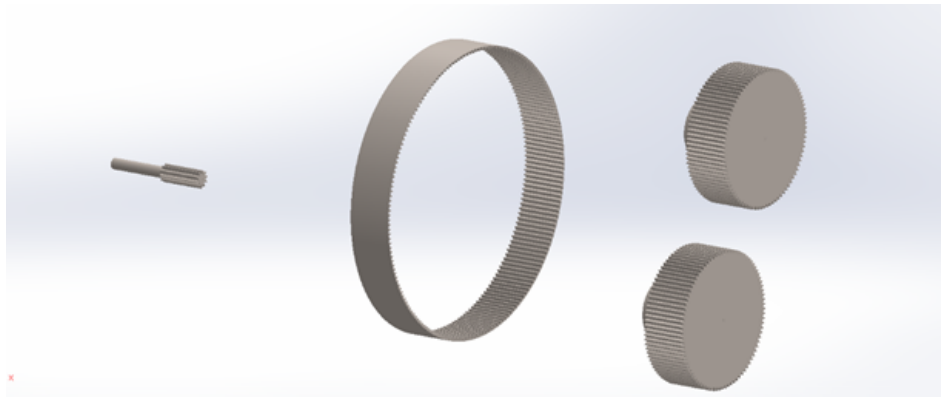


Figure 4.43: Caption 1

#### 4.31.4 Housing:

Enclosed system for protection against dust and debris. Which lightweight aluminum were used to reduce the weight of the gear box.

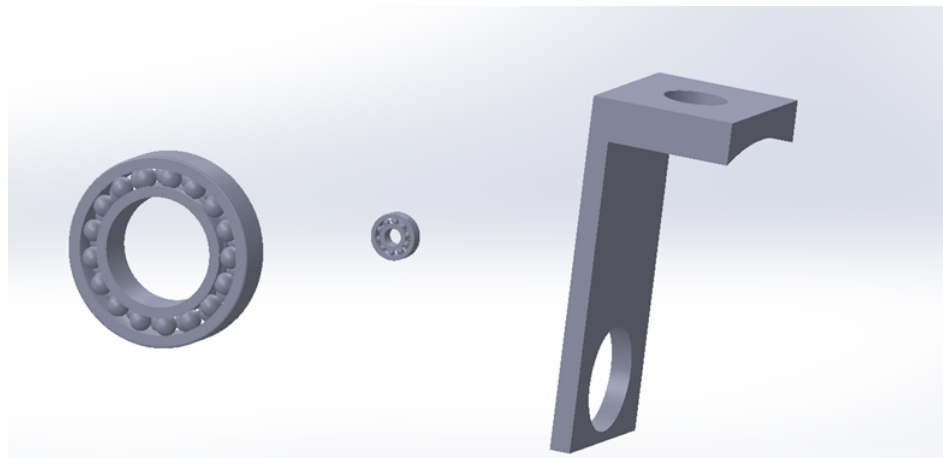


Figure 4.44: Caption 1

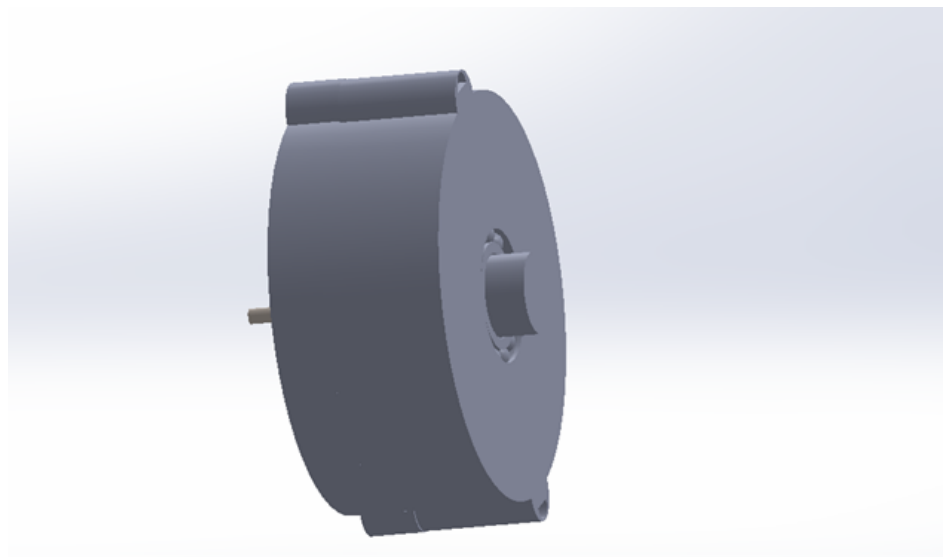


Figure 4.45: Caption 1

#### 4.31.5 Assembly

The parts were then assembled in SolidWorks for a check on appropriateness and compatibility.

### 4.32 CALCULATION AND ANALYSIS

Simulations done in SolidWorks to test performances of the design:

#### 4.32.1 GEARBOX CALCULATION

- ring gear → 190 Teeth [120 mm  $\phi$ ] [Tr]
- PLAMET Gear → 90 Teeth [Tp]

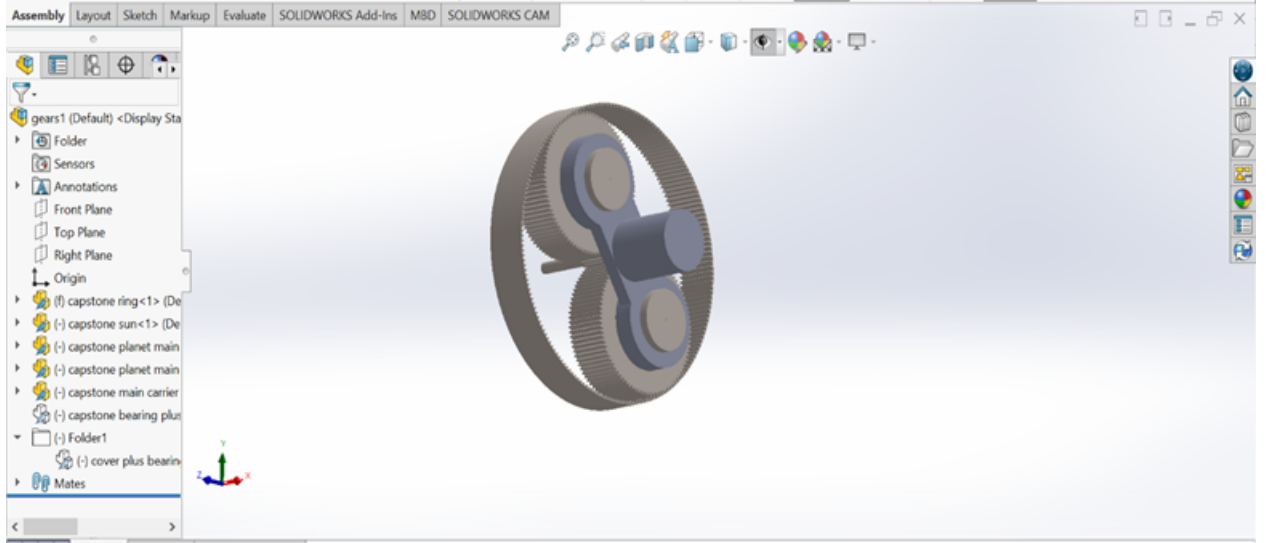


Figure 4.46: Add caption here

- Sun gear → 10 Teeth [Ts]

GEAR RATIO : NOTE I want a high ratio of 20 : 1

$$20 = 1 + \frac{T_r}{T_s}$$

$$\frac{T_r}{T_s} = 19$$

$$T_r = 19T_s$$

The planet does not affect the ratio but determines the spacing of the sun and ring gears.

Rearranging:

$$\frac{T_r}{T_s} = 19$$

$$IF T_s = 10$$

$$T_r = 19 \times 10 = 190$$

from  $T_r - T_s = 2T_p \rightarrow$  Spacing in the ring

$$190 - 10 = 2T_p$$

$$T_p = 90$$

$$\rightarrow 1 + \frac{T_r}{T_s} \Rightarrow 1 + \frac{190}{10} = 20$$

$$\rightarrow 20 : 1$$

→ 1500 input speed ÷ 20 (gear ratio) ⇒ 75 rmp output speed

Considering

Nema 23 stepper motor

Nominal power → 240 Watts

Nominal voltage → 484

Nominal current → 5 A

Maminal rotation → 1500 rpm

$$T_{\text{in}} = \frac{P \times 60}{2\pi \times N} = \frac{240 \times 60}{2\pi \times 1500} \Rightarrow T_{\text{in}} = 1.53 \text{ Nm}$$

- This calalation is assumed 100% efficiency, Real - Idorly will be slightly lower due to losses [heat, friction]

$$\begin{aligned} T_{\text{out}} &= T_{\text{in}} \times R_{\text{atio}} \times \eta \\ &= 1.53 \times 20 \times 0.94 \\ &= 28.2 \text{ Nm} \end{aligned}$$

$$\begin{aligned} \eta [\text{ efficiency}] &= \frac{\text{Out put power}}{\text{Input poise}} \times 100\% = \frac{75 \times 28.2}{1500 \times 1.53} \\ &= \frac{2,115}{2,280} = 0.927 = 92\% \end{aligned}$$

## 4.33 MOTION ANALYSIS:

Wheels' rotation and torque transfer in the gearbox simulated.  
Result: Smooth motion with efficiency in power transmission.

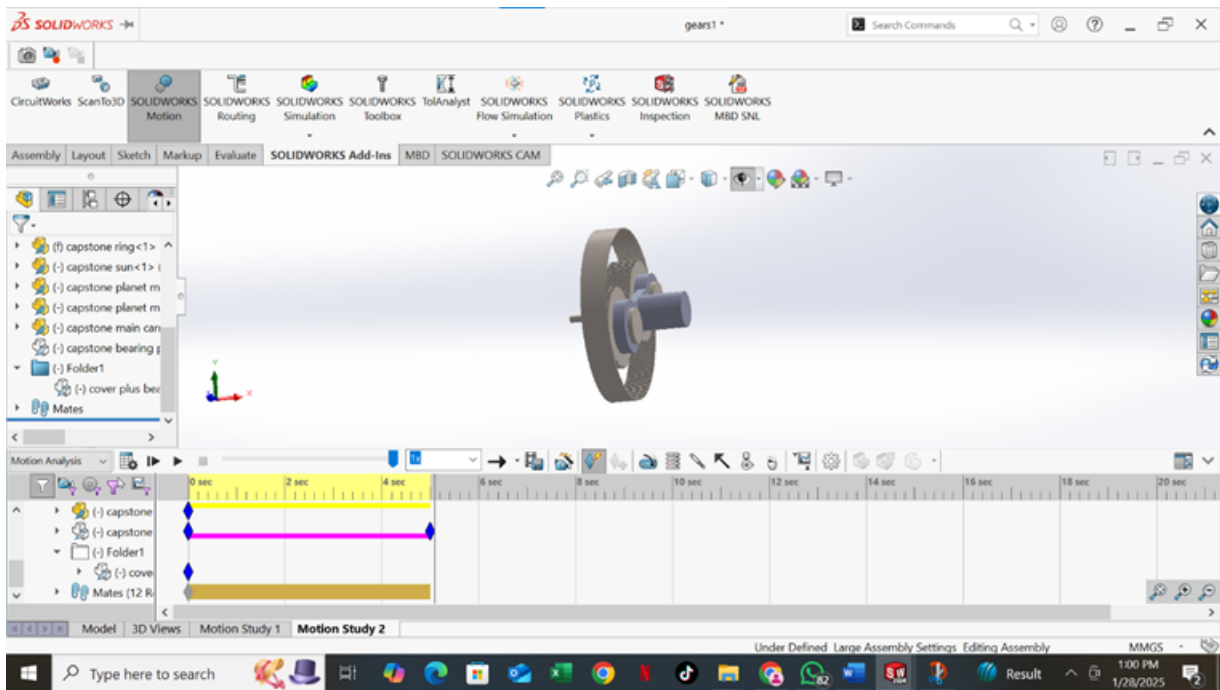


Figure 4.47: Add caption here

### Material Selection

Wheels: Natural rubber, corrosion resistant and high load capacity.

Gears: Hardened Steel for increased strength and wear resistance

Shafts: Steel for durability

Housing: aluminum protection

### Results and Discussion

The final design was able to meet all the specified requirements, which included load capacity, torque output, and manufacturability. The simulations proved that the system was structurally sound and could operate without hitches under realistic conditions .

#### **4.34 CONCLUSION**

It should not only be functional, but also practical, manufacturable, and economic, taking into consideration all the constraints. The literature survey focuses on the fact that the gearbox-equipped drive wheel system is a main concern in the design of an AGV. Material selection, load-carrying capacity, torque optimization, and manufacturability are the key factors to be considered. In this paper, design and simulation for performance improvement of the AGV using SolidWorks are proposed to overcome these bottlenecks and help in the development of reliable high-performance drive systems for AGVs.

The middle drive wheels with an integrated gearbox were designed and further validated for use in an AGV. The system was reliable, efficient, and easy to manufacture. Future work can be the physical development of the prototype and performance testing at site applications..

## **4.35 GREGORY'S CHAPTER**

### **4.36 INTRODUCTION**

Bearing wheels and caster wheels are integral components in various industrial and commercial applications, facilitating mobility, load distribution, and operational efficiency. These wheels are commonly found in material handling equipment, automotive systems, and heavy machinery, where they ensure seamless movement and reduced friction. The efficiency and durability of these components directly impact productivity, safety, and cost-effectiveness in different industries.

Designing an effective bearing or caster wheel system involves several critical factors, including material selection, load-bearing capacity, resistance to environmental conditions, and compliance with industry standards such as ISO 3691-4:2020. Material properties play a vital role in determining the strength, wear resistance, and overall performance of the wheels. Common materials used in bearing wheels include AISI 1045 steel for shafts and AISI 52100 chrome steel for bearings, both of which offer high durability and load-handling capabilities.

The study of bearing and caster wheels also involves analyzing mechanical constraints, including torque requirements, frictional forces, and stress distribution. Ensuring optimal performance requires comprehensive calculations, including shaft diameter determination, bearing life assessment, and stress-strain analysis. Additionally, environmental considerations such as exposure to moisture, temperature variations, and corrosive elements influence the selection of materials and protective coatings.

Manufacturing constraints must also be addressed to maintain cost-effectiveness and efficiency in production. Precision machining, heat treatment processes, and surface finishing techniques are necessary to achieve the desired durability and performance characteristics. Furthermore, safety factors such as load limitations, stability, and braking mechanisms must be considered to prevent operational hazards and equipment failure.

This project aims to develop a systematic approach to designing and evaluating bearing and caster wheels while addressing real-world challenges. By integrating theoretical calculations with finite element analysis (FEA), this study seeks to enhance the reliability, efficiency, and sustainability of these components. The findings will contribute to improving material selection, optimizing load distribution, and ensuring compliance with industry regulations, ultimately leading to more robust and long-lasting wheel systems.

## **4.37 LITERATURE REVIEW**

Research on bearing wheels and caster wheels has extensively explored their mechanical properties, material composition, and industrial applications. Several studies have emphasized the significance of material selection in determining the durability and efficiency of these components. According to Smith et al. (2020), AISI 1045 steel is widely used for shaft manufacturing due to its high tensile strength and resistance to mechanical fatigue. Similarly, AISI 52100 chrome steel is preferred for bearings due to its excellent hardness, wear resistance, and ability to withstand high loads.

Lubrication and friction management play crucial roles in ensuring the longevity of bearing systems. Studies by Brown and Pietra (2018) highlight that improper lubrication can lead to increased friction, wear, and premature failure of bearings. Advanced lubrication techniques, such as sealed bearings and self-lubricating materials, have been explored to enhance performance and minimize maintenance requirements.

The impact of environmental factors on bearing and caster wheel performance has also been a key area of research. According to Can and Ozkarahan (2019), exposure to high humidity and extreme temperatures can accelerate corrosion and degrade material integrity. Protective coatings, such as zinc plating and polymer encapsulation, have been recommended to improve resistance against environmental hazards.

Manufacturing techniques and precision engineering have further influenced the development of high-performance bearing and caster wheels. Recent advancements in computer-aided design (CAD) and finite element analysis (FEA) have enabled engineers to optimize designs for maximum efficiency. Studies by Johnson et al. (2021) indicate that simulation-based testing allows for accurate prediction of load distribution, stress concentrations, and potential failure points, leading to more reliable designs.

Safety considerations in wheel design have also been extensively analyzed. Research by Lee and Kim (2022) emphasizes the importance of braking mechanisms and stability enhancements in caster wheel applications, particularly in medical and industrial equipment. Proper weight distribution and impact resistance are essential factors in preventing accidents and improving operational safety.

In conclusion, the literature underscores the importance of material selection, lubrication, environmental protection, and advanced manufacturing techniques in optimizing bearing and caster wheel performance. The integration of modern engineering tools and industry standards ensures that these components meet the growing demands of industrial applications while maintaining safety, durability, and efficiency. This study builds upon existing research to develop a comprehensive approach to designing and evaluating bearing and caster wheel systems.

## **4.38 REALISTIC CONSTRAINTS**

### **4.38.1 Material Constraints**

Bearing wheels and caster wheels require high-strength materials for load-bearing capacity and durability. AISI 1045 steel is chosen for the shaft due to its excellent mechanical properties, including high yield strength (530 MPa) and good machinability. AISI 52100 chrome steel is used for bearings due to its superior hardness and wear resistance. However, these materials are susceptible to corrosion in humid environments, necessitating protective coatings or stainless alternatives. The choice of rubber or polyurethane for the wheel itself impacts rolling resistance, wear rate, and temperature resistance.

### **4.38.2 Manufacturing Constraints**

Manufacturing challenges include precision machining of shafts and bearings to ensure proper tolerances. Heat treatment processes are required for AISI 52100 bearings to achieve the necessary hardness. Forging and casting limitations impact cost and production scalability. Bearings must meet ISO 3691-4:2020 standards, which impose strict requirements on tolerances and material integrity. The availability of raw materials and manufacturing costs also influence design decisions.

### **4.38.3 Mechanical Constraints**

Bearing wheels and caster wheels must withstand dynamic loads and impacts without failure. Bearings must be designed to handle radial and axial loads efficiently. Torque calculations ensure that the system operates within safe stress limits. Misalignment and excessive vibration can reduce bearing life, requiring proper lubrication and mounting techniques. The wheel's rolling friction, influenced by surface conditions and load distribution, impacts efficiency.

### **4.38.4 Environmental Constraints**

Environmental factors such as temperature variations, moisture, and chemical exposure affect material performance. Bearings exposed to extreme temperatures may experience reduced lubrication effectiveness, leading to higher friction and wear. Caster wheels used in outdoor environments must resist UV degradation and corrosion. Sustainable material choices and waste reduction strategies are essential to meet environmental regulations.

#### **4.38.5 Safety Constraints**

Safety considerations include ensuring that the wheels can withstand maximum load without failure. Overloading can lead to bearing fatigue and catastrophic failure. Proper braking mechanisms must be integrated into caster wheel systems to prevent uncontrolled movement. Bearings must comply with safety standards such as ISO 3691-4:2020 to prevent accidents due to bearing failure. Ergonomic considerations also play a role in reducing strain on operators handling heavy loads.

### **4.39 CHAPTER FOUR: METHODS USED TO DESIGN THE PROJECT**

#### **4.39.1 Objectives**

1. Shaft Diameter Calculation: Ascertain the ideal shaft diameter by considering material qualities and bending moments, making sure the shaft can support operational loads.
2. Bearing selection and torque calculation: Choose a bearing size and type that satisfies the operational lifespan and dynamic load requirements, then calculate the necessary torque.
3. Safety and Efficiency Optimization: To balance performance and cost-efficiency, take safety considerations into account and choose materials as efficiently as possible.
4. Conformity: Verify that the design conforms with applicable industry standards, especially ISO 3691-4:2020, which regulates dependability and safety in load-bearing systems.

#### **4.39.2 Methodology**

#### **4.39.3 Bearing selection**

##### **4.39.3.1 Inputs and Assumptions**

1. Wheel radius (R): 110 mm
2. Load on the wheel (F): 981 N
3. Maximum speed (v): 1.25 m/s
4. Shaft material: Steel (e.g., AISI 1045)
  - Yield strength:  $\sigma_y=250$  MPa
5. Bearing material: Chrome steel (e.g., AISI 52100)
6. Bearings catalog: We'll pick based on calculated load and RPM.
7. Factor of safety (FOS): 2.0 for shaft design.

#### 4.39.3.2 Shaft Diameter Calculation

**Angular Velocity** Convert the speed into angular velocity ( $\omega$ ) to determine the RPM.

$$\omega = \frac{v}{R} \quad (4.18)$$

Substitute values in eq. (4.18):

$$\omega = \frac{1.25}{0.110} = 11.36 \text{ rad/s}$$

Convert  $\omega$  to RPM:

$$RPM = \omega \times 602\pi = 11.36 \times 602\pi \approx 21484.99 \text{ RPM}$$

**Bending Moment and Shaft Diameter** For a wheel shaft, the critical load is the bending moment due to the force F. Assuming a simple beam supported at the bearing points:

$$M = F \times L \quad (4.19)$$

Where L is the distance from the bearing to the load. Assume L=50 mm=0.05 m( minimum according to the ISO 3691-4:2020 standard):

$$M = 981 \times 0.05 = 49.05 \text{ Nm}$$

Using the **maximum shear stress theory** for a solid circular shaft, the shaft diameter is calculated from:

$$d = (16M/\pi\tau_{max})^{1/3} \quad (4.20)$$

Where:

- $\tau_{max}$ : Allowable shear stress =  $\sigma_y/2 \times FOS = 250/2 \times 2 = 62.5 \text{ MPa} = 62.5 \times 10^6 \text{ Pa}$

Substitute values in eq. (4.20):

$$d = (16 \times 49.05 / \pi \times 62.5 \times 10^6)^{1/3} = 0.012 \text{ mm}$$

#### 4.39.3.3 Bearing Selection

**Load on the Bearing** The radial load on the bearing is equal to the load on the wheel:

$$Fr = 981 \text{ N}$$

**Dynamic Load Rating** Using the bearing life equation:

$$C = Fr \times (L/1,000,000)^{\frac{1}{3}}$$

Where:

- L: Bearing life in revolutions. Assume L=10<sup>6</sup> revolutions.

$$C = 981 \times (10^6 / 1,000,000)^{1/3} = 981 N$$

From a standard bearing catalog, a **deep groove ball bearing** with a dynamic load rating C>981 N and an inner diameter matching the shaft size (d=12 mm) is selected:

- **Bearing Type:** Deep groove ball bearing (e.g., 6201 series).
- **Verification :**

#### 4.39.3.4 Material Properties of AISI 1045 Steel

**Yield Strength ( $\sigma_y$ ):** Approximately 530 MPa

**Ultimate Tensile Strength ( $\sigma_u$ ):** Approximately 625 MPa

#### 4.39.3.5 Calculation

##### 1. **Cross-Sectional Area (A):**

$$A = \pi \left( \frac{d}{2} \right)^2 = \pi \left( \frac{12 \text{ mm}}{2} \right)^2 \approx 113.1 \text{ mm}^2$$

##### 2. **Stress ( $\sigma$ ):**

A shaft of 12mm diameter made of AISI 1045 steel can safely bear a load of 981N, as the induced stress is well within the material's yield and ultimate tensile strengths.

$$\sigma = \frac{F}{A} = \frac{981 \text{ N}}{113.1 \text{ mm}^2} \approx 8.67 \text{ MPa}$$

**3.3 Number of Balls in the Bearing** To determine the diameter of the balls in the bearing when we are supposed to have 9 balls( i tried all the number less than 9 , they were not compatible with the standard), we can use the following formula:

$$z = \frac{\pi(D+d)}{2d_b} \quad (4.21)$$

where:

- $z$  is the number of balls.
- $D$  is the outer diameter of the bearing.
- $d$  is the inner diameter of the bearing.
- $db$  is the diameter of each ball.

Given:

- $z=9$
- $D = 32 \text{ mm}$
- $d = 12 \text{ mm}$

We need to solve for  $db$ :

$$9=\pi(32+12)/2db$$

$$9=\pi\times44/2db$$

$$db=22\pi/9$$

$$db\approx7.68 \text{ mm}$$

For a 6201 bearing:

- Number of balls: Typically 7–9 balls.
- Ball diameter: beyond 4.5 mm.

#### 4.39.3.6 Material Selection

##### **Shaft Material: AISI 1045 Steel**

- Reason: High strength, good machinability, and readily available.

##### **Bearing Material: AISI 52100 Chrome Steel**

- Reason: High hardness, wear resistance, and durability under dynamic loads.

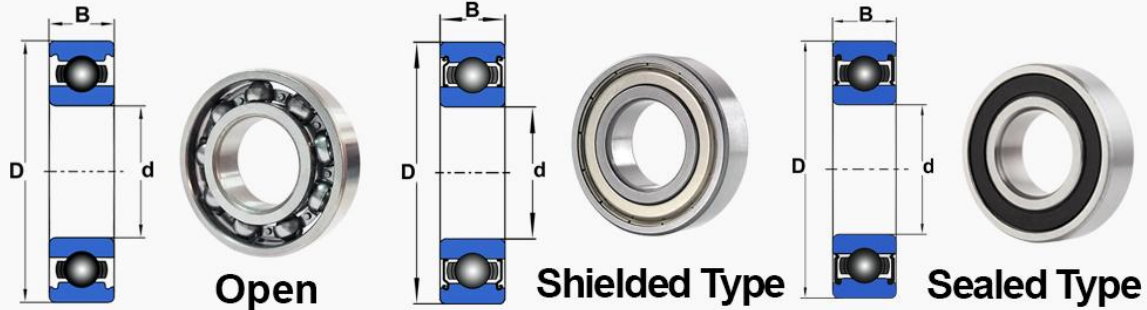
#### 4.39.3.7 Compatibility Check

A deep groove ball bearing that meets these specifications is the **NSK 6201** bearing. Here are the details:

- **Inner Diameter (ID):** 12 mm
- **Outer Diameter (OD):** 32 mm

- **Width (W):** 10 mm
- **Material:** AISI 52100 Chrome Steel
- **Load Capacity:** Suitable for the given load and speed requirements

# NSK Deep Groove Ball Bearing



d	D	B	$r_{min}$	Boundary Dimensions (mm)				Basic Load Ratings (N) {kgf}				Factor	Limiting Speeds (rpm)				Bearing Numbers			
				$C_r$		$C_{0r}$		$C_r$		$C_{0r}$			Grease		Oil		Open	Shielded	Sealed	
				$C_r$	$C_{0r}$	$C_r$	$C_{0r}$	$f_0$	$C_r$	$C_{0r}$	$f_0$		Open Z · ZZ V · VV	DU DDU	Open Z					
<b>10</b>	19	5	0.3	1 720	840	175	86	14.8	34 000	24 000	40 000		<b>6800</b>	<b>ZZ</b>	<b>VV</b>	<b>DD</b>				
	22	6	0.3	2 700	1 270	275	129	14.0	32 000	22 000	38 000		<b>6900</b>	<b>ZZ</b>	<b>VV</b>	<b>DD</b>				
	26	8	0.3	4 550	1 970	465	201	12.4	30 000	22 000	36 000		<b>6000</b>	<b>ZZ</b>	<b>VV</b>	<b>DDU</b>				
	30	9	0.6	5 100	2 390	520	244	13.2	24 000	18 000	30 000		<b>6200</b>	<b>ZZ</b>	<b>VV</b>	<b>DDU</b>				
	35	11	0.6	8 100	3 450	825	350	11.2	22 000	17 000	26 000		<b>6300</b>	<b>ZZ</b>	<b>VV</b>	<b>DDU</b>				
<b>12</b>	21	5	0.3	1 920	1 040	195	106	15.3	32 000	20 000	38 000		<b>6801</b>	<b>ZZ</b>	<b>VV</b>	<b>DD</b>				
	24	6	0.3	2 890	1 460	295	149	14.5	30 000	20 000	36 000		<b>6901</b>	<b>ZZ</b>	<b>VV</b>	<b>DD</b>				
	28	7	0.3	5 100	2 370	520	241	13.0	28 000	—	32 000		<b>16001</b>	—	—	—				
	28	8	0.3	5 100	2 370	520	241	13.0	28 000	18 000	32 000		<b>6001</b>	<b>ZZ</b>	<b>VV</b>	<b>DDU</b>				
	32	10	0.6	6 800	3 050	695	310	12.3	22 000	17 000	28 000		<b>6201</b>	<b>ZZ</b>	<b>VV</b>	<b>DDU</b>				
<b>15</b>	37	12	1	9 700	4 200	990	425	11.1	20 000	16 000	24 000		<b>6301</b>	<b>ZZ</b>	<b>VV</b>	<b>DDU</b>				
	24	5	0.3	2 070	1 260	212	128	15.8	28 000	17 000	34 000		<b>6802</b>	<b>ZZ</b>	<b>VV</b>	<b>DD</b>				
	28	7	0.3	4 350	2 260	440	230	14.3	26 000	17 000	30 000		<b>6902</b>	<b>ZZ</b>	<b>VV</b>	<b>DD</b>				
	32	8	0.3	5 600	2 830	570	289	13.9	24 000	—	28 000		<b>16002</b>	—	—	—				
	32	9	0.3	5 600	2 830	570	289	13.9	24 000	15 000	28 000		<b>6002</b>	<b>ZZ</b>	<b>VV</b>	<b>DDU</b>				
<b>17</b>	35	11	0.6	7 650	3 750	780	380	13.2	20 000	14 000	24 000		<b>6202</b>	<b>ZZ</b>	<b>VV</b>	<b>DDU</b>				
	42	13	1	11 400	5 450	1 170	555	12.3	17 000	13 000	20 000		<b>6302</b>	<b>ZZ</b>	<b>VV</b>	<b>DDU</b>				
	26	5	0.3	2 630	1 570	268	160	15.7	26 000	15 000	30 000		<b>6803</b>	<b>ZZ</b>	<b>VV</b>	<b>DD</b>				
	30	7	0.3	4 600	2 550	470	260	14.7	24 000	15 000	28 000		<b>6903</b>	<b>ZZ</b>	<b>VV</b>	<b>DDU</b>				
	35	8	0.3	6 000	3 250	610	330	14.4	22 000	—	26 000		<b>16003</b>	—	—	—				
<b>20</b>	35	10	0.3	6 000	3 250	610	330	14.4	22 000	13 000	26 000		<b>6003</b>	<b>ZZ</b>	<b>VV</b>	<b>DDU</b>				
	40	12	0.6	9 550	4 800	975	490	13.2	17 000	12 000	20 000		<b>6203</b>	<b>ZZ</b>	<b>VV</b>	<b>DDU</b>				
	47	14	1	13 600	6 650	1 390	675	12.4	15 000	11 000	18 000		<b>6303</b>	<b>ZZ</b>	<b>VV</b>	<b>DDU</b>				
	32	7	0.3	4 000	2 470	410	252	15.5	22 000	13 000	26 000		<b>6804</b>	<b>ZZ</b>	<b>VV</b>	<b>DD</b>				
	37	9	0.3	6 400	3 700	650	375	14.7	19 000	12 000	22 000		<b>6904</b>	<b>ZZ</b>	<b>VV</b>	<b>DDU</b>				
<b>22</b>	42	8	0.3	7 900	4 450	810	455	14.5	18 000	—	20 000		<b>16004</b>	—	—	—				
	42	12	0.6	9 400	5 000	955	510	13.8	18 000	11 000	20 000		<b>6004</b>	<b>ZZ</b>	<b>VV</b>	<b>DDU</b>				
	47	14	1	12 800	6 600	1 300	670	13.1	15 000	11 000	18 000		<b>6204</b>	<b>ZZ</b>	<b>VV</b>	<b>DDU</b>				
	52	15	1.1	15 900	7 900	1 620	805	12.4	14 000	10 000	17 000		<b>6304</b>	<b>ZZ</b>	<b>VV</b>	<b>DDU</b>				
	44	12	0.6	9 400	5 050	960	515	14.0	17 000	11 000	20 000		<b>60/22</b>	<b>ZZ</b>	<b>VV</b>	<b>DDU</b>				
	50	14	1	12 900	6 800	1 320	695	13.5	14 000	9 500	16 000		<b>62/22</b>	<b>ZZ</b>	<b>VV</b>	<b>DDU</b>				
	56	16	1.1	18 400	9 250	1 870	940	12.4	13 000	9 500	16 000		<b>63/22</b>	<b>ZZ</b>	<b>VV</b>	<b>DDU</b>				

Figure 4.48: caption here not added by Gregory

#### 4.39.4 Torque calculation

##### 4.39.4.1 Given Data:

- Gross Vehicle Weight: 300 kg
- Weight per Drive Wheel: 100 kg
- Maximum Incline Angle:  $8^\circ$
- Maximum Velocity: 1.5 m/s
- Surface: Concrete
- Type of Bearing: Deep Groove Ball Bearing (NSK 6201)
- Wheel Type: Rubber Tires
- Drive Wheel Diameter: 95 mm (0.095 m)

##### 4.39.4.2 Load Analysis:

###### 1. Load Calculation:

$$F = W = 100 \text{ kg} \times 9.81 \text{ m/s}^2 = 981 \text{ N}$$

###### 2. Wheel Rotational Speed:

$$r = 0.22 \text{ m}/2 = 0.11 \text{ m}$$

$$\text{Circumference} = \pi \times d = \pi \times 0.22 \text{ m} = 0.6909 \text{ m}$$

Wheel Rotational Speed=Linear Speed

$$\text{Circumference} = 1.25 \text{ m/s} / 0.6909 \text{ m} \approx 1.81 \text{ r/s} \approx 108.6 \text{ RPM}$$

###### 3. Required Torque:

$$T = F \times r = 981 \text{ N} \times 0.11 \text{ m} = 107.91 \text{ Nm}$$

Considering efficiency and safety:

$$\text{Efficiency}(85\%), T_{motor} = T_t / \text{Eff.} = 107.91 \text{ Nm} / 0.85 = 126.95 \text{ Nm}$$

(without bearing)

###### 4. Torque Required for Acceleration: Assuming $\alpha=1 \text{ m/s}^2$ :

Require Tractive effort (Ft)

$$F_t = m t \times \alpha = 300 \text{ kg} \times 1 \text{ m/s}^2 = 300 \text{ N}$$

Force must be provided by frictional force at the wheel

$$T = Ft \times r = 300N \times 0.11m = 33Nm$$

### 5. Effect of Inclination:

$$\theta = 3^\circ = 0.0524 rad$$

$$Gravity Component = 300 \times 9.81 \times \sin(0.0524) \approx 154.11N$$

$$T_{incline} = F_{gravity} \times r = 154.11N \times 0.11m = 16.9521Nm$$

### 6. Torque Due to Friction: Assuming $\mu=0.002$ (coef. friction): $16.9521\text{ Nm}$

$$F_{friction} = \mu \times R = 0.002 \times 981N = 1.962N \text{ (R: radial load)}$$

$$Torque Due to Friction = Ff \times r = 1.962N \times 0.006m = 0.011772Nm \text{ (r=bore radius)}$$

### Total Torque Required:

$$T_{total} = T_1 + T_{friction} = 33Nm + 0.011772Nm = 33.211772Nm$$

### Verification:

- The NSK 6201 bearing has a basic dynamic load rating of 7.28 kN, which is sufficient to handle the load of 981 N.
- The calculated torque values and rotational speed are within the bearing's specifications.

### 4.39.5 Results

The outcomes of the computations and validation procedures are as follows:

#### 4.39.5.1 Shaft Measurements

12 mm is the calculated shaft diameter.

Approximately 8.67 MPa of induced stress is much less than the material's yield strength of 250 MPa.

#### 4.39.5.2 Bearing Details:

NSK 6201 deep groove ball bearing model.

Dimensions:

- 12 mm in diameter within.
- 32 mm in diameter outside.
- Capacity to load: Equipped to manage loads that are above the designated 981 N.
- Ball diameter: 7.68 mm, which meets catalog requirements for nine balls.

#### **4.39.5.3 Observance of Standards**

By following ISO 3691-4:2020 guidelines, the design guarantees load-handling systems' dependability and safety. For operating performance, the shaft and bearing dimensions meet the minimal requirements.

#### **4.39.5.4 Total Torque Required:**

The dynamic load needed is 28.2Nm

### **4.40 CONCLUSION AND FUTURE WORKS**

The selection and design of bearing wheels and castor wheels require careful consideration of material properties, mechanical performance, and environmental factors to ensure durability and efficiency. In this project, the NSK 6201 bearing was chosen for its high performance and reliability. The NSK 6201 bearing is a single-row deep groove ball bearing known for its ability to handle both radial and axial loads, making it ideal for various industrial applications.

SolidWorks was used for 3D modeling and simulation, providing an accurate representation of the bearing and castor wheel assemblies. The finite element analysis (FEA) conducted within the software helped identify potential failure points and refine the design to enhance structural integrity. This approach significantly improved the efficiency of the design process, reducing the need for physical prototyping and minimizing costs.

The design and manufacturing process adhered to the ISO 3691-4:2020 guidelines, which specify safety requirements and verification for driverless industrial trucks and their systems. These guidelines ensure that the bearing and castor wheels meet the necessary safety standards, including braking systems, speed control, load handling, and stability. Compliance with these standards is crucial for the safe and efficient operation of industrial trucks.

Future work should focus on real-world validation of the proposed design through experimental testing and field applications. Additionally, the integration of smart sensors for real-time load monitoring and predictive maintenance could enhance operational efficiency and extend the service life of the components. Sustainable material alternatives should also be explored to align with environmental regulations and industry trends toward eco-friendly solutions.

In conclusion, this project successfully demonstrated a structured approach to the design and analysis of bearing wheels and castor wheels. By leveraging SolidWorks for design validation and incorporating theoretical and empirical analysis, the study provides a comprehensive framework for developing durable and high-performance wheel systems. Further

advancements in materials and digital manufacturing technologies will continue to improve these components, ensuring reliability in industrial applications.

## 4.41 ROS

The Robot Operating System (ROS) is a set of software libraries and tools that help you build robot applications. From drivers to state-of-the-art algorithms, and with powerful developer tools, [13] To effectively approach ROS programming, it's essential to first understand the foundational concepts of ROS and its package management system. We will explore key ROS components, including the ROS master, nodes, parameter server, messages, and services. Along the way, we will also discuss the necessary steps for installing ROS and initiating work with the ROS master.

In the subsequent sections, we will explore the following topics:

- Why ROS?
- the ROS filesystem level.
- ROS computation graph level.
- ROS community level.

## TECHNICAL REQUIREMENTS

To follow this chapter, the only thing you need is a standard computer running Ubuntu 20.04 LTS or a Debian 10 GNU/Linux distribution.



Figure 4.49: Ubuntu 20.04

## **4.42 WHY ROS?**

[1] Robot Operating System (ROS) is a flexible framework that provides various tools and libraries for writing robotic software. It offers several powerful features to help developers in tasks such as message passing, distributed computing, code reusing, and implementing state-of-the-art algorithms for robotic applications. The ROS project was started in 2007 by Morgan Quigley and its development continued at Willow Garage, a robotics research lab for developing hardware and open source software for robots. The goal of ROS was to establish a standard way to program robots while offering off-the-shelf software components that can be easily integrated with custom robotic applications. There are many reasons to choose ROS as a programming framework, and some of them are as follows:

### **4.42.1 High-end capabilities:**

ROS comes with ready-to-use functionalities. For example, the Simultaneous Localization and Mapping (SLAM) and Adaptive Monte Carlo Localization (AMCL) packages in ROS can be used for having autonomous navigation in mobile robots, while the MoveIt package can be used for motion planning for robot manipulators. These capabilities can directly be used in our robot software without any hassle. In several cases, these packages are enough for having core robotics tasks on different platforms. Also, these capabilities are highly configurable; we can fine-tune each one using various parameters.

### **4.42.2 Tons of tools:**

The ROS ecosystem is packed with tons of tools for debugging, visualizing, and having a simulation. The tools, such as rqt\_gui, RViz, and Gazebo, are some of the strongest open source tools for debugging, visualization, and simulation. A software framework that has this many tools is very rare.

### **4.42.3 Support for high-end sensors and actuators:**

ROS allows us to use different device drivers and the interface packages of various sensors and actuators in robotics. Such high-end sensors include 3D LIDAR, laser scanners, depth sensors, actuators, and more. We can interface these components with ROS without any hassle.

### **4.42.4 Inter-platform operability:**

The ROS message-passing middleware allows communication between different programs. In ROS, this middleware is known as nodes. These nodes can be programmed in any

language that has ROS client libraries. We can write high-priority nodes in C++ or C and other nodes in Python or Java.

#### 4.42.5 Modularity:

One of the issues that can occur in most standalone robotic applications is that if any of the threads of the main code crash, the entire robot application can stop. In ROS, the situation is different; we are writing different nodes for each process, and if one node crashes, the system can still work.

#### 4.42.6 Concurrent resource handling:

Handling a hardware resource via more than two processes is always a headache. Imagine that we want to process an image from a camera for face detection and motion detection; we can either write the code as a single entity that can do both, or we can write a single-threaded piece of code for concurrency. If we want to add more than two features to threads, the application behavior will become complex and difficult to debug. But in ROS, we can access devices using ROS topics from the ROS drivers. Any number of ROS nodes can subscribe to the image message from the ROS camera driver, and each node can have different functionalities. This can reduce the complexity in computation and also increase the debugging ability of the entire system.

Most high-end robotics companies are now porting their software to ROS. This trend is also visible in industrial robotics, in which companies are switching from proprietary robotic applications to ROS. Now that we know why it is convenient to study ROS, we can start introducing its core concepts. There are mainly three levels in ROS: the filesystem level, the computation graph level, and the community level. We will briefly have a look at each level.

### 4.43 THE ROS FILESYSTEM LEVEL

ROS is more than a development framework. We can refer to ROS as a meta-OS, since it offers not only tools and libraries but even OS-like functions, such as hardware abstraction, package management, and a developer toolchain. Like a real operating system, ROS files are organized on the hard disk in a particular manner, as depicted in the following diagram: Here are the explanations for each block in the filesystem:

- **Packages:** The ROS packages are a central element of the ROS software. They contain one or more ROS programs (nodes), libraries, configuration files, and so on, which are organized together as a single unit. Packages are the atomic build and release items in the ROS software.

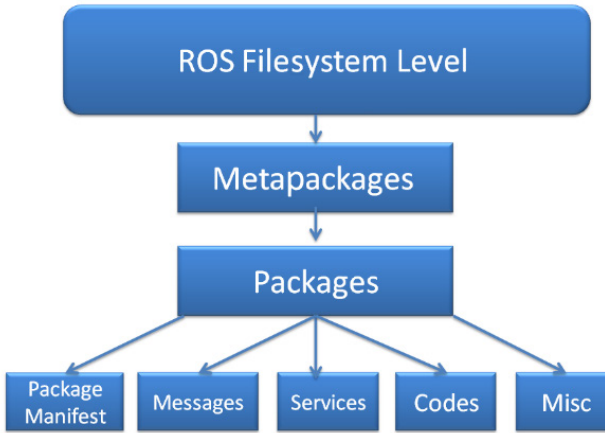


Figure 4.50: ROS filesystem level

- **Package manifest:** The package manifest file is inside a package and contains information about the package, author, license, dependencies, compilation flags, and so on. The package.xml file inside the ROS package is the manifest file of that package.
- **Metapackages:** The term metapackage refers to one or more related packages that can be loosely grouped. In principle, metapackages are virtual packages that don't contain any source code or typical files usually found in packages.
- **Metapackages manifest:** The metapackage manifest is similar to the package manifest, with the difference being that it might include packages inside it as runtime dependencies and declare an export tag.
- **Messages (.msg):** We can define a custom message inside the msg folder inside a package (my\_package/msg/MyMessageType.msg). The extension of the message file is .msg.
- **Services (.srv):** The reply and request data types can be defined inside the srv folder inside the package (my\_package/srv/MyServiceType.srv).
- **Repositories:** Most of the ROS packages are maintained using a Version Control System (VCS) such as Git, Subversion (SVN), or Mercurial (hg). A set of files placed on a VCS represents a repository.

The following screenshot gives you an idea of the files and folders of a package that we are going to create in the upcoming sections:

#### 4.44 ROS PACKAGES

The typical structure of a ROS package is shown here:

```

ros_pkg
├── action
│   └── demo.action
├── CMakeLists.txt
├── include
│   └── ros_pkg
│       └── demo.h
├── msg
│   └── message.msg
└── src
    └── demo.cpp
└── srv
    └── service.srv

```

Figure 4.51: List of files inside the package

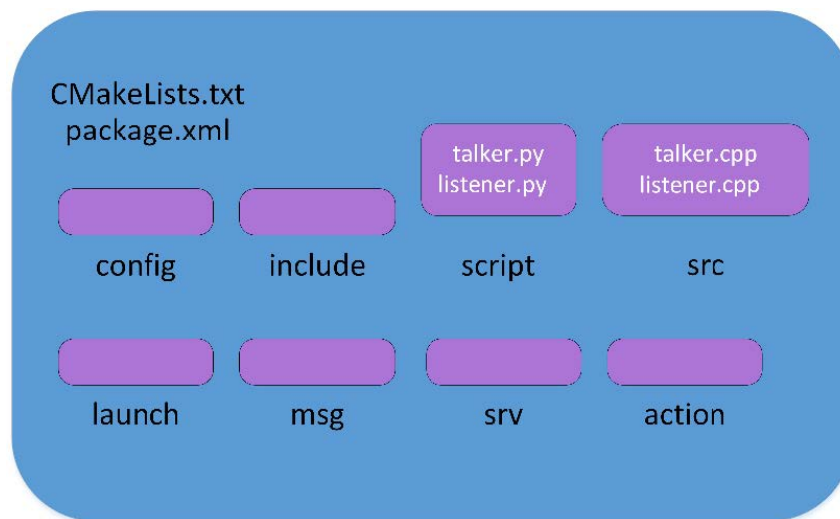


Figure 4.52: Structure of a typical C++ ROS package

- **config:** All configuration files that are used in this ROS package are kept in this folder. This folder is created by the user and it is a common practice to name the folder config as this is where we keep the configuration files.
- **include/package\_name:** This folder consists of headers and libraries that we need to use inside the package.
- **script:** This folder contains executable Python scripts. In the block diagram, we can see two example scripts.
- **src:** This folder stores the C++ source codes.
- **launch:** This folder contains the launch files that are used to launch one or more ROS nodes.
- **msg:** This folder contains custom message definitions.
- **srv:** This folder contains the services definitions.

- **action:** This folder contains the action files. We will learn more about these kinds of files in the next chapter.
- **package.xml:** This is the package manifest file of this package.
- **CMakeLists.txt:** This file contains the directives to compile the package.

We need to know some commands for creating, modifying, and working with ROS packages. Here are some of the commands we can use to work with ROS packages:

- **catkin\_create\_pkg:** This command is used to create a new package.
- **rospack:** This command is used to get information about the package in the filesystem.
- **catkin\_make:** This command is used to build the packages in the workspace.
- **rosdep:** This command will install the system dependencies required for this package.

To work with packages, ROS provides a bash-like command called rosbash (<http://wiki.ros.org/rosbash>), which can be used to navigate and manipulate the ROS package. Here are some of the rosbash commands:

- **roscd:** This command is used to change the current directory using a package name, stack name, or a special location. If we give the argument a package name, it will switch to that package folder.
- **rosdp:** This command is used to copy a file from a package.
- **rosed:** This command is used to edit a file using the vim editor.
- **rosrun:** This command is used to run an executable inside a package.

The definition of package.xml in a typical package is shown in the following code:

```

1      <?xml version="1.0"?>
2      <package>
3          <name>hello world</name>
4          <version>0.0.1</version>
5          <description>The hello world package</description>
6          <maintainer email="example@gmail.com">example</maintainer>
7          <buildtool_depend>catkin</buildtool_depend>
8          <buildtool_depend>roscpp</build_depend>
9          <build_depend>rospy</build_depend>
10         <build_depend>std_msgs</build_depend>
```

```
11 <run_depend>roscpp</run_depend>
12 <run_depend> rospy</run_depend>
13 <run_depend> std_msgs</run_depend>
14 <export>
15 </export> </package>
```

The package.xml file also contains information about the compilation. The `<build_depend></build_depend>` tag includes the packages that are necessary for building the source code of the package. The packages inside the `<run_depend></run_depend>` tags are necessary for running the package node at runtime.

## 4.45 ROS METAPACKAGES

Metapackages are specialized packages that require only one file; that is, a package.xml file. Metapackages simply group a set of multiple packages as a single logical package. In the package.xml file, the metapackage contains an export tag, as shown here:

```
1 <export>
2 <metapackage/>
3 </export>
```

Also, in metapackages, there are no `<buildtool_depend>` dependencies for catkin; there are only `<run_depend>` dependencies, which are the packages that are grouped inside the metapackage.

The ROS navigation stack is a good example of somewhere that contains metapackages. If ROS and its navigation package are installed, we can try using the following command by switching to the navigation metapackage folder:

```
1 roscd navigation
```

Open package.xml using your text editor (gedit, in the following case):

```
1 gedit package.xml
```

This is a lengthy file; here is a stripped-down version of it: This file contains several

```
1      <?xml version="1.0"?>
2      <package>
3          <name>navigation</name>
4          <version>1. 14. 0</version>
5          <description>
6              A 2D navigation stack that takes in information from
7                  ↳ odometry, sensor
8              streams, and a goal pose and outputs safe velocity commands
9                  ↳ that are sent
10             to a mobile base.
11         </description>
12         <url>http : //wiki.ros.org/navigation</url>
13         <buildtool_depend>catkin</buildtool_depend>
14         <run_depend>amcl</run_depend>
15         ...
16         <export>
17             <metapackage/>
18         </export>
19     </package>
```

Figure 4.53: Structure of the package.xml metapackage

pieces of information about the package, such as a brief description, its dependencies, and the package version.

## 4.46 ROS MESSAGES

ROS nodes can write or read data of various types. These different types of data are described using a simplified message description language, also called ROS messages. These data type descriptions can be used to generate source code for the appropriate message type in different target languages. Even though the ROS framework provides a large set of robotic-specific messages that have already been implemented, developers can define their own message type inside their nodes. The message definition can consist of two types: fields and constants. The field is split into field types and field names. The field type is the data type of the transmitting message, while the field name is the name of it.

Here is an example of message definitions:

```
1     int32 number
```

```
1     string name
```

```
1     float32 speed
```

Here, the first part is the field type and the second is the field name. The field type is the data type, and the field name can be used to access the value from the message. For example, we can use `msg.number` to access the value of the `number` field from the message.

Here is a table showing some of the built-in field types that we can use in our message:

### Built-in Field Types for Message Definition

Primitive type	Serialization	C++	Python
bool (1)	Unsigned 8-bit int	uint8_t (2)	bool
int8	Signed 8-bit int	int8_t	int
uint8	Unsigned 8-bit int	uint8_t	int (3)
int16	Signed 16-bit int	int16_t	int
uint16	Unsigned 16-bit int	uint16_t	int
int32	Signed 32-bit int	int32_t	int
uint32	Unsigned 32-bit int	uint32_t	int
int64	Signed 64-bit int	int64_t	long
uint64	Unsigned 64-bit int	uint64_t	long
float32	32-bit IEEE float	float	float
float64	64-bit IEEE float	double	float
string	ascii string (4)	std::string	string
time	secs/nsecs unsigned 32-bit ints	ros::Time	rospy.Time
duration	secs/nsecs signed 32-bit ints	ros::Duration	rospy.Duration

Table 4.18: Primitive types and their serialization in C++ and Python.

ROS provides a set of complex and more structured message files that are designed to cover a specific application's necessity, such as exchanging common geometrical (geometry\_msgs) or sensor (sensor\_msgs) information. These messages are composed of different primitive types. A special type of ROS message is called a message header. This header can carry information, such as time, frame of reference or frame\_id, and sequence number. Using the header, we will get numbered messages and more clarity about which component is sending the current message. The header information is mainly used to send data such as robot joint transforms. Here is the definition of the header:

1        uint32 seq

1        time stamp

```
1     string frame_id
```

The `rosmg` command tool can be used to inspect the message header and the field types. The following command helps view the message header of a particular message:

```
1     rosmg show std_msgs/Header
```

This will give you an output like the preceding example's message header. We will look at the `rosmg` command and how to work with custom message definitions later in this chapter.

## 4.47 THE ROS SERVICES

ROS services are a type of request/response communication between ROS nodes. One node will send a request and wait until it gets a response from the other. Similar to the message definitions when using the .msg file, we must define the service definition in another file called .srv, which must be kept inside the `srv` subdirectory of the package.

An example service description format is as follows:

```
1 #Request message type
2 string req
3 ---
4 #Response message type
5 string res
```

The first section is the message type of the request, which is separated by `---`, while the next section contains the message type of the response. In these examples, both Request and Response are strings.

## 4.48 THE ROS COMPUTATION GRAPH LEVEL

Computation in ROS is done using a network of ROS nodes. This computation network is called the computation graph. The main concepts in the computation graph are **ROS nodes**, **master**, **parameter server**, **messages**, **topics**, **services**, and **bags**. Each concept in the graph is contributed to this graph in different ways.

The ROS communication-related packages, including core client libraries, such as `roscpp` and `rospython`, and the implementation of concepts, such as topics, nodes, parameters, and services, are included in a stack called `ros_comm` ([http://wiki.ros.org/ros\\_comm](http://wiki.ros.org/ros_comm)).

This stack also consists of tools such as `rostopic`, `rosparam`, `rosservice`, and `rosnode` to introspect the preceding concepts.

The `ros_comm` stack contains the ROS communication middleware packages, and these packages are collectively called the **ROS graph layer**.

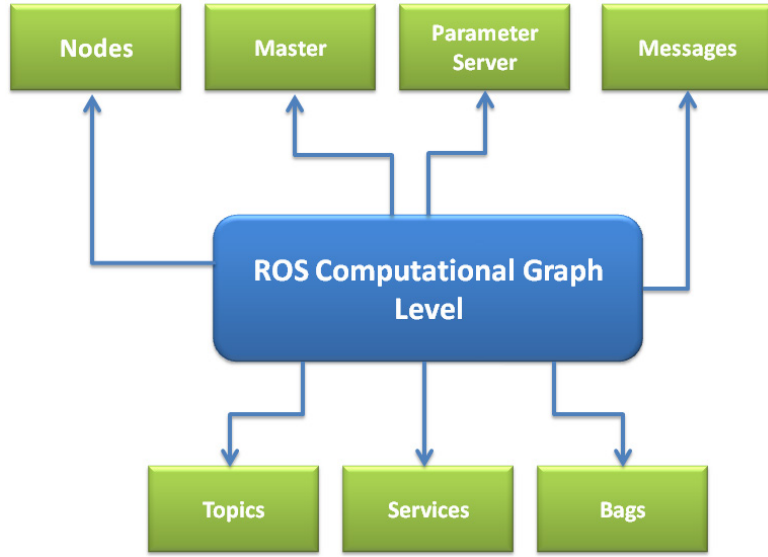


Figure 4.54: Structure of the ROS graph layer

#### 4.48.1 Nodes

Nodes are the processes that have computation. Each ROS node is written using ROS client libraries. Using client library APIs, we can implement different ROS functionalities, such as the communication methods between nodes, which is particularly useful when the different nodes of our robot must exchange information between them. One of the aims of ROS nodes is to build simple processes rather than a large process with all the desired functionalities. Being simple structures, ROS nodes are easy to debug.

#### 4.48.2 Master

The ROS master provides the name registration and lookup processes for the rest of the nodes. Nodes will not be able to find each other, exchange messages, or invoke services without a ROS master. In a distributed system, we should run the master on one computer; then, the other remote nodes can find each other by communicating with this master.

#### 4.48.3 Parameter server

The parameter server allows you to store data in a central location. All the nodes can access and modify these values. The parameter server is part of the ROS master.

#### 4.48.4 Topics

Each message in ROS is transported using named buses called topics. When a node sends a message through a topic, then we can say the node is publishing a topic. When a node receives a message through a topic, then we can say that the node is subscribing to a

topic. The publishing node and subscribing node are not aware of each other's existence. We can even subscribe to a topic that might not have any publisher. In short, the production of information and its consumption are decoupled. Each topic has a unique name, and any node can access this topic and send data through it so long as they have the right message type.

#### 4.48.5 Logging

ROS provides a logging system for storing data, such as sensor data, which can be difficult to collect but is necessary for developing and testing robot algorithms. These are known as bagfiles. Bagfiles are very useful features when we're working with complex robot mechanisms.

The following graph shows how the nodes communicate with each other using topics:

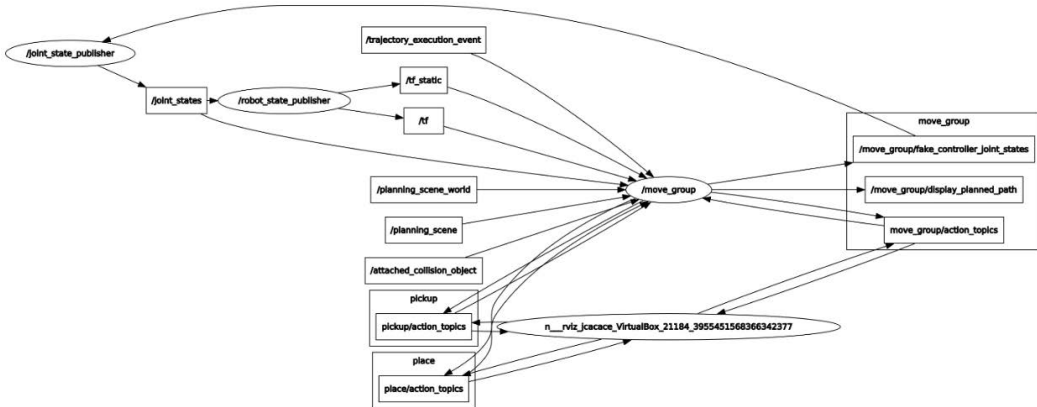


Figure 4.55: Graph of communication between nodes using topics

The topics are represented by rectangles, while the nodes are represented by ellipses. The messages and parameters are not included in this graph. These kinds of graphs can be generated using a tool called **rqt\_graph** ([http://wiki.ros.org/rqt\\_graph](http://wiki.ros.org/rqt_graph)).

## 4.49 ROS NODES

ROS nodes have computations using ROS client libraries such as `roscpp` and `rospy`. A robot might contain many nodes; for example, one node processes camera images, one node handles serial data from the robot, one node can be used to compute odometry, and so on.

Using nodes can make the system fault-tolerant. Even if a node crashes, an entire robot system can still work. Nodes also reduce complexity and increase debug-ability compared to monolithic code because each node is handling only a single function.

All running nodes should have a name assigned to help us identify them. For example, `/camera_node` could be the name of a node that is broadcasting camera images.

There is a rosbash tool for introspecting ROS nodes. The `rosnode` command can be used to gather information about an ROS node. Here are the usages of `rosnode`:

- `rosnode info [node_name]`: This will print out information about the node.
- `rosnode kill [node_name]`: This will kill a running node.
- `rosnode list`: This will list the running nodes.
- `rosnode machine [machine_name]` : This will list the nodes that are running on a particular machine or a list of machines.
- `rosnode ping`: This will check the connectivity of a node.
- `rosnode cleanup`: This will purge the registration of unreachable nodes.

some example nodes that use the roscpp client and discuss how ROS nodes that use functionalities such ROS topics, service, messages, and actionlib work.

## 4.50 ROS MESSAGES

messages are simple data structures that contain field types. ROS messages support standard primitive data types and arrays of primitive types.

We can access a message definition using the following method. For example, to access `std_msgs/msg/String.msg` when we are using the roscpp client, we must include `std_msgs/String.h` for the string message definition.

In addition to the message data type, ROS uses an MD5 checksum comparison to confirm whether the publisher and subscriber exchange the same message data types.

ROS has a built-in tool called `rosmsg` for gathering information about ROS messages. Here are some parameters that are used along with `rosmsg`:

- `rosmsg show [message_type]`: This shows the message's description.
- `rosmsg list`: This lists all messages.
- `rosmsg md5 [message_type]`: This displays md5sum of a message.
- `rosmsg package [package_name]`: This lists messages in a package.
- `rosmsg packages [package_1] [package_2]`: This lists all packages that contain messages.

## 4.51 ROS TOPICS

Using topics, the ROS communication is unidirectional. Differently, if we want a direct request/response communication, we need to implement ROS services. The ROS nodes communicate with topics using a TCP/IP-based transport known as **TCPROS**. This method is the default transport method used in ROS. Another type of communication is **UDPROS**, which has low latency and loose transport and is only suited for teleoperations. The ROS topic tool can be used to gather information about ROS topics. Here is the syntax of this command:

- **rostopic bw /topic**: This command will display the bandwidth being used by the given topic.
- **rostopic echo /topic**: This command will print the content of the given topic in a human-readable format. Users can use the -p option to print data in CSV format.
- **rostopic find /message\_type**: This command will find topics using the given message type.
- **rostopic hz /topic**: This command will display the publishing rate of the given topic.
- **rostopic info /topic**: This command will print information about an active topic.
- **rostopic list**: This command will list all the active topics in the ROS system.
- **rostopic pub /topic message\_type args**: This command can be used to publish a value to a topic with a message type.
- **rostopic type /topic**: This will display the message type of the given topic.

## 4.52 ROS SERVICES

In ROS services, one node acts as a ROS server in which the service client can request the service from the server. If the server completes the service routine, it will send the results to the service client. For example, consider a node that can provide the sum of two numbers that has been received as input while implementing this functionality through an ROS service. The other nodes of our system might request the sum of two numbers via this service. In this situation, topics are used to stream continuous data flows.

The ROS service definition can be accessed by the following method. For example, `my_package/srv/Image.srv` can be accessed by `my_package/Image`.

In ROS services, there is an MD5 checksum that checks in the nodes. If the sum is equal, then only the server responds to the client.

There are two ROS tools for gathering information about the ROS service. The first tool is **rossrv**, which is similar to **rosmsg**, and is used to get information about service types. The next command is **rosservice**, which is used to list and query the running ROS services.

Let's explain how to use the **rosservice** tool to gather information about the running services:

- **rosservice call /service args**: This tool will call the service using the given arguments.
- **rosservice find service\_type**: This command will find the services of the given service type.
- **rosservice info /services**: This will print information about the given service.
- **rosservice list**: This command will list the active services running on the system.
- **rosservice type /service**: This command will print the service type of a given service.
- **rosservice uri /service**: This tool will print the service's ROSRPC URI.

## 4.53 ROS BAGFILES

The **rosbag** command is used to work with rosbag files. A bag file in ROS is used for storing ROS message data that's streamed by topics. The .bag extension is used to represent a bag file.

Bag files are created using the **rosbag record** command, which will subscribe to one or more topics and store the message's data in a file as it's received. This file can play the same topics that they are recorded from, and it can remap the existing topics too.

Here are the commands for recording and playing back a bag file:

- **rosbag record [topic\_1] [topic\_2] -o [bag\_name]**: This command will record the given topics into the bag file provided in the command. We can also record all topics using the -a argument.
- **rosbag play [bag\_name]**: This will play back the existing bag file.

The full, detailed list of commands can be found by using the following command in a Terminal:

```
1 rosbag play -h
```

There is a GUI tool that we can use to handle how bag files are recorded and played back called `rqt_bag`. To learn more about `rqt_bag`, go to [https://wiki.ros.org/rqt\\_bag](https://wiki.ros.org/rqt_bag).

## 4.54 THE ROS MASTER

The ROS master is much like a DNS server, in that it associates unique names and IDs to the ROS elements that are active in our system. When any node starts in the ROS system, it will start looking for the ROS master and register the name of the node in it. So, the ROS master has the details of all the nodes currently running on the ROS system. When any of the node's details change, it will generate a callback and update the node with the latest details. These node details are useful for connecting each node.

When a node starts publishing to a topic, the node will give the details of the topic, such as its name and data type, to the ROS master. The ROS master will check whether any other nodes are subscribed to the same topic. If any nodes are subscribed to the same topic, the ROS master will share the node details of the publisher to the subscriber node. After getting the node details, these two nodes will be connected. After connecting to the two nodes, the ROS master has no role in controlling them. We might be able to stop either the publisher node or the subscriber node according to our requirements. If we stop any nodes, they will check in with the ROS master once again. This same method is used for the ROS services.

As we've already stated, the nodes are written using ROS client libraries, such as `roscpp` and `rospy`. These clients interact with the ROS master using **XML Remote Procedure Call (XMLRPC)**-based APIs, which act as the backend of the ROS system APIs.

The `ROS_MASTER_URI` environment variable contains the IP and port of the ROS master. Using this variable, ROS nodes can locate the ROS master. If this variable is wrong, communication between the nodes will not take place. When we use ROS in a single system, we can use the IP of a localhost or the name `localhost` itself. But in a distributed network, in which computation is done on different physical computers, we should define `ROS_MASTER_URI` properly; only then will the remote nodes be able to find each other and communicate with each other. We only need one master in a distributed system, and it should run on a computer in which all the other computers can ping it properly to ensure that remote ROS nodes can access the master.

The following diagram(fig. 4.56) shows how the ROS master interacts with publishing and subscribing nodes, with the publisher node publishing a string type topic with a Hello World message and the subscriber node subscribing to this topic: When the publisher node starts advertising the Hello World message in a particular topic, the ROS master gets the details of the topic and the node. It will check whether any node is subscribing to the same topic. If no nodes are subscribing to the same topic at that time, both nodes will remain unconnected. If the publisher and subscriber nodes run at the same time, the ROS master will exchange the details of the publisher to the subscriber, and they will connect and exchange data through ROS topics.

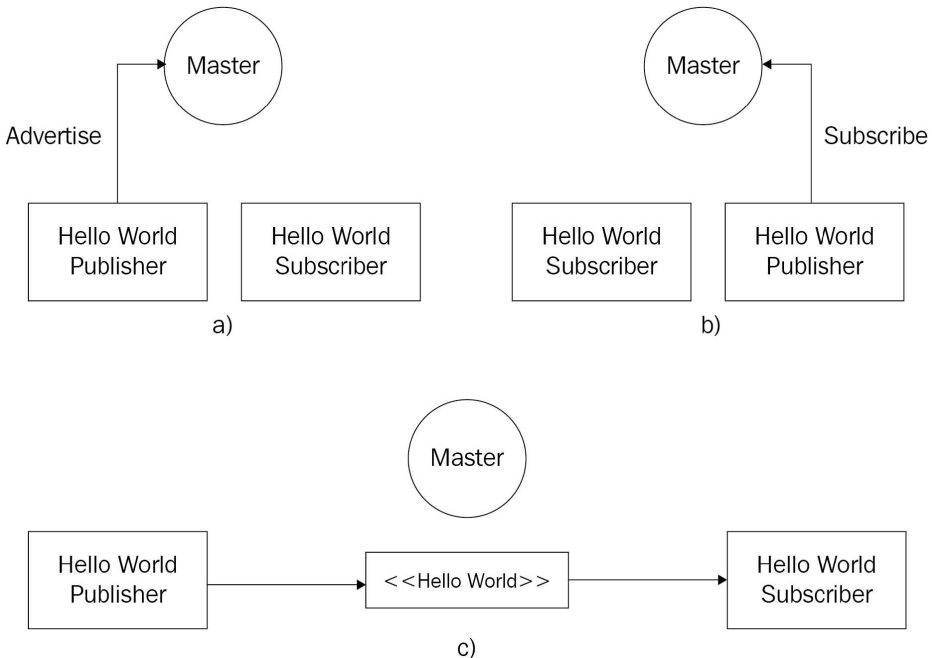


Figure 4.56: Communication between the ROS master and Hello World publisher and subscriber

## 4.55 ROS PARAMETER

When programming a robot, we might have to define robot parameters to tune our control algorithm, such as the robot controller gains P, I, and D of a standard proportional integral derivative controller. When the number of parameters increases, we might need to store them as files. In some situations, these parameters must be shared between two or more programs. In this case, ROS provides a parameter server, which is a shared server in which all the ROS nodes can access parameters from this server. A node can read, write, modify, and delete parameter values from the parameter server.

We can store these parameters in a file and load them into the server. The server can store a wide variety of data types and even dictionaries. The programmer can also set the scope of the parameter; that is, whether it can be accessed by only this node or all the nodes.

The parameter server supports the following XMLRPC data types:

- 32-bit integers
- Booleans
- Strings
- Doubles

- ISO8601 dates
- Lists
- Base64-encoded binary data

We can also store dictionaries on the parameter server. If the number of parameters is high, we can use a YAML file to save them. Here is an example of the YAML file parameter definitions:

```
/camera/name : 'nikon' #string_type
/camera/fps : 30 #integer
/camera/exposure : 1.2 #float
/camera/active : true #boolean
```

The `rosparam` tool is used to get and set the ROS parameter from the command line. The following are the commands for working with ROS parameters:

- `rosparam set [parameter_name] [value]`: This command will set a value in the given parameter.
- `rosparam get [parameter_name]`: This command will retrieve a value from the given parameter.
- `rosparam load [YAML_file]`: The ROS parameters can be saved into a YAML file. It can load them into the parameter server using this command.
- `rosparam dump [YAML_file]`: This command will dump the existing ROS parameters into a YAML file.
- `rosparam delete [parameter_name]`: This command will delete the given parameter.
- `rosparam list`: This command will list existing parameter names.

These parameters can be changed dynamically when you're executing a node that uses these parameters by using the `dynamic_reconfigure` package ([http://wiki.ros.org/dynamic\\_reconfigure](http://wiki.ros.org/dynamic_reconfigure)).

## 4.56 ROS DISTRIBUTIONS

ROS updates are released with new ROS distributions. A new distribution of ROS is composed of an updated version of its core software and a set of new/updated ROS packages. ROS follows the same release cycle as the Ubuntu Linux distribution: a new version of ROS is released every 6 months. Typically, for each Ubuntu LTS version, an **LTS** version of ROS is released. **Long Term Support (LTS)** means that the released software will be maintained for a long time (5 years in the case of ROS and Ubuntu).

Built-in Field Types for Message Definition				
Distro	Release date	Poster	Turtle	EOL date
ROS Noetic Ninjemy (Recommended)	May 23rd, 2020			May, 2025 (Focal EOL)
ROS Melodic Morenia	May 23rd, 2018			June 27, 2023 (Bionic EOL)
ROS Lunar Loggerhead	May 23rd, 2017			May, 2019
ROS Kinetic Kame	May 23rd, 2016			April, 2021 (Xenial EOL)

Table 4.20: ROS Distributions Table

## 4.57 RUNNING THE ROS MASTER AND THE ROS PARAMETER SERVER

Before running any ROS nodes, we should start the ROS master and the ROS parameter server. We can start the ROS master and the ROS parameter server by using a single command called **roscore**, which will start the following programs:

- ROS master
- ROS parameter server
- rosout logging nodes

The rosout node will collect log messages from other ROS nodes and store them in a log file, and will also re-broadcast the collected log message to another topic. The /rosout topic is published by ROS nodes using ROS client libraries such as roscpp and rospy, and this topic is subscribed by the rosout node, which rebroadcasts the message in another topic called /rosout\_agg. This topic contains an aggregate stream of log messages. The roscore command should be run as a prerequisite to running any ROS nodes. The following screenshot shows the messages that are printed when we run the roscore command in a Terminal.

Use the following command to run roscore on a Linux Terminal:

```
1 roscore
```

After running this command, we will see the following text in the Linux Terminal:

The terminal window displays the output of the roscore command. The output is annotated with numbers 1 through 5, highlighting specific parts of the log:

- Annotation 1:** Logs disk usage checking. It starts with "... Logging to /home/jcacace/.ros/log/a50123ca-4354-11eb-b33a-e3799b7b952f/roslaunch-robot-2558.log", followed by "Checking log directory for disk usage. This may take a while.", and ends with "Done checking log file disk usage. Usage is <1GB."
- Annotation 2:** Starts the roslaunch server. The message is "started roslaunch server http://robot:33837/" followed by "ros\_comm version 1.15.9".
- Annotation 3:** Displays system parameters. It shows "/rosdistro: noetic" and "/rosversion: 1.15.9".
- Annotation 4:** Starts the ROS master. The message is "auto-starting new master process[master]: started with pid [2580]" followed by "ROS\_MASTER\_URI=http://robot:11311/".
- Annotation 5:** Starts the rosout logging node. The message is "setting /run\_id to a50123ca-4354-11eb-b33a-e3799b7b952f" followed by "process[rosout-1]: started with pid [2590]" and "started core service [/rosout]."

Figure 4.57: Terminal messages while running the roscore command

- In section 1, we can see that a log file is created inside the `~/.ros/log` folder for collecting logs from ROS nodes. This file can be used for debugging purposes.
- In section 2, the command starts a ROS launch file called `roscore.xml`. When a launch file starts, it automatically starts `rosmaster` and the ROS parameter server. The `roslaunch` command is a Python script, which can start `rosmaster` and the ROS parameter server whenever it tries to execute a launch file. This section shows the address of the ROS parameter server within the port.
- In section 3, we can see parameters such as `rosdistro` and `rosversion` being displayed in the Terminal. These parameters are displayed when it executes `roscore.xml`. We will look at `roscore.xml` in more detail in the next section.
- In section 4, we can see that the `rosmaster` node is being started with `ROS_MASTER_URI`, which we defined earlier as an environment variable.
- In section 5, we can see that the `rosout` node is being started, which will start subscribing to the `/rosout` topic and rebroadcasting it to `/rosout_agg`.

The following is the content of `roscore.xml`:

```

1 <launch>
2   <group ns="/">
3     <param name="rosversion" command="rosversion roslaunch" />
4     <param name="rosdistro" command="rosversion -d" />
5     <node pkg="rosout" type="rosout" name="rosout"
6       respawn="true"/>
7   </group>
8 </launch>

```

When the `roscore` command is executed, initially, the command checks the command-line argument for a new port number for `rosmaster`. If it gets the port number, it will start listening to the new port number; otherwise, it will use the default port. This port number and the `roscore.xml` launch file will be passed to the `roslaunch` system. The `roslaunch` system is implemented in a Python module; it will parse the port number and launch the `roscore.xml` file.

In the `roscore.xml` file, we can see that the ROS parameters and nodes are encapsulated in a group XML tag with a `/` namespace. The group XML tag indicates that all the nodes inside this tag have the same settings.

The `rosversion` and `rostdistro` parameters store the output of the `rosversion roslaunch` and `rosversion -d` commands using the `command` tag, which is a part of the ROS param tag. The `command` tag will execute the command mentioned in it and store the output of the command in these two parameters.

`rosmaster` and the parameter server are executed inside `roslaunch` modules via the `ROS_MASTER_URI` address. This happens inside the `roslaunch` Python module.

`ROS_MASTER_URI` is a combination of the IP address and port that `rosmaster` is going to listen to. The port number can be changed according to the given port number in the `roscore` command.

#### 4.57.1 Checking the `roscore` command's output

Let's check out the ROS topics and ROS parameters that are created after running `roscore`. The following command will list the active topics in the Terminal:

```
1 rostopic list
```

The list of topics is as follows, as per our discussion of the `rosout` node's `subscribe /rosout` topic. This contains all the log messages from the ROS nodes. `/rosout_agg` will rebroadcast the log messages:

```
1 /rosout
2 /rosout_agg
```

The following command lists the parameters that are available when running `roscore`. The following command is used to list the active ROS parameter:

```
1 rosparam list
```

These parameters are mentioned here; they provide the ROS distribution name, version, the address of the `roslaunch` server, and `run_id`, where `run_id` is a unique ID associated with a particular run of `roscore`:

```
1 /rostdistro
2 /roslaunch/uris/host_robot_virtualbox_51189
3 /rosversion
4 /run_id
```

The list of ROS services that's generated when running roscore can be checked by using the following command:

```
1 rosservice list
```

The list of services that are running is as follows:

```
1 /rosout/get_loggers  
2 /rosout/set_logger_level
```

These ROS services are generated for each ROS node, and they are used to set the logging levels.

## 4.58 SIMULATION ENVIRONMENT

## 4.59 INTRODUCTION TO THE SIMULATION ENVIRONMENT

In developing a control strategy for mobile robots such as Automated Guided Vehicles (AGVs), simulation plays a crucial role in testing software components, robot behavior, and control algorithms across various environments. Before physically building the robotic system, running a simulation provides a risk-free and cost-effective approach to refining its design and functionality. By simulating the robot's behavior in a controlled virtual environment, different algorithms can be tested and optimized to ensure efficient navigation, obstacle avoidance, and perception without the risk of hardware damage.

The simulation environment was built using the **Robot Operating System (ROS)** and the **Gazebo** simulator, with the `gazebo_ros` package. `RViz` was utilized for real-time visualization of sensor data and robot trajectories, while `OpenCV` handled computer vision tasks such as *line following* and *QR code detection*. The following sections provide detailed insights into their implementation and role in the project.

## 4.60 TOOLS AND FRAMEWORK

### 4.60.1 Gazebo

Gazebo was initially developed in 2002 to facilitate the simulation of ground robot applications in both indoor and outdoor environments [14]. Over the years, it has evolved into a mature open-source project widely adopted by the global robotics community for various applications. Gazebo follows a modular architecture, incorporating four key components essential for robot simulation:

- **Physics Engine Support** – Gazebo integrates multiple physics engines to handle collision detection, contact dynamics, and reaction forces between rigid bodies.
- **Sensor Simulation** – It provides a comprehensive library of commonly used robotic sensors, including cameras, LiDAR, sonar, GPS, and IMUs, along with configurable noise models for realistic sensor emulation.
- **Multiple Interfaces** – The simulator supports various interfaces for programmatic interaction, including C++ for developing plugins.
- **Graphical User Interface (GUI)** – Gazebo features an interactive 3D environment that enables users to visualize and manipulate the simulated world in real-time.



Figure 4.58: Gazebo Simulator

Gazebo is a robust simulation tool integrated with the Robot Operating System (ROS), designed to simulate robotic and sensor applications in both indoor and outdoor 3D environments. It follows a Client-Server architecture coupled with a topic-based Publish/Subscribe model for inter-process communication, enabling efficient data exchange between the various components of the system.

For dynamic simulations, Gazebo leverages several high-performance physics engines, including the Open Dynamics Engine (ODE) [15], Bullet [16], Simbody [17], and the Dynamic Animation and Robotics Toolkit (DART) [18]. These engines handle rigid-body physics simulations, providing highly accurate interactions between objects. Additionally, Gazebo employs the Object-Oriented Graphics Rendering Engine (OGRE) [19] for 3D graphics rendering, generating realistic visual environments that enhance the simulation experience.

In this architecture, the Gazebo Client sends control data, such as the coordinates of simulated objects, to the Server, which then manages real-time control of the virtual robot. Gazebo also supports distributed simulation, allowing the Client and Server to run on separate machines, which can be beneficial for scaling and performance.

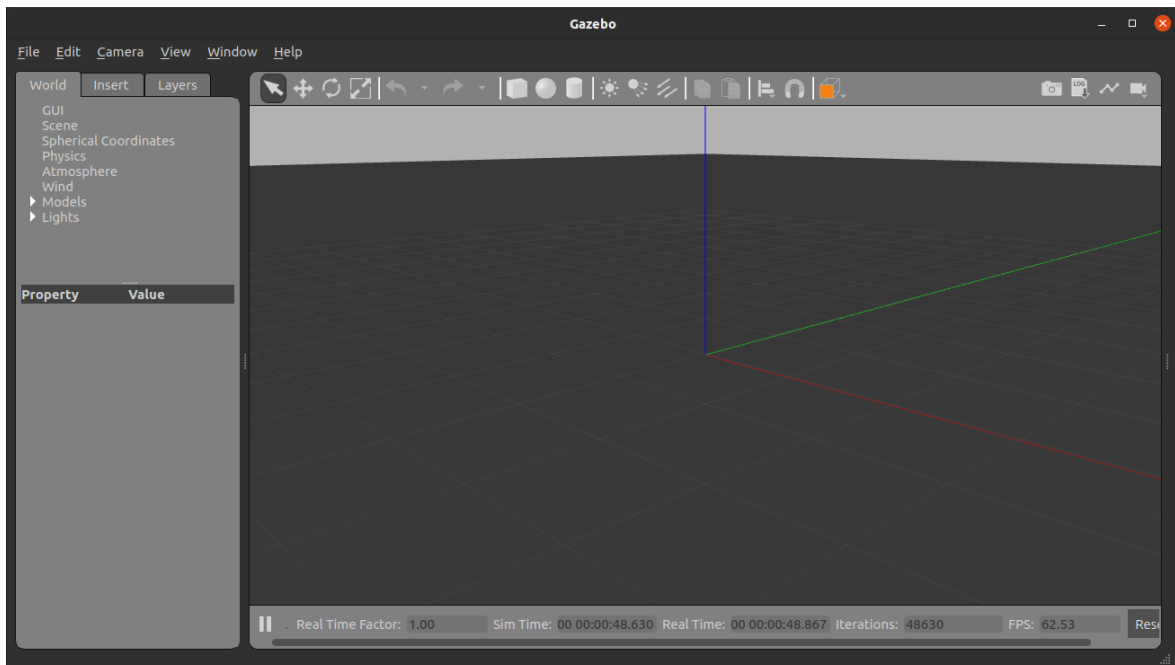


Figure 4.59: Empty world in Gazebo

The ROS Plugin for Gazebo ensures integration between the two platforms, enabling direct communication with ROS. This allows both simulated and real robots to be controlled using the same software interface, making Gazebo an ideal platform for testing, developing, and validating robotic systems in a virtual environment before deployment on physical hardware.

This plugin facilitates bi-directional communication through ROS topics, services, and actions, allowing sensor data from Gazebo—such as LiDAR, cameras, and IMUs—to be published as ROS messages while also enabling ROS-based velocity and trajectory commands to control simulated robots. Additionally, the plugin supports `ros_control`, making it possible to implement position, velocity, and effort controllers, which are essential for tuning PID loops before testing them on real actuators.

```

1   <launch>
2
3     <arg name="model" default="$(env TURTLEBOT3_MODEL)"
4       ↳ doc="model type [burger, waffle, waffle_pi]" />
5
6     <arg name="x_pos" default="0.0"/>
7     <arg name="y_pos" default="0.0"/>
8     <arg name="z_pos" default="0.0"/>
9
10
11    <include file="$(find gazebo_ros)/launch/empty_world.launch">
12      <arg name="world_name"
13        ↳ value="$(find turtlebot3_gazebo)/worlds/empty.world"/>
14
15      <arg name="paused" value="false"/>
16      <arg name="use_sim_time" value="true"/>
17      <arg name="gui" value="true"/>
18      <arg name="headless" value="false"/>
19      <arg name="debug" value="false"/>
20
21    </include>
22
23
24    <param name="robot_description" command=
25      "$(find xacro)/xacro --inorder
26      $(find turtlebot3_description)/
27      urdf/turtlebot3_$(arg model).urdf.xacro" />
28
29
30    <node pkg="gazebo_ros" type="spawn_model" name="spawn_urdf"
31      ↳ args="-urdf -model turtlebot3_$(arg model) -x $(arg x_pos) -y
32          $(arg y_pos) -z $(arg z_pos) -param robot_description" />
33
34  </launch>
```

The provided example demonstrates how the **ROS Plugin for Gazebo** enables the spawning and control of a robot model within a simulated environment, enabling **smooth and efficient integration** with the **Robot Operating System (ROS)**. The launch file initializes an empty **Gazebo** world and loads a robot model described in a **URDF (Unified Robot Description Format)** file using the `spawn_model` node from the `gazebo_ros` package. Additionally,

the `robot_state_publisher` node is included to publish the robot's joint states, ensuring that its transformations can be visualized and utilized in **ROS-based frameworks** such as **MoveIt** or **RViz**. This integration allows developers to test **robot behaviors, sensor data integration, and control algorithms** in a virtual environment before deploying them on physical hardware.

It facilitates bi-directional communication through **ROS topics, services, and actions**, enabling sensor data from Gazebo—such as **LiDAR, cameras, and IMUs**—to be published as **ROS messages** while also allowing **ROS-based velocity and trajectory commands** to control simulated robots. Additionally, the plugin supports `ros_control`, enabling the implementation of **position, velocity, and effort controllers**, which are essential for tuning **PID loops** before applying them to real actuators.

This specific example shows a **ROS launch file** that spawns a **TurtleBot3** model shown fig. 4.60 in an empty **Gazebo** simulation environment. This file provides flexibility by allowing users to specify the **TurtleBot3 model type** (burger, waffle, or waffle\_pi) and configure the **robot's initial position**. It also sets critical simulation parameters, such as **enabling GUI rendering, synchronizing ROS time with Gazebo simulation time, and dynamically loading the robot's description** based on the selected model type. The launch file ensures a well-structured simulation environment where **robotic software, motion planning, and perception algorithms** can be tested under realistic conditions.

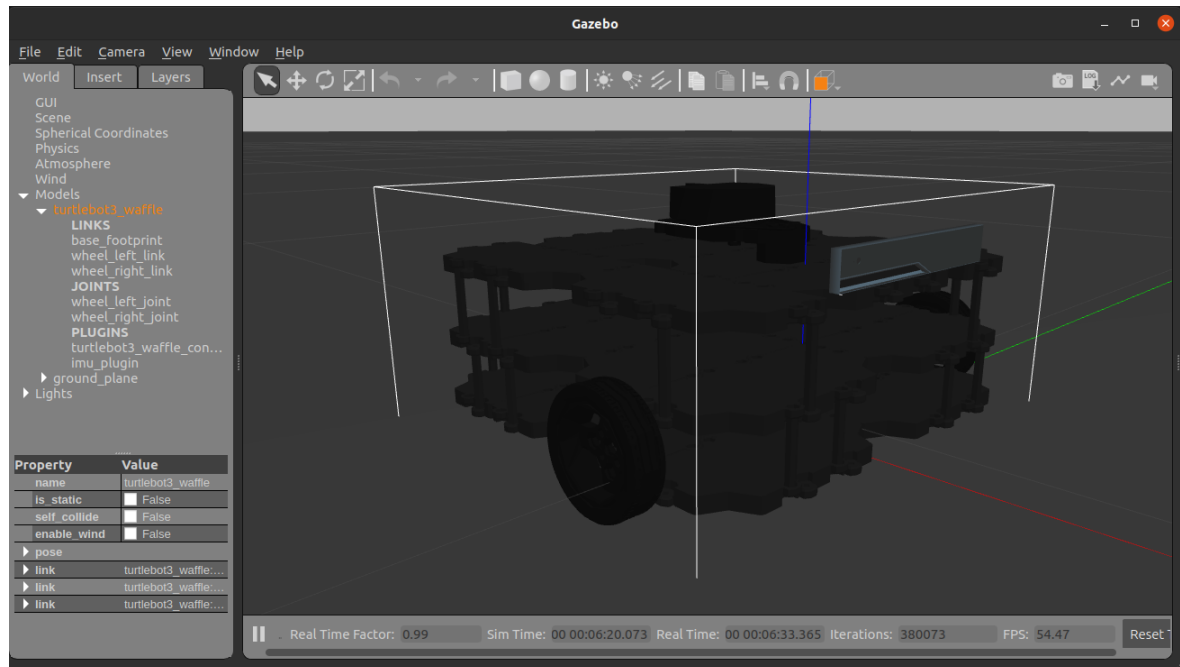


Figure 4.60: TurtleBot3 Waffle spawned in empty world

The Gazebo Graphical User Interface (GUI) provides an interactive environment for users to visualize and manipulate their simulated worlds in real-time. One of the key features

of the GUI is the set of side tabs, which organize various tools and functionalities. Among these, the left side pannel that appears fig. 4.61 World, Insert, and Layers tabs are particularly important for managing the simulation environment and objects within it.

The **World Tab** in Gazebo's GUI allows users to manage and configure the properties of the simulation world, providing several options for modifying the environment settings. Users can adjust the **gravity settings** to control the strength of gravity in the simulation, select the **physics engine** (such as **ODE**, **Bullet**, or **DART**) to determine the level of simulation fidelity and performance, and customize **time and weather conditions**, including factors like sunlight, fog, and rain. Additionally, the World tab provides detailed information about the models within the simulation, including their **joints** and **links**. Users can visualize and modify the connections between different parts of a robot or object, defining how they move and interact with each other. The **links** represent rigid bodies, while **joints** define the relative motion between those bodies, such as revolute, prismatic, or fixed joints. This tab plays a crucial role in fine-tuning the simulation environment and robot behavior, ensuring that the simulation behaves as expected for the application at hand. It is an essential tool for accurately replicating real-world conditions and testing robotic systems in varied scenarios.

The **Insert Tab** allows users to add various objects and components to the simulation environment. Users can insert robot models, lights, sensors, and even other world elements, which helps populate the simulation for testing and development. Additionally, the tab makes it easy to add custom plugins or adjust the robot's attributes in the virtual world.

The **Layers Tab** provides control over the visibility of different elements within the simulation. Users can toggle the visibility of models, sensors, and other objects in the scene to focus on specific parts of the simulation. This helps streamline the workspace, especially when dealing with complex environments and large-scale simulations.

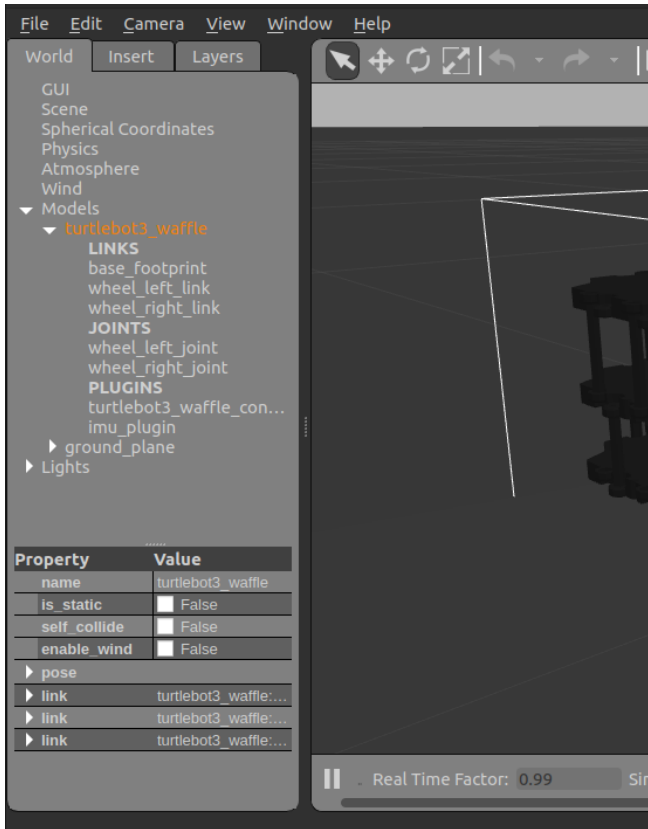


Figure 4.61: Gazebo Graphical User Interface left side pannel

The lower part of the Gazebo GUI displayed in fig. 4.62 provides critical real-time simulation information and performance metrics. One of the most important features is the **Real-Time Factor (RTF)**, which indicates the ratio between real-time and simulated time. This factor helps users determine how efficiently the simulation is running, with values close to 1.0 indicating that the simulation is running in real-time. If the RTF is greater than 1.0, it suggests that the simulation is running faster than real time, while a value less than 1.0 indicates that it is running slower.

In addition to RTF, it also displays **Sim Time**, which shows the simulation's elapsed time. This is useful for tracking the progression of events in the simulation and synchronizing it with other systems. The **Real Iterations** and **Sim Iterations** counters provide insight into the number of iterations performed by the simulation per second for real-time and simulated time, respectively. Monitoring these values helps users assess the efficiency of the simulation and diagnose performance issues if the simulation is not proceeding as expected.

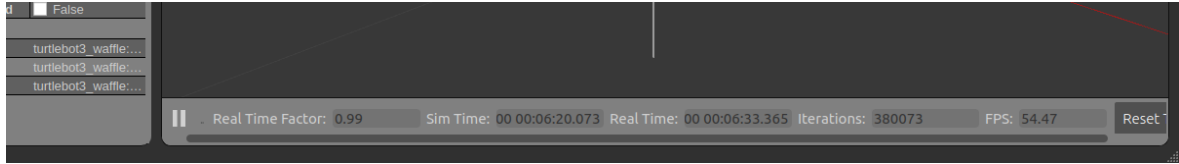


Figure 4.62: Gazebo Graphical User Interface lower part

The top part of the Gazebo GUI (fig. 4.63) provides several essential controls and information related to the simulation's overall operation. At the top-left corner, users will find the **File** menu, which includes options to open, save, and manage Gazebo worlds. It also allows users to load and save configurations, and set preferences for simulation settings.

In addition, the top part of the GUI provides options for manipulating the lighting within the simulation. Users can select from **Point**, **Spot**, and **Directional** lights to illuminate different parts of the world. Point lights emit light in all directions from a single point, Spot lights create a focused beam of light, and Directional lights simulate sunlight, casting parallel rays in a specific direction. This allows for realistic and customizable lighting in the simulation environment.

The **Selection Light** tool enables users to adjust the lighting between two or more objects in the simulation, offering more control over how objects are illuminated and how shadows are cast in the environment.

Moreover, the GUI allows users to switch between different **perspective views**, such as top-down, side, or camera views, to inspect and interact with the simulation from different angles.



Figure 4.63: Gazebo Graphical User Interface top part

Right-clicking on an object in the Gazebo simulation environment brings up a context-sensitive menu that allows users to perform a variety of actions to interact with and manipulate the object. The options available in this menu include:

1. **Move To:** This option allows users to move a selected object to a specified location in the simulation world. After selecting this option, users can click on a point in the world to which the object will be moved, making it easier to position objects accurately within the environment.

2. **Follow:** The Follow option enables users to make the camera follow a particular object in the simulation. When this option is activated, the camera will automatically track the

movement of the selected object, allowing users to observe its behavior from a fixed perspective, which can be useful when testing robot movements or simulating dynamic scenarios.

**3. Edit:** The Edit option opens a set of interactive tools that allow users to modify the properties of the selected object, such as its position, orientation, size, and material properties.

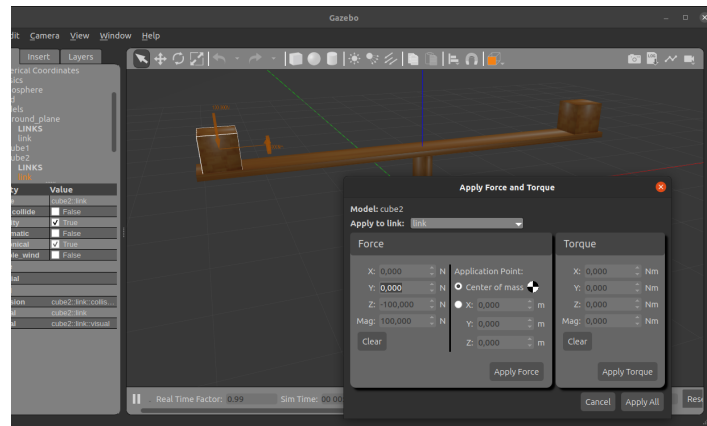


Figure 4.64: Example of force applied on one side of a seesaw in gazebo

**4. Apply Force/Torque:** This option gives users the ability to apply a force or torque to the selected object, which is especially useful for testing how the object reacts under various physical conditions. fig. 4.64 shows how users can specify the direction, magnitude, and duration of the applied force or torque, allowing for controlled experiments on the object's behavior within the simulated environment.

#### 4.60.2 RViz

**RViz** (ROS Visualization) is an open-source 3D visualization tool that provides real-time graphical representations of robotic systems.

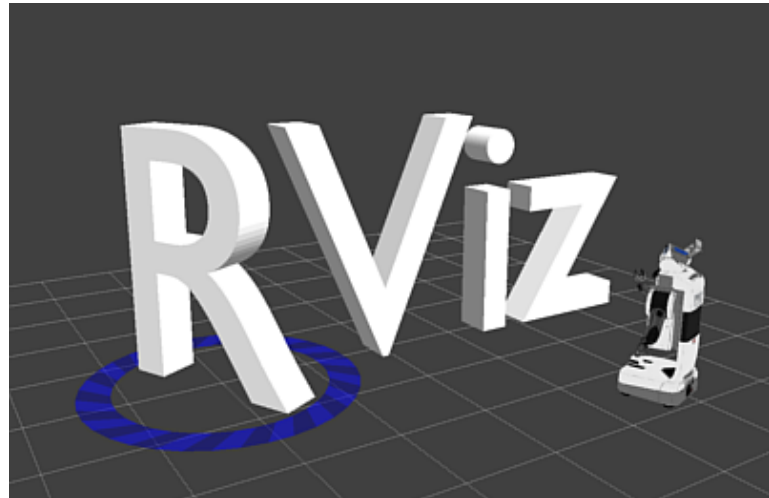


Figure 4.65: Rviz (Ros Visualization)

It serves two primary purposes: (1) visualizing sensor data, such as LiDAR scans, point clouds from 3D sensors (e.g., RealSense, Kinect), and camera images, in an intuitive 3D environment; and (2) enabling interactive control of robotic systems by sending commands like navigation goals or waypoints. In this project, RViz was used extensively to monitor sensor outputs, validate navigation algorithms, and debug the robot's behavior during simulation. Its seamless integration with ROS topics and plugins made it an indispensable tool for visualizing complex data streams, such as laser range finder (LRF) distances and Point Cloud Data (PCD), without requiring additional programming.

## **4.61 IMPLEMENTATION OF THE SIMULATION ENVIRONMENT**

The implementation of the simulation environment is carefully designed to ensure that the results obtained in simulation closely reflect real-world performance. Most simulation parameters, including the robot's dimensions, mass properties, sensor specifications, and environmental conditions, are selected to match the specifications outlined in the competition framework. This ensures that the robot developed based on simulation results can seamlessly transition from a virtual setting to real-world deployment with minimal modifications.

A key aspect of this simulation is the accurate modeling of robot dynamics, actuator characteristics, and sensor behavior. The physics engine parameters, such as friction coefficients, and sensor noise models, are tuned to replicate real-world conditions as precisely as possible. Additionally, the design of the virtual environment, including terrain features, obstacles, and lighting conditions, is configured to match the competition setup. This allows for realistic testing and validation of navigation and control algorithms.

By incorporating these considerations, the simulation provides a reliable testing ground for developing and refining motion planning, perception, and control strategies. This approach reduces the gap between simulated and real-world performance, ensuring that insights gained from the virtual environment translate effectively to the physical robot. However, like any simulation-based approach, there are inherent advantages and disadvantages when using simulators to test robot behaviors, as discussed in [20].

Despite these limitations, careful selection of simulation parameters—such as physics engine settings, sensor noise models, and environmental conditions—enhances the accuracy of the virtual testing environment. The following subsections detail the implementation of the robot model, world design, and control and sensor integration, outlining how each component contributes to achieving a high-fidelity simulation.

#### 4.61.1 Robot Model ( URDF/SDF )

#### 4.61.2 World Design

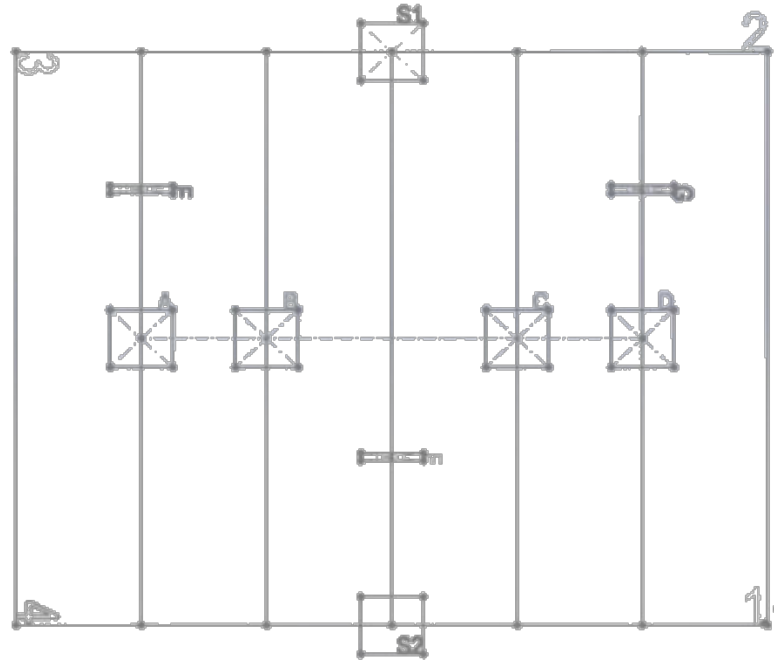


Figure 4.66: Teknofest competition real map layout

The simulation environment was designed to replicate the competition layout in fig. 4.66 as closely as possible. The terrain was constructed using custom models to accurately mimic the competition area, incorporating key features such as a **white wooden floor**, **black lines for path following**, **platforms for load dynamics**, **obstacles**, and **friction variations** to simulate real-world conditions.

In Gazebo, this entire environment is saved as a world file, which includes all the models, textures, and configurations necessary to recreate the simulation. The world file is written in the Simulation Description Format (SDF), an XML-based format used to describe the properties and behavior of objects and environments in Gazebo.

SDF allows for easy definition of physical properties, geometries, lighting, and sensor configurations, making it a versatile and standard way to represent simulation environments. The SDF format ensures that the simulation setup is reproducible, shareable, and can be modified easily for different testing scenarios. Similar to the Unified Robot Description Format (URDF), which is used for defining robot models in ROS, SDF provides a structured way to describe objects and environments. While URDF focuses primarily on robot kinematics and geometry, SDF is more comprehensive and extends its capabilities to encompass the full environment, including physics properties, sensor configurations, and world dynamics.

The world file was made through the design of individual SDF files for each model within the environment. These individual models were first defined with each having its own dedicated SDF file. Once the models were completed, they were then integrated into a single world file, named `competition_area.world` (in SDF format). This world file serves as the central configuration, bringing together all the models, their properties, and the environment settings.

#### 4.61.2.1 Environment Layout

Designed to replicate the competition area closely the world contains custom models were created to represent key elements of the space, ensuring that the robot's interaction with its surroundings is as realistic as possible. Key components of the environment layout include the following:

- **Flooring and Pathways:** A **white wooden floor** was chosen to resemble the actual competition floor, providing a surface with consistent friction properties for the robot to interact with. The **black lines for path following** were added on the white floor according to the competition specifications, acting as markers for the robot's autonomous navigation algorithms to follow.

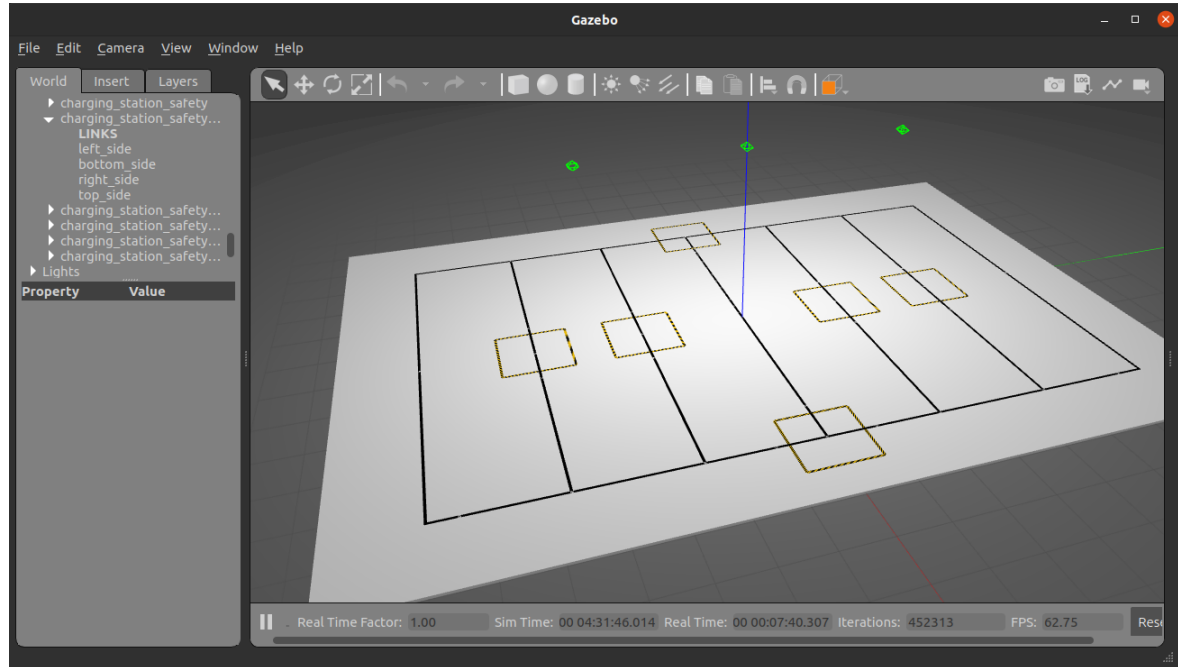


Figure 4.67: White wooden floor with black lines in gazebo

The black lines for path following were also incorporated into the simulation as individual objects within the Gazebo environment. Each line was treated as a separate

model to allow easy modifications, such as adjusting their position, length, or orientation, without affecting the rest of the simulation environment. This modular approach makes it easier to tweak the lines for different test scenarios, ensuring flexibility and quick adjustments during development and testing.

```
1      ...
2      <wall_time>1738074256 296636706</wall_time>
3      <iterations>117145</iterations>
4      <model name='black_line'>
5          <pose>0 0 0.06 0 -0 0</pose>
6          <scale>1 1 1</scale>
7          <link name='line_link'>
8              <pose>0 0 0.06 0 -0 0</pose>
9              <velocity>0 0 0 0 -0 0</velocity>
10             <acceleration>0 0 0 0 -0 0</acceleration>
11             <wrench>0 0 0 0 -0 0</wrench>
12         </link>
13     </model>
14     <model name='black_line_clone'>
15         <pose>0 2.33333 0.06 0 -0 0</pose>
16         <scale>1 1 1</scale>
17         <link name='line_link'>
18             <pose>0 2.33333 0.06 0 -0 0</pose>
19             <velocity>0 0 0 0 -0 0</velocity>
20             <acceleration>0 0 0 0 -0 0</acceleration>
21             <wrench>0 0 0 0 -0 0</wrench>
22         </link>
23     </model>
24     <model name='black_line_clone_0'>
25         <pose>0 4.666 0.06 0 -0 0</pose>
26         <scale>1 1 1</scale>
27         ...
```

Additionally, QR code tags were placed at key locations, such as loading/unloading points, stations, and before turns, to provide the robot with precise location information.

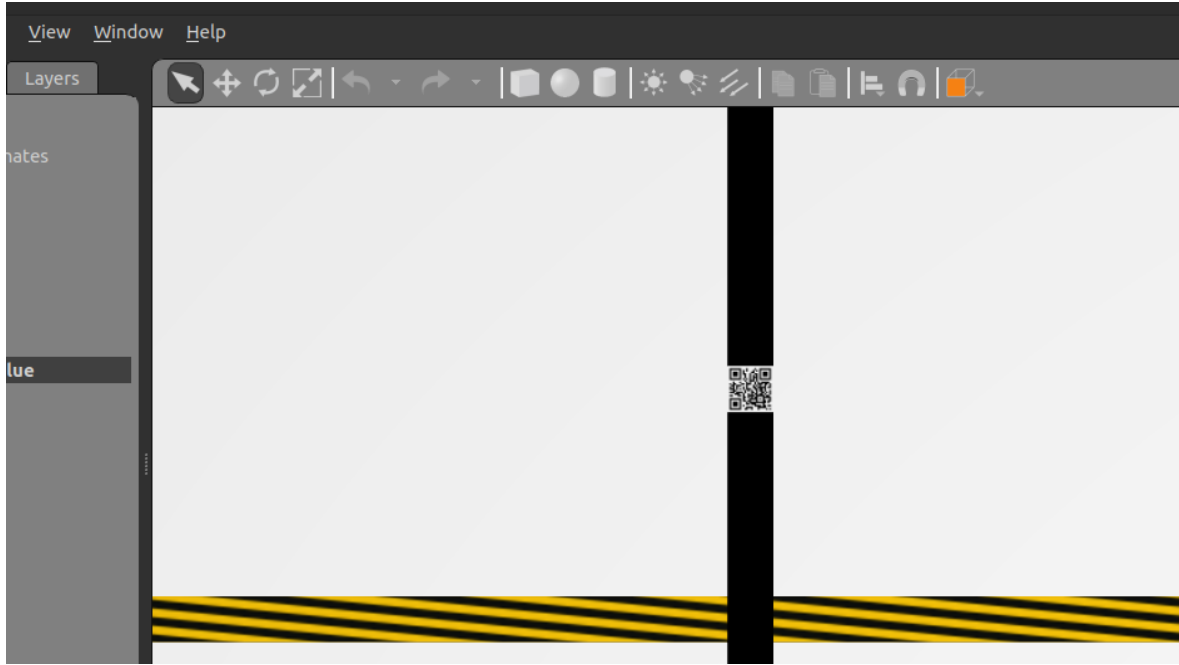


Figure 4.68: Example of Qr Code tag before a loading point

the `<friction>` tag parameters of the white floor, displayed in fig. 4.67, were specifically chosen to replicate the conditions of wood flooring. The static friction coefficient was set to 0.4, representing the resistance to the start of sliding motion. The dynamic friction coefficient was set to 0.35, modeling the friction while the robot is already sliding. These values were carefully selected to ensure that the robot's interactions with the floor behave as expected in real-world conditions.

The `<static>` tag ensures that the floor model is fixed and does not move during the simulation. The `<pose>` tag is used to position the floor in the environment, placing it just slightly above the ground to avoid collision with the ground plane. The `<collision>` tag defines the physical properties for detecting interactions, including the geometry of the floor as a box shape. Additionally, the `<visual>` tag defines how the floor appears in the simulation, with the material set to a white color to represent the wooden floor's appearance.

```

1   <model name='wooden_floor'>
2     <static>1</static>
3     <pose>0 0 0.01 0 -0 0</pose>
4     <link name='floor_link'>
5       <collision name='floor_collision'>
6         <geometry>
7           <box>
8             <size>12 17 0.1</size>
9           </box>
10          </geometry>
11          <max_contacts>10</max_contacts>
12          <surface>
13            <contact>
14              <ode/>
15            </contact>
16            <bounce/>
17            <friction>
18              <ode/>
19              <torsional>
20                <ode/>
21              </torsional>
22              <static_friction>0.4</static_friction> <!-- Adjusted for
23                ← wooden floor -->
24              <dynamic_friction>0.35</dynamic_friction> <!-- Adjusted
25                ← for wooden floor -->
26            </friction>
27          </surface>
28        </collision>
29        <visual name='floor_visual'>
30          <geometry>
31            <box>
32              <size>12 17 0.1</size>
33            </box>
34          </geometry>
35          <material>
36            <ambient>1 1 1 1</ambient>
37            <diffuse>1 1 1 1</diffuse>
38          </material>

```

```

39      <enable_wind>0</enable_wind>
40      <kinematic>0</kinematic>
41    </link>
42  </model>
43

```

- **Obstacles and Load Platforms:** The environment includes various **obstacles** such as walls and dynamic objects, designed to challenge the robot's obstacle avoidance and path planning abilities. **Platforms for load dynamics** were added to simulate loading and unloading points, where the robot needs to deliver or pick up objects, mimicking the tasks required during the competition.



Figure 4.69: Competition area bounded by ad hoardings

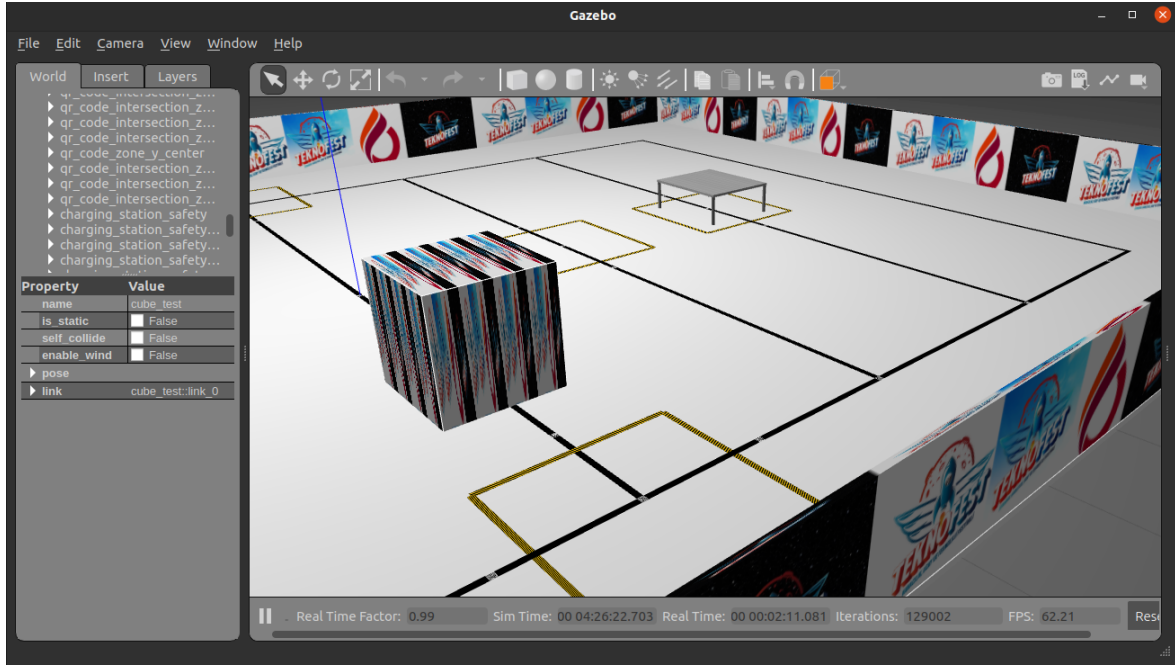


Figure 4.70: Competition area line interrupted by permanent obstacle

The platform model, as shown in the code snippet, is designed with a central table surface and four supporting legs. The structure is composed of multiple links, where each leg is defined separately, and they are all connected to the table surface through fixed joints.

The `<model>` tag defines the platform, which includes the physical properties and geometric shapes of the table and legs.

Each link, such as `table_surface` and `front_left_leg`, `front_right_leg`, etc., has its own inertial properties (`<inertial>`) and a collision geometry defined under the `<collision>` tag.

For instance, the `<collision>` tag for the table surface has a defined friction property, with a coefficient of 1 for both static and dynamic friction, simulating a high-friction surface. This friction coefficient can be adjusted to simulate the specific characteristics of a material, such as wood or metal.

Each leg is represented as a cylinder, with its own collision properties and friction settings, ensuring realistic interaction with the robot during the simulation. The friction properties of each leg are defined in the `<surface>` `<friction>` section using `ode` settings. These settings also include the `<bounce>` and `<contact>` properties, which help simulate realistic physical interactions between the objects in the environment. Each of these legs also has a specific pose and position in the simulation.

The joints, such as `front_left_joint`, connect each leg to the table surface with a

fixed type, meaning that the legs do not move relative to the table. The pose of each joint defines the exact position and orientation of the legs in the simulation environment.

The overall pose of the platform, including its position in the world, is defined at the end of the model, specifying the coordinates and orientation for the platform's placement in the simulation.

Additionally, the platform's visual properties are set using the `<visual>` tag, with a custom material representing the surface texture, such as stainless steel, applied to the table's surface. To ensure accurate physical interactions, the `<inertial>` tag defines the mass and moments of inertia of the platform and its legs, ensuring a realistic response to forces and torques applied during the simulation. The `<collision>` tag specifies the geometric shape used for physics calculations, which may be simplified compared to the visual model to improve computational efficiency while maintaining accurate contact and collision responses. The platform's legs also incorporate both `<collision>` and `<inertial>` properties, allowing them to contribute to the overall stability of the structure while ensuring that the physics engine correctly simulates interactions such as impacts, weight distribution, and external forces acting on the table.

```

1   <model name='platform'>
2     <link name='table_surface'>
3       <inertial>
4         <mass>13.98</mass>
5         <inertia>
6           <ixx>0.1</ixx>
7           <ixy>0</ixy>
8           <ixz>0</ixz>
9           <iyy>0.1</iyy>
10          <iyz>0</iyz>
11          <izz>0.1</izz>
12        </inertia>
13        <pose>0 0 0 0 -0 0</pose>
14      </inertial>
15      <collision name='surface_collision'>
16        <pose>0 0 0.367 0 -0 0</pose>
17        <geometry>
18          <box>
19            <size>1.1 0.95 0.03</size>
20          </box>

```

```
21      </geometry>
22      <surface>
23          <friction>
24              <ode>
25                  <mu>1</mu>
26                  <mu2>1</mu2>
27          </ode>
28          <torsional>
29              <ode/>
30          </torsional>
31      </friction>
32      <contact>
33          <ode/>
34      </contact>
35      <bounce/>
36      </surface>
37      <max_contacts>10</max_contacts>
38  </collision>
39  ...
```

```

1      ...
2      <visual name='surface_visual'>
3          <pose>0 0 0 0.367 0 -0 0</pose>
4          <geometry>
5              <box>
6                  <size>1.1 0.95 0.03</size>
7              </box>
8          </geometry>
9          <material>
10         <script>
11             <uri>model://platform/materials/scripts</uri>
12             <uri>model://platform/materials/textures</uri>
13             <name>stainless_steel_texture</name>
14         </script>
15     </material>
16 </visual>
17 ...
18

```

```

1      ...
2      <link name='front_left_leg'>
3          <inertial>
4              <mass>2.796</mass>
5              <inertia>
6                  <ixx>0.01</ixx>
7                  <ixy>0</ixy>
8                  <ixz>0</ixz>
9                  <iyy>0.01</iyy>
10                 <iyz>0</iyz>
11                 <izz>0.01</izz>
12             </inertia>
13             <pose>0 0 0 0 -0 0</pose>
14         </inertial>
15         <collision name='collision'>
16             <pose>0.53 0.455 0.1835 0 -0 0</pose>
17             <geometry>
18                 <cylinder>
19                     <radius>0.02</radius>

```

```

20           <length>0.367</length>
21       </cylinder>
22   </geometry>
23   <surface>
24       <friction>
25           <ode>
26               <mu>1</mu>
27               <mu2>1</mu2>
28           </ode>
29           <torsional>
30               <ode/>
31           </torsional>
32       </friction>
33   <contact>
34       <ode>
35           <kp>100000</kp>
36           <kd>1</kd>
37       </ode>
38   </contact>
39   <bounce/>
40 </surface>
41   <max_contacts>10</max_contacts>
42 </collision>
43 <visual name='visual'>
44     <pose>0.53 0.455 0.1835 0 -0 0</pose>
45     <geometry>
46         <cylinder>
47             <radius>0.02</radius>
48             <length>0.367</length>
49         </cylinder>
50     </geometry>
51     <material>
52         <script>
53             <uri>file:///media/materials/scripts/gazebo.material</uri>
54             <name>Gazebo/Grey</name>
55         </script>
56     </material>
57 </visual>
58 <self_collide>0</self_collide>

```

```
59      <enable_wind>0</enable_wind>
60      <kinematic>0</kinematic>
61    </link>
62    <link name='front_right_leg'>
63      <inertial>
64        <mass>2.796</mass>
65        <inertia>
66          <ixx>0.01</ixx>
67          <ixy>0</ixy>
68          <izz>0</izz>
69        . . .
```

Ad hoardings and obstacles were incorporated into the environment using a simple yet effective approach. A cube shape was used to create the basic geometry of these objects, with their dimensions adjusted to meet the specific requirements of the simulation. Textures were applied to the cubes to give them the appearance of real-world hoardings and obstacles, ensuring that they serve as realistic visual and physical barriers within the simulation.

These objects were assigned physical properties, such as mass and friction, and collisions were defined to ensure proper interaction with the robot. The hoardings and permanent obstacles were defined as static objects to prevent them from moving during the simulation, ensuring they remain fixed in place as intended.

The following lines provide an example of the visual and collision properties for the hoardings. These lines demonstrate how the hoardings models were assigned the name `cube_test` during the individual SDF design phase of the world. The code defines the geometry, textures, and physical properties for the hoardings.

```

1     ...
2     model name='cube_test_clone_clone'>
3         <link name='link_0'>
4             <inertial>
5                 <mass>1</mass>
6                 <inertia>
7                     <ixx>0.166667</ixx>
8                     <ixy>0</ixy>
9                     <ixz>0</ixz>
10                    <iyy>0.166667</iyy>
11                    <iyz>0</iyz>
12                    <izz>0.166667</izz>
13                </inertia>
14                <pose>0 0 0 0 -0 0</pose>
15            </inertial>
16            <pose>-0 -0 0 0 -0 0</pose>
17            <visual name='visual'>
18                <pose>0 0 0 0 -0 0</pose>
19                <geometry>
20                    <box>
21                        <size>0.05 16.9 1</size>
22                    </box>
23                </geometry>
24                <material>
```

```

25      <lighting>1</lighting>
26      <script>
27          <uri>model://cube_test/materials/scripts</uri>
28          <uri>model://cube_test/materials/textures</uri>
29          <name>teknofest_logo</name>
30      </script>
31      <shader type='pixel' />
32  </material>
33  <transparency>0</transparency>
34  <cast_shadows>1</cast_shadows>
35 </visual>
36 <collision name='collision'>
37     <laser_retro>0</laser_retro>
38     <max_contacts>10</max_contacts>
39     <pose>0 0 0 0 -0 0</pose>
40     <geometry>
41         <box>
42             <size>0.05 16.9 1</size>
43         </box>
44     </geometry>
45     <surface>
46         <friction>
47             <ode>
48                 <mu>1</mu>
49                 <mu2>1</mu2>
50                 <fdir1>0 0 0</fdir1>
51                 <slip1>0</slip1>
52                 <slip2>0</slip2>
53             </ode>
54             <torsional>
55                 <coefficient>1</coefficient>
56                 <patch_radius>0</patch_radius>
57                 <surface_radius>0</surface_radius>
58                 <use_patch_radius>1</use_patch_radius>
59             <ode>
60                 <slip>0</slip>
61             </ode>
62         </torsional>
63     </friction>
64     <bounce>

```

```

65      <restitution_coefficient>0</restitution_coefficient>
66      <threshold>1e+06</threshold>
67    </bounce>
68    <contact>
69      <collide_without_contact>0</collide_without_contact>
70      <collide_without_contact_bitmask>1</collide_without_c ]>
71      ↳  ontact_bitmask>
72      <collide_bitmask>1</collide_bitmask>
73    <ode>
74      <soft_cfm>0</soft_cfm>
75      <soft_erp>0.2</soft_erp>
76      <kp>1e+13</kp>
77      <kd>1</kd>
78      <max_vel>0.01</max_vel>
79      <min_depth>0</min_depth>
80    </ode>
81    <bullet>
82      <split_impulse>1</split_impulse>
83      <split_impulse_penetration_threshold>-0.01</split_i ]>
84      ↳  mpulse_penetration_threshold>
85      <soft_cfm>0</soft_cfm>
86      <soft_erp>0.2</soft_erp>
87      <kp>1e+13</kp>
88      <kd>1</kd>
89    </bullet>
90  </contact>
91  </surface>
92 </collision>
93 <self_collide>0</self_collide>
94 <enable_wind>0</enable_wind>
95 <kinematic>0</kinematic>
96 </link>
97 <static>1</static>
98 <allow_auto_disable>1</allow_auto_disable>
99 <pose>-6.06431 0.045196 0.46 0 -0 0</pose>
100 <enable_wind>0</enable_wind>
</model>
...

```

The design of the QR codes followed a similar approach to most other models in

the world. Each QR code was represented by a textured cube, with textures made to resemble the unique images that contain the right location information.

```

1      <?xml version='1.0'?>
2      <sdf version='1.7'>
3          <model name='qr_code'>
4              <link name='link_0'>
5                  <pose>0 0 0 0 0 0</pose>
6                  <visual name='visual'>
7                      <pose>0 0 0 0 0 0</pose>
8                      <geometry>
9                          <box>
10                             <size>0.05 0.05 0.001</size>    <!-- Increase size
11                                -- of the box -->
12                         </box>
13                     </geometry>
14                     <material>
15                         <lighting>1</lighting>
16                         <script>
17                             <uri>model://qr_code/materials/scripts</uri>
18                             <uri>model://qr_code/materials/textures</uri>
19                             <name>qr_code_content</name>
20                         </script>
21                         <shader type='pixel' />
22                     </material>
23                     <transparency>0</transparency>
24                     <cast_shadows>1</cast_shadows>
25                 </visual>
26             </link>
27             <static>1</static>
28             <allow_auto_disable>1</allow_auto_disable>
29         </model>
30     </sdf>

```

The above SDF code represents the individual model of the QR code. It contains only visual information and does not define any physical properties, as the QR code is used for location identification within the simulation. The model is defined as static to prevent movement and includes a texture that simulates the unique QR code image.

To simplify the referencing of points on the map in fig. 4.66, the area was divided into several well-defined zones. This subdivision facilitates the robot's movement management by allowing specific tasks to be assigned to each zone. All tags were then

assigned unique values based on their relative locations to critical points such as loading/unloading stations, intersections, and key passage points. These QR codes serve as essential reference markers, enabling the robot's localization system to determine its exact position and adjust its trajectory accordingly.

- **Station 1:** Located between corners 1 and 4, this zone represents station 1.
- **Station 2:** Located between corners 2 and 3, this zone corresponds to station 2.
- **Zone A:** Contains the loading/unloading point A.
- **Zone B:** Contains the loading/unloading point B.
- **Zone C:** Contains the loading/unloading point C.
- **Zone D:** Contains the loading/unloading point D.

The QR code's content is specified using a `material` element in the SDF model. The `qr_code_contents.material` file defines the texture that represents the unique image of the QR code. The `material` file is referenced within the `visual` element of the QR code model using a `<script>` tag, which links to the texture folder containing the QR code images.

By separating the texture definition into the `qr_code_contents.material` file, it allows for easy updates and maintenance of the QR codes used in the simulation without needing to modify the main model files.

```
1      ...
2      {
3          texture_unit
4          {
5              texture intersection_zone_c_station_1.png
6          }
7      }
8  }
9
10
11 material intersection_zone_c_station_2
12 {
13     technique
14     {
15         pass
16         {
17             texture_unit
```

```

18     {
19         texture intersection_zone_c_station_2.png
20     }
21 }
22 }
23 }

24

25 material intersection_zone_d_station_1
26 {
27     technique
28     {
29         pass
30         {
31             texture_unit
32             {
33                 texture intersection_zone_d_station_1.png
34             }
35         }
36     }
37 }

38

39 material intersection_zone_d_station_2
40 {
41     technique
42     {
43         pass
44         {
45             texture_unit
46             {
47                 texture intersection_zone_d_station_2.png
48             }
49         }
50     }
51 }

52

53 material intersection_zone_x_station_1
54 {
55     technique
56     {
57         pass

```

```

58     {
59         texture_unit
60         {
61             texture intersection_zone_x_station_1.png
62         }
63     }
64 }
65
66
67 material intersection_zone_x_station_2
68 {
69     technique
70     {
71         pass
72         {
73             texture_unit
74             {
75                 texture intersection_zone_x_station_2.png
76             }
77         }
78     }
79 }
80
81 material intersection_zone_y_station_1
82 {
83     technique
84     {
85         pass
86         {
87             texture_unit
88             {
89                 texture intersection_zone_y_station_1.png
90             }
91         }
92     }
93 }
94
95 material intersection_zone_y_station_2
96 {
97     technique

```

```

98     {
99         pass
100        {
101            texture_unit
102            {
103                texture intersection_zone_y_station_2.png
104            }
105        }
106    }
107 }
108 ...

```



Figure 4.71: Qr code tag placed at the intersection of line of the zone C and the station 2

- **Random Clutter Generation:** Procedural generation methods were used to add **random clutter**, simulating items or obstacles that may appear unpredictably, requiring the robot to adapt to ever-changing environments.
- **Real-World Simulation Features:** External environmental factors such as wind were not simulated, as the competition setting assumes an indoor environment. Basic ambient and directional lighting were configured to ensure consistent visibility for sensor-based perception tasks.

Poor lighting similar to conditions in fig. 4.72 can introduce challenges such as motion blur, sensor noise, and shadow distortions, making it difficult for cameras to differentiate objects from the background. Additionally, extreme lighting conditions, such as glare or overexposure, may lead to incorrect sensor readings, affecting navigation and localization accuracy.

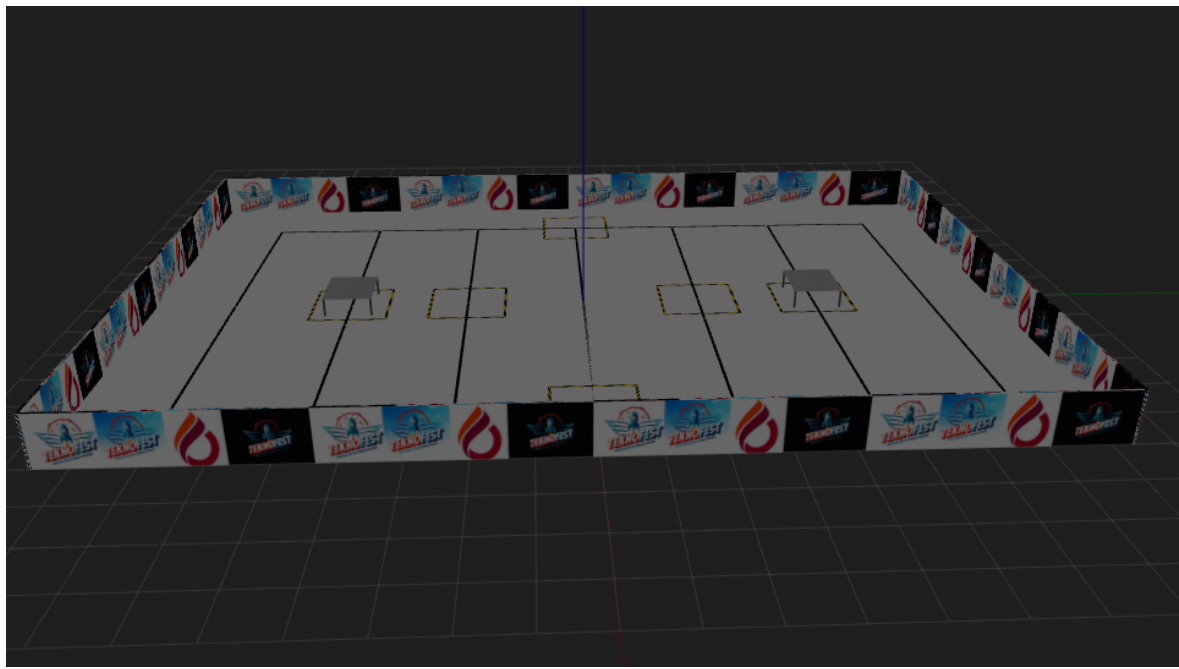


Figure 4.72: Effect of lighting conditions in simulation environment

On the other hand, good lighting shown in fig. 4.73 improves the performance of vision-based tasks such as object detection and QR code recognition. A well-lit environment with uniform brightness and minimal shadows ensures that cameras and sensors receive clear and consistent data, reducing the chances of misinterpretation due to varying illumination levels.

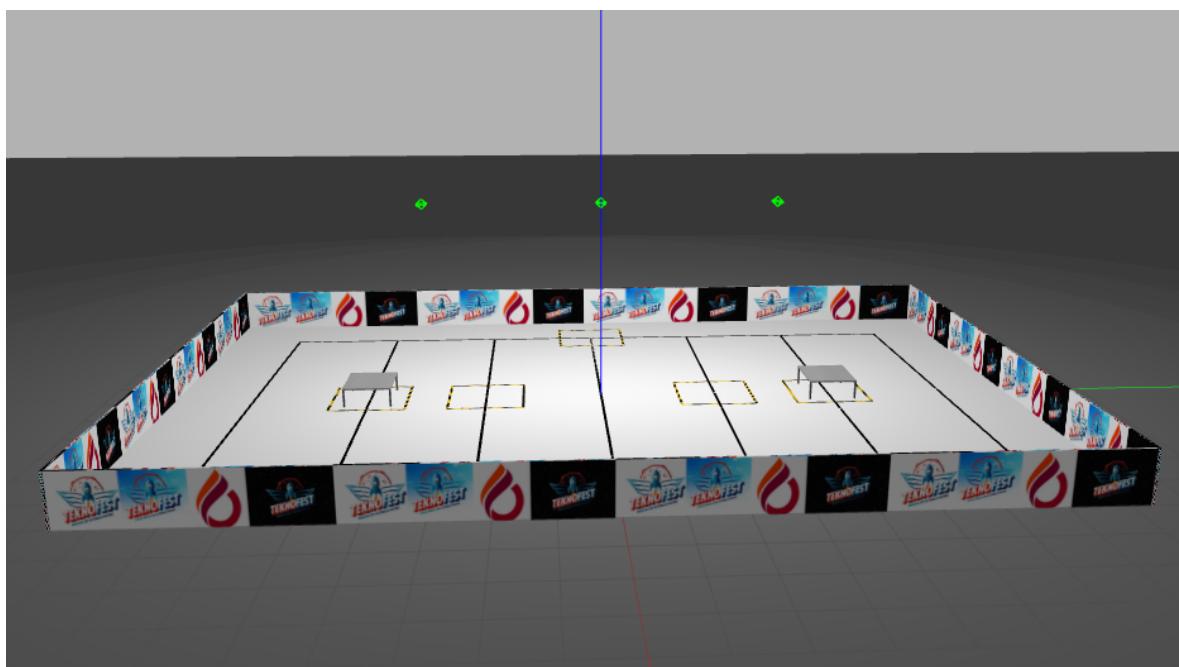


Figure 4.73: Effect of lighting conditions in simulation environment

#### **4.61.2.2 Physics Configuration**

I should maybe say more about this

#### **4.61.2.3 Realism Enhancements**

Is it necessary ?

#### **4.61.3 Control and sensor Integration**

You should be able to do something about this

### **4.62 VALIDATION OF THE SIMULATION**

### **4.63 CHALLENGES AND SOLUTIONS**

## 4.64 URDF

## 4.65 UNDERSTANDING ROBOT MODELING USING URDF

The Unified Robot Description Format (URDF) is an XML file format used to describe the physical properties of a robot in robotics applications, in particular within the Robot Operating System (ROS) ecosystem. It specifies the robot structure (links, joints, sensors and actuators etc.)

URDF can represent the kinematic and dynamic description of the robot, the visual representation of the robot, and the collision model of the robot. The following tags are the commonly used URDF tags to compose a URDF robot model:

### 4.65.1 link:

The link tag represents the single link of a robot. Using this tag, we can model a robot link and its properties. The modeling includes the size, the shape, and the color; it can even import a 3D mesh to represent the robot link. We can also provide the dynamic properties of the link, such as the inertial matrix and the collision properties. The syntax is as follows:

```
1 <link name="<name of the link>">
2   <inertial>.....</inertial>
3   <visual> .....</visual>
4   <collision>.....</collision>
5 </link>
```

The following is a representation of a single link. The Visual section represents the real link of the robot, and the area surrounding the real link is the Collision section. The Collision section encapsulates the real link to detect a collision before hitting the real link:

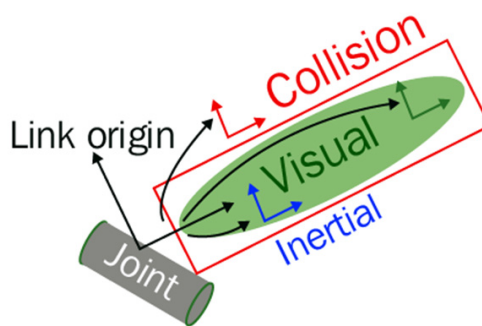


Figure 4.74: A visualization of the URDF link [1]

#### 4.65.2 joint:

The `joint` tag represents a robot joint. We can specify the kinematics and dynamics of the joint and set the limits of the joint movement and its velocity. The joint tag supports the different types of joints, such as revolute, continuous, prismatic, fixed, floating, and planar. The syntax is as follows:

```
1 <joint name="<name of the joint>">
2   <parent link="link1"/>
3   <child link="link2"/>
4   <calibration .... />
5   <dynamics damping = ..../>
6   <limit effort = ..../>
7   </joint>
```

A URDF joint is formed between two links; the first is called the Parent link, and the second is called the Child link. Note that a single joint can have a single parent and multiple children at the same time. The following is an illustration of a joint and its links:

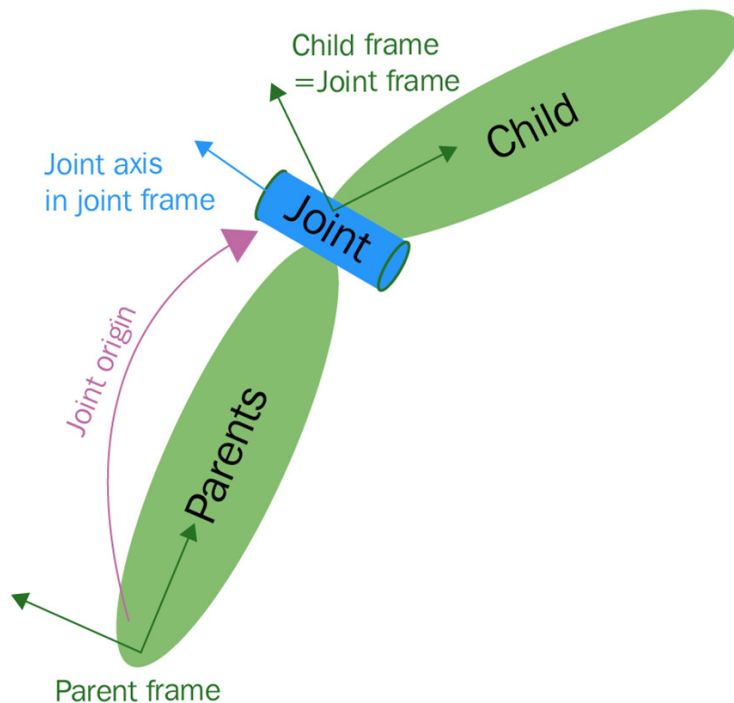


Figure 4.75: A visualization of the URDF joint [1]

#### 4.65.3 robot:

This tag encapsulates the entire robot model that can be represented using URDF. Inside the robot tag, we can define the name of the robot, the links, and the joints of the robot. The syntax is as follows:

```
1 <robot name="<name of the robot>">
2   <link> .....
```

A robot model consists of connected links and joints. Here is a visualization of the robot model:

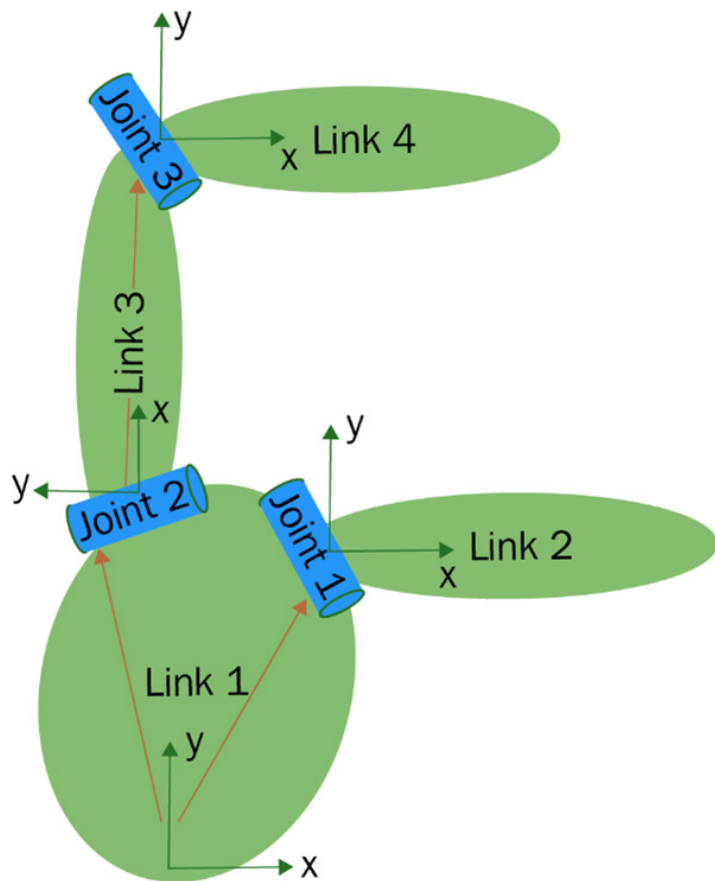


Figure 4.76: A visualization of a robot model with joints and links [1]

#### 4.65.4 gazebo:

This tag is used when we include the simulation parameters of the Gazebo simulator inside the URDF. We can use this tag to include gazebo plugins, gazebo material properties, and more. The following shows an example that uses gazebo tags:

```
1 <gazebo reference="link_1">
2   <material>Gazebo/Black</material>
3 </gazebo>
```

You can find more about URDF tags at [wiki.ros \[21\]](#). We are now ready to use the elements listed earlier to create a new robot from scratch. In the next section, we are going to create a new ROS package containing a description of the different robots.

#### 4.65.5 Adding physical and collision properties to a URDF model

Before simulating a robot in a robot simulator, such as Gazebo or CoppeliaSim, we need to define the robot link's physical properties, such as geometry, color, mass, and inertia, as well as the collision properties of the link. Good robot simulations can be obtained only if the robot dynamic parameters (for instance, its mass, inertia, and more) are correctly specified in the urdf file. In the following code, we include these parameters as part of the base\_link:

```
1 <link name="base_link">
2 ...
3   <collision>
4     <geometry>
5       <box size="0.9 0.85 0.5"/>
6     </geometry>
7       <origin xyz="0.0 0.0 0.025" rpy="0.0 0.0 0.0"/>
8   </collision>
9   <inertial>
10    <origin xyz="0 0 0" rpy="0 0 0"/>
11    <mass value="35"/>
12    <inertia ixx="3.2" ixy="0.0" ixz="0.0" iyy="4" iyz="0.0" izz="$3.9"/>
13  </inertial> </link>
```

#### 4.65.6 Transmission:

The `transmission` tag is used to model the relationship between a robot's joints and actuators (such as motors, servos, or other mechanical devices that provide motion). It defines how power or motion is transferred from an actuator to a joint in the robot's structure. The `<transmission>` tag usually works with `<joint>` and `<actuator>` tags to specify how an actuator controls the motion of the robot's joints:

```
1   <robot name="example_robot">
2
3     <!-- Define the joint -->
4     <joint name="joint_1" type="revolute">
5       <parent link="base_link"/>
6       <child link="link_1"/>
7       <axis xyz="0 0 1"/>
8       <limit effort="10.0" velocity="1.0" lower="-1.57" upper="1.57"/>
9     </joint>
10
11    <!-- Define the transmission -->
12    <transmission name="trans_1">
13      <type>transmission_interface/SimpleTransmission</type>
14      <joint name="joint_1"/>
15      <actuator name="motor_1">
16        <mechanicalReduction>100.0</mechanicalReduction> <!-- Gear ratio
17          ↳ -->
18        </actuator>
19      </transmission>
20
21      <!-- Define the actuator (motor) -->
22      <gazebo>
23        <plugin name="motor_1_plugin" filename="libgazebo_motor_plugin.so">
24          <motor_type>electric</motor_type>
25          <max_power>100.0</max_power>
26        </plugin>
27      </gazebo>
28
29    </robot>
```

<joint>: The joint joint\_1 connects the base\_link to link\_1 and allows rotational movement. It has limits on effort and velocity. <transmission>: The transmission trans\_1 links joint\_1 to the actuator (motor motor\_1). It uses the SimpleTransmission type. <mechanicalReduction>: The actuator has a gear reduction of 100:1, meaning for every 100 rotations of the motor, the joint will rotate once. <actuator>: This specifies the motor (motor\_1) that will control joint\_1. <gazebo>: This block includes a Gazebo plugin (libgazebo\_motor\_plugin.so) to simulate the motor's behavior in a Gazebo simulation environment, with specific motor properties like motor\_type and max\_power.

### in summary:

#### Dependencies for URDF Simulation in Gazebo

Step	Component	Effect if Missing
1	Links (<link>)	The robot has no physical structure, making it impossible to define shapes, visualize, or interact with physics.
2	Joints (<joint>)	The robot will be completely rigid. No movement or articulation between parts is possible.
3	Inertia (<inertial>)	Gazebo will generate warnings or unstable behavior because the physics engine relies on mass and inertia properties to simulate motion correctly.
4	Collision (<collision>)	The robot will pass through objects and not interact with the environment physically. It may also affect contact-based sensors.
5	Gazebo Plugin (<plugin>)	The robot cannot interact with Gazebo's physics, controllers, or sensors. Features like camera feeds, joint control, and custom physics will not work.
6	Gazebo Simulation	The robot cannot be tested in a realistic environment with physics, gravity, and other external forces. It remains a static model without dynamic behavior.
7	Transmission (<transmission>)	Motors will not work. Even if controllers are added, they will not be able to apply forces to move the joints.

Table 4.21: Essential Dependencies for Simulating a URDF in Gazebo

## 4.66 CREATING URDF MODEL

After learning about URDF and its important tags, we can start some basic modeling using URDF. The robot's URDF model comprises eight rigid links and seven joints, designed to balance geometric simplicity with functional accuracy. The central chassis (base\_link), modeled as a rectangular prism, forms the structural foundation. Symmetrically attached to

this base are two cylindrical wheels (`left_wheel`, `right_wheel`), each connected via continuous rotation joints to enable differential steering. A vertical lifting mechanism, represented as a cylinder (`lifting_mechanism`), extends upward from the chassis through a prismatic joint, providing linear motion for height adjustment. Rigidly mounted atop this actuator is a box-shaped platform (`platform`), secured by a fixed joint to ensure stability. Three sensor units—two cameras (`camera1`, `camera2`) and a LiDAR (`lidar`)—are modeled as compact boxes and affixed to the platform through additional fixed joints, ensuring precise perceptual alignment. By prioritizing minimalistic shapes (cylinders for rotational elements, boxes for planar surfaces) and logical joint configurations (two continuous, one prismatic, and four fixed), the design achieves computational efficiency while retaining fidelity to the robot's core mechanical and sensing capabilities.

#### 4.66.1 Understanding robot modeling using xacro

The flexibility of URDF reduces when we work with complex robot models. Some of the main features that URDF is missing include simplicity, reusability, modularity, and programmability. If someone wants to reuse a URDF block 10 times in their robot description, they can copy and paste the block 10 times. If there is an option to use this code block and make multiple copies with different settings, it will be very useful while creating the robot description. The URDF is a single file and we can't include other URDF files inside it. This reduces the modular nature of the code. All code should be in a single file, which reduces the code's simplicity. Also, if there is some programmability, such as adding variables, constants, mathematical expressions, and conditional statements in the description language, it will be more userfriendly. Robot modeling using xacro meets all of these conditions. Some of the main features of xacro are as follows:

- **Simplify URDF:** xacro is a cleaned-up version of URDF. It creates macros inside the robot description and reuses the macros. This can reduce the code length. Also, it can include macros from other files and make the code simpler, more readable, and more modular.
- **Programmability:** The xacro language supports a simple programming statement in its description. There are variables, constants, mathematical expressions, conditional statements, and more that make the description more intelligent and efficient.

Instead of `.urdf`, we need to use the `.xacro` extension for xacro files. Here is an explanation of the xacro code:

```

1 <?xml version="1.0"?>
2 <robot xmlns:xacro="http://www.ros.org/wiki/xacro" name="my_robot">
```

These lines specify a namespace that is needed in all xacro files to parse the xacro file. After specifying the namespace, we need to add the name of the xacro file. In the next section.

#### 4.66.2 Using properties

Using xacro, we can declare constants or properties that are the named values inside the xacro file, which can be used anywhere in the code. The main purpose of these constant definitions is that instead of giving hardcoded values on links and joints, we can keep constants, and it will be easier to change these values rather than finding the hardcoded values and then replacing them. An example of using properties is given here. We declare the length and radius of the base link and the pan link. So, it will be easy to change the dimension here rather than changing the values in each one:

```

1 <!-- body value -->
2 <xacro:property name="base_length" value="0.9" />
3 <xacro:property name="base_width" value="0.85" />
4 <xacro:property name="base_hight" value="0.5" />
5
6 <!-- Wheel values -->
7 <xacro:property name="wheel_r" value="0.15" />
8 <xacro:property name="wheel_length" value="0.05" />
9
10 <!-- Lidar values -->
11 <xacro:property name="lidar_r" value="0.1" />
12 <xacro:property name="lidar_l" value="0.05" />
```

We can use the value of the variable by replacing the hardcoded value with the following definition:

```

1 <link name="base_link">
2   <visual>
3     <geometry>
4       <box size="${base_length} ${base_width} ${base_hight}" />
5     </geometry>
6     <origin xyz="0.0 0.0 ${base_hight/2.0}" rpy="0.0 0.0 0.0" />
```

```

7     <material name="green"/>
8   </visual>
```

Here, the value 0.9, is replaced with "base\_length", and "0.85" is replaced with "base\_width".

#### 4.66.3 Using the math expression

We can build mathematical expressions inside \$ using basic operations such as +, -, \*, /, unary minus, and parentheses. Exponentiation and modulus are not supported yet. The following is a simple math expression used inside the code:

```

1   <link name="platform_link">
2     <visual>
3       <geometry>
4         <box
5           → size="${base_length/1.5} ${base_width/1.5} ${base_hight/8}"/>
6         </geometry>
7         <origin xyz="0.0 0.0 0" rpy="0.0 0.0 0.0"/>
8         <material name="green"/>
   </visual>
```

#### 4.66.4 Using macros

One of the main features of xacro is that it supports macros. We can use xacro to reduce the length of complex definitions. Here is a xacro definition we used in our code to specify inertial values:

```

1   <xacro:macro name="box_inertia" params="m l w h xyz rpy">
2     <inertial>
3       <origin xyz="${xyz}" rpy="${rpy}"/>
4       <mass value="${m}"/>
5       <inertia ixx="${(m/12)*(h*h + l*l)}" ixy="0.0" ixz="0.0"
6         → iyy="${(m/12)*(w*w + l*l)}" iyz="0.0"
7         → izz="${(m/12) * (w*w + h*h)}"/>
   </inertial>
 </xacro:macro>
```

Here, the macro is named box\_inertia, and its parameters are {m ,l ,w ,h ,xyz ,rpy}. we can pass these parameters as a values or as a xacro property:

```

1 <xacro:box_inertia m="5.0" l="${2*base_length}" w="${2*base_width}"
2   ↵ h="${2*base_hight}" xyz="0.0 0.0 ${base_hight/2.0}"
3   ↵ rpy="0.0 0.0 0.0"/>

```

#### 4.66.5 Including other xacro files

We can extend the capabilities of the robot xacro by including the xacro definition of sensors using the xacro:include tag. The following code snippet shows how to include a sensor definition in the robot xacro:

```

1 <xacro:include filename="$(find ros_robot_pkg)/urdf/definition.xacro"/>

```

Here, we include a xacro file to call the definitions and the constants.

### 4.67 VISUALIZING THE 3D ROBOT MODEL IN RVIZ

After designing the URDF, we can view it on RViz. We can create a launch file and put the following code into the launch folder:

```

1 <launch>
2 <param name="robot_description" command=
3   ↵ "$(find xacro)/xacro $(find the_pkg_name)/.../my_robot.urdf.xacro"
4   ↵ />
5 <node name="robot_state_publisher" pkg="robot_state_publisher"
6   ↵ type="robot_state_publisher" />
7 <node name="rviz" pkg="rviz" type="rviz"
8   ↵ args="-d $(find the_pkg_name)/rviz/config.rviz" />
9 <node name="joint_state_publisher" pkg="joint_state_publisher"
10  type="joint_state_publisher"/>
11 <node name="joint_state_publisher_gui" pkg="joint_state_publisher_gui"
12   ↵ type="joint_state_publisher_gui"/>
13 <!-- Controller Manager -->
14   <node name="controller_spawner" pkg="controller_manager"
15     ↵ type="spawner" respawn="false" output="screen"
16       args="diff_drive_controller" />
17 </launch>

```

The `<launch>` tag is the root tag that defines the entire launch file. All the nodes and parameters that need to be launched are specified within this tag.

The `<param>` tag sets the `robot_description` parameter, which specifies the URDF or XACRO file that contains the robot's description. In this case, the `command` attribute runs the `xacro` tool to process the `my_robot.urdf.xacro` file located in the package specified by the `the_pkg_name`.

The `<node>` tag launches the `robot_state_publisher` node. This node reads the robot's description and publishes the state of the robot (e.g., joint positions, transformations) to ROS topics. It uses the `robot_description` parameter that was set earlier.

The next `<node>` tag launches RViz, the visualization tool used to display the robot in a 3D environment. The `args` attribute specifies a pre-configured RViz setup file (`config.rviz`) located in the package `the_pkg_name`. This setup is used for visualizing the robot model and its movements.

The subsequent `<node>` tags launch two joint state publisher nodes.

The `joint_state_publisher` node publishes the joint states (such as the positions of robot joints) to ROS topics. The `joint_state_publisher_gui` node includes a graphical user interface (GUI) that allows users to interactively control the joint states of the robot.

Finally, the `<node>` tag for the `controller_spawner` node is responsible for spawning and managing robot controllers. The node is part of the `controller_manager` package, and the `spawner` executable is used to spawn a controller, in this case, `diff_drive_controller`. The `respawn` attribute is set to `false`, so the node will not automatically respawn if it crashes. The `output` attribute ensures that the output from the node is printed to the screen.

We can launch the model using the following command:

```
1 roslaunch the_pkg_name launch_file_name.launch
```

If everything works correctly, we will get a pan-and-tilt mechanism in RViz, as shown here:

#### 4.67.1 Interacting with joints in Rviz

In the previous version of ROS, the GUI of `joint_state_publisher` was enabled thanks to a ROS parameter called `use_gui`. To start the GUI in the launch file, this parameter had to be set to true before starting the `joint_state_publisher` node. In the current version of ROS, launch files should be updated to launch `joint_state_publisher_gui` instead of using `joint_state_publisher` with the `use_gui` parameter.

We can see that an extra GUI came along with RViz; it contains sliders to control the Whell joints and the lifting platform joint. This GUI is called the Joint State Publisher Gui node and belongs to the `joint_state_publisher_gui` package:

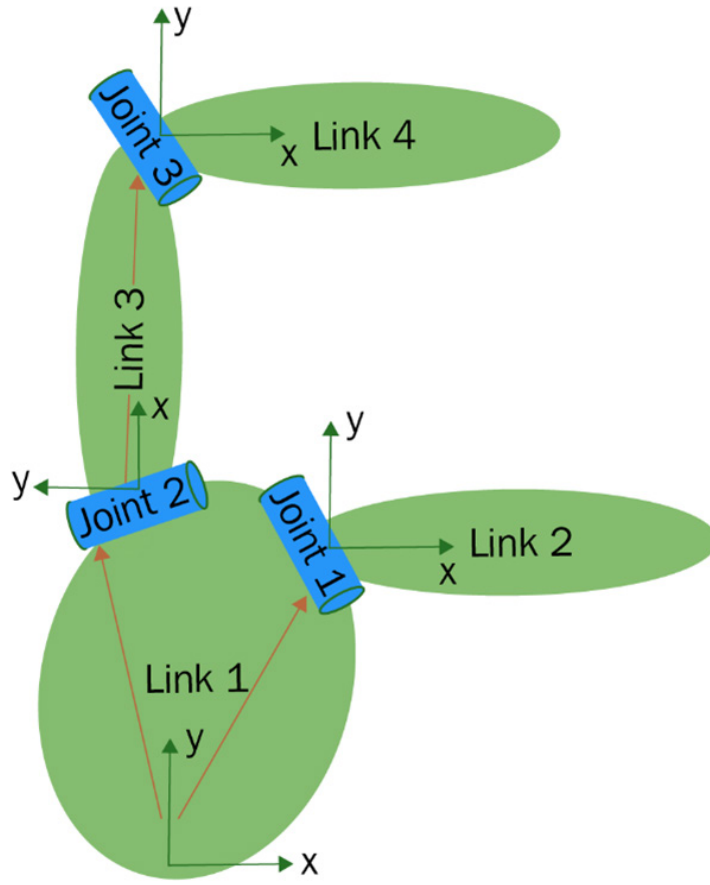


Figure 4.77: A visualization of a robot model with Rviz

```

1 <node name="joint_state_publisher_gui" pkg="joint_state_
2 publisher_gui" type="joint_state_publisher_gui" />

```

We can include this node in the launch file using the following statement. The limits of pan-and-tilt should be mentioned inside the joint tag:

```

1 <joint name="platform_lift_joint" type="prismatic">
2   <origin xyz="0.0 0.0 ${base_hight / 2}" rpy="0.0 0.0 0.0"/>
3   <parent link="base_link"/>
4   <child link="platform_lift_link"/>
5   <axis xyz="0 0 1"/> <!-- Movement along the Z-axis -->
6   <!-- Motion range and limits -->
7   <limit lower="0.0" upper="${base_hight/2}" effort="50"
8     velocity="1.0"/>
</joint>

```

The `<limit>` tag defines the limits of effort, velocity, and angle. In this scenario, effort is the maximum force supported by this joint, expressed in Newton; lower and upper indicate the lower and upper limits of the joint, in radians for the revolute joint and in meters for the prismatic joints. velocity is the maximum joint velocity expressed in m/s. The following screenshot shows the user interface that is used to interact with the robot joints: In this user

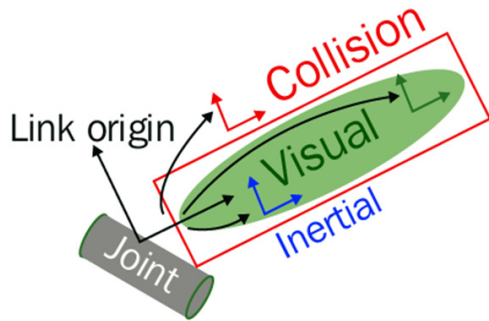


Figure 4.78: The joint level of the platform lifting mechanism

interface, we can use the sliders to set the desired joint values. The basic elements of a urdf file have been discussed. In the next section, we will add additional physical elements to our robot model.

## **4.68 NAVIGATION**

Autonomous navigation is a rapidly growing field and has become a pivotal area of research and application in robotics, with numerous applications in industries such as transportation, manufacturing, and warehousing. One of the fundamental tasks for autonomous robots is the ability to navigate their environment independently with minimal human intervention, that is a crucial factor or a key milestone for the development of intelligent systems capable of interacting with the real world. Among the various techniques used for autonomous navigation, line following remains one of the most essential and widely researched methods, especially for mobile robots, where the robot must track a specific line on the ground. While it may appear straightforward, line following involves a variety of challenges, including sensor calibration, precise control of the robot's motors, and handling of unpredictable environmental factors. For this project the primary objective was eventually designing and developing a simulated robot capable of accomplishing a specific task while following a line and avoiding obstacles and maintain accurate control over its movements within a simulated environment using the **Robot Operating System (ROS)**, which is widely used in both research and industry due to its flexibility, modularity, and wide range of libraries and tools. ROS provides a powerful framework for developing and simulating robotic applications.

### **METHODS USED TO DESIGN:**

It is necessary outline the methodology used to design the robot, its navigation system, and the simulation environment. The method should cover both the hardware (even though it's simulated) and software design, as well as the control algorithms used to ensure the robot follows the line autonomously.

The design of the autonomous line-following robot involved a series of methodical steps to ensure the successful integration of hardware (simulated), software (ROS-based), and control algorithms to enable autonomous navigation. The following sections describe the approach taken to design and implement the robot and its navigation system in the simulation environment.

## **4.69 FOR LINE DETECTION AND FOLLOWING:**

### **4.69.1 Camera-based Vision Method:**

Using **cameras** for line-following is an advanced approach in robotics, where the robot uses visual information to detect and track a line or path. This technique, often referred to as

**vision-based line following**, involves utilizing computer vision algorithms to process images captured by the robot's camera and determine the robot's position relative to the line. To use a camera for line-following, the camera is needed to be mounted on the robot, typically facing downward or slightly tilted to capture the surface on which the line is drawn which is the case with the robot used for this project.

This process was accomplished through many steps via simulation such :

## SETTING UP THE SIMULATION ENVIRONMENT

The simulation platform was set up with the following components:

- **Robot Model:** The robot in the simulation should have a camera mounted on it. The robot model could be a differential-drive robot, a mobile platform with wheels, or a more complex robot with additional sensors. **The robot model used is a differential-drive mobile robot.**
- **Camera Sensor:** Simulated cameras in the environment will capture images of the ground, where the line is located. The camera was set up to view downward, directly in front of the robot.
- **Line (Path):** lines on the ground can be created in the simulation. The line can be straight, curved, or even follow a more complex path. For this project black lines were drawn within the world created in Gazebo.
- **Simulator:** The simulation platform used is:

**Gazebo:** Commonly used with **ROS** (Robot Operating System) for robot control and visualization.

## IMAGE PROCESSING FOR LINE DETECTION

After setting up the simulated robot and camera, the robot will need to process the images captured by the camera to detect the line. The core part of this system involves **image processing** and **vision algorithms**.

- **Steps for Image Processing:**
- **Capture Image from the Camera:**

In the simulation, it is necessary to get access to the camera feed in real-time. With **ROS**, there can be subscriber to the camera's image topic such **/camera/rgb/image\_raw**

- **Convert the Image to Grayscale:**

**grayscale conversion** can be used to reduce the complexity of the image. Since the line will typically have a contrasting colour (black or white), working with a grayscale image makes it easier to detect the line.

- **Thresholding** will convert the grayscale image into a binary image where the line is white (or black) and the background is the opposite colour. You can use a simple threshold or adaptive thresholding for better results in varying lighting conditions.

- **Detect the Line:**

Once the image is binary, **edge detection**, **contour detection**, or **Hough Transform** can be used to detect the line. For instance, you can use **Hough Line Transform** to detect straight lines. For the project they were combined and used together for line detection.

- **Determine the Robot's Position Relative to the Line:**

The **centroid** of a detected line is calculated to measure or estimate how far the robot is from the centre of the line in the camera frame.

#### 4.69.2 1.2 Control Algorithm for Line Following

Once the line is detected, the robot needs to be controlled to follow it. The basic principle is to adjust the robot's steering based on its position relative to the line. PID Controller algorithm can be used to keep the robot following line in a steady way.

The **PID (Proportional-Integral-Derivative)** controller is commonly used in line-following robots.

- **Proportional:** The steering correction is proportional to how far the robot is from the line's centre.
- **Integral:** This helps eliminate accumulated errors over time.
- **Derivative:** This predicts and reacts to the rate of change in the error (speed of deviation).

#### 4.69.3 1.3 Integrating the Line Following with the Simulator

Finally, the image processing and control algorithms needed to be integrated into the simulation environment. With ROS this integration is usually made through Gazebo. When **ROS** is used the robot can be set up with a simulated camera and subscribe to the camera feed. ROS provides libraries like CV BRIDGE to convert the ROS image messages into

## 4.70 FOR BUILDING MAP

### 4.70.1 LIDAR

The map was built using SLAM (Simultaneous Localization and Mapping) in a simulation thanks to the lidar sensor. Using LIDAR (Light Detection and Ranging) with SLAM (Simultaneous Localization and Mapping) is a common and effective approach for building a map of an environment while simultaneously localizing the robot within that environment. In ROS, LIDAR is often used as the primary sensor for SLAM, especially for 2D SLAM algorithms like GMapping and Hector SLAM. The algorithm used for SLAM was GMapping in this project. The lidar can be used to avoid obstacles as well.

### 4.70.2 QR Code Scanning

QR Code Detection with OpenCV was used, the OpenCV's QRCodeDetector detects and decode QR codes in the robot's camera feed. The QR code are used to help the robot to navigate autonomously, the QR code information to know its current position and calculate the closest path to the destination.

After building the map , it will be saved for autonomous navigation purpose.

## 4.71 REALISTIC CONSTRAINTS

## 4.72 COMPUTATIONAL-POWER-AND-RESOURCES

### 4.72.1 cpu-and-gpu-limitations

- CPU Limitations: Simulations, especially those involving complex algorithms like SLAM or sensor fusion, can be CPU-intensive. The computational demand increases with the complexity of the robot's tasks, such as real-time mapping, localization, or decision-making. A limited CPU performance could cause delays, lag, or even make real-time processing difficult.
- GPU Constraints: If you're using computer vision algorithms (e.g., QR code recognition, camera-based line-following), a GPU can greatly accelerate image processing. However, not all simulations leverage GPU power, and if the GPU is not sufficient or not utilized properly, the simulation could run slower or experience bottlenecks.

### 4.72.2 memory-ram-constraints

- High Memory Usage: Simulations that involve large environments, dense sensor data

(such as LIDAR point clouds), or high-resolution images can require a significant amount of RAM. If the memory usage exceeds the available capacity, it can lead to slow performance, crashes, or even the inability to run the simulation at all.

- Data Storage for Sensor Data: Storing large amounts of sensor data (e.g., from LIDAR, cameras, IMUs) generated during a simulation can strain the system's storage, especially if you need to log or save sensor outputs for later analysis. In a large-scale simulation, this could be a limiting factor.

#### 4.72.3 real-time-performance

- Real-Time Simulation Constraints: Achieving real-time performance in simulations can be difficult, especially when dealing with complex tasks such as real-time SLAM or path planning. The simulation might not run at the required frame rate (e.g., 30Hz or higher), leading to delays in robot control and decision-making.
- Simulation Time vs Real Time: If the simulation is not running at real-time speed (1:1 with physical time), it can make it harder to validate time-sensitive behaviors. For example, a robot using SLAM may not update its map fast enough in a simulation that runs too slowly, affecting navigation and decision-making in real-world applications.

### 4.73 COMPLEXITY-OF-THE-SIMULATED-ENVIRONMENT

#### 4.73.1 size-and-detail-of-the-simulation

- Environmental Complexity: Large and complex simulated environments with many dynamic obstacles, detailed textures, and various types of surfaces can be computationally expensive. More detailed environments require more processing power to render, simulate physics, and handle sensor data.
- Realistic Physics: Physics engines in simulations (e.g., Gazebo, V-REP) simulate the interactions between the robot and the environment, including forces like friction, gravity, and object collisions. While necessary for realistic testing, these physics simulations can be computationally demanding, especially in dynamic environments with many objects.

#### 4.73.2 dynamic-objects-and-movements

- Real-Time Object Simulation: When simulating environments with moving objects (e.g., pedestrians or vehicles), the computation required to simulate their motion and

interactions with the robot can add significant overhead. This becomes particularly challenging if multiple objects are moving in complex patterns at the same time.

## 4.74 SIMULATING-SENSOR-DATA

### 4.74.1 a.-sensor-data-processing-load

- LIDAR and Point Cloud Data: LIDAR sensors generate large amounts of data, especially in 3D environments. Processing the point cloud data in real time requires significant computing resources, particularly when applying algorithms like SLAM to build and update maps. The more data points and the larger the map, the more processing power is required.
- Camera Data for Visual Processing: Cameras generate high-resolution images that need to be processed for tasks like QR code detection or line-following. Processing these images (especially with advanced computer vision techniques such as feature detection or deep learning) can be computationally expensive. Depending on the image resolution and the complexity of the detection algorithms, this could put a strain on the available computing resources.

### 4.74.2 real-time-sensor-fusion

- Combining Data from Multiple Sensors: If you are fusing data from multiple sensors (e.g., combining LIDAR, IMU, camera data for SLAM), the computational load increases significantly. Sensor fusion algorithms, such as Kalman Filters or particle filters, need to process data from all sensors in real time, which may not be feasible with limited computational resources.

## 4.75 ALGORITHMIC-CONSTRAINTS

### 4.75.1 a.-computational-cost-of-slam

- SLAM Algorithm Complexity: Algorithms used for SLAM (like Extended Kalman Filters, GraphSLAM, or particle filters) are computationally expensive, especially when the robot has to map a large area in real-time. As the environment grows, the number of calculations needed to maintain and update the map increases, potentially leading to slower performance or the need for more powerful hardware.
- Map Size and Resolution: The higher the resolution and accuracy of the map, the more computational resources are required to store and update it. Large maps with high-

detail features demand significant memory and processing power to handle updates, store the data, and process localization.

#### 4.75.2 b.-path-planning-and-decision-making

- Complex Path Planning Algorithms: Path planning algorithms, such as A\*, RRT, or D\* algorithms, may require substantial computational resources depending on the complexity of the environment. If your robot is navigating a large or cluttered environment, calculating collision-free paths in real-time becomes a challenge, especially if there are many dynamic obstacles to avoid.
- Decision-Making Algorithms: When the robot makes decisions based on sensor input, running machine learning algorithms or decision trees to determine the next action (e.g., go towards a QR code or follow a line) can also be computationally expensive. Depending on the complexity of the logic, this could limit the speed and responsiveness of the simulation.

### 4.76 SIMULATION-SOFTWARE-LIMITATIONS

#### 4.76.1 simulation-engine-efficiency

- Performance of the Simulation Engine: Different simulation platforms (Gazebo, V-REP, Webots, etc.) have varying levels of efficiency. Some simulators might be highly optimized for certain types of robots or algorithms, while others may be slower or require more resources to simulate complex systems. Choosing the right simulation platform for your application is critical for balancing performance and accuracy.
- Plugin Overhead: Many simulators rely on plugins for additional functionality (e.g., camera sensors, LIDAR). The more plugins you add or the more complex the plugin behavior, the more computational overhead is introduced. This can affect simulation performance, especially in large-scale environments or real-time applications.

#### 4.76.2 parallelization-and-multithreading

- Limited Parallel Processing: Not all simulation environments or algorithms are well-optimized for parallel processing, which means that tasks may not fully utilize multi-core CPUs or GPUs. For example, in simulations involving real-time SLAM, the ability to parallelize sensor data processing or SLAM computation can significantly reduce the computational load, but not all algorithms or environments support this effectively.

- Threading Issues: Running multiple processes (e.g., sensor readings, actuator control, SLAM) in parallel in a simulation may introduce issues such as deadlock or race conditions if not properly managed. This can lead to slower simulation times or unresponsive behavior in your robot model.

## 4.77 SIMULATING-REAL-TIME-CONSTRAINTS

### 4.77.1 real-time-control-vs.-simulation-speed

- Synchronization Issues: Achieving true real-time performance is difficult in a simulation. Many simulations allow you to adjust the time scale (e.g., running the simulation faster than real time for testing), but this introduces the issue that the control algorithms might not have the same timing constraints they would in a real robot. Ensuring that the simulation runs with a fixed time step, synchronized with the robot's control loops, is essential but can be computationally demanding.
- Hardware-in-the-loop (HIL) Simulation: When integrating real hardware with a simulator (e.g., for testing SLAM on real sensors), the latency and real-time computation required can cause performance bottlenecks. This is especially true if communication between the simulation and physical robot hardware is slow or not synchronized properly.

# Chapter 5

## CONCLUSION AND FUTURE WORKS

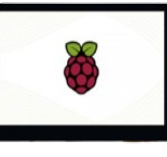
### 5.1 COST

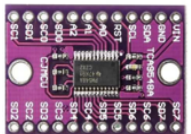
Table 5.1: here is the list of components

Components	Quantity	Price(per Unit)	ref
Raspberry Pi 4 8GB RAM	1	3127.03 ₺	
ESP32-S3-DevKitC-1-N8R8 - ESP32-S3-WROOM-1	2	1220 ₺	
Closed Loop Stepper Driver V4.1 0-8.0A 24-48VDC CL57T	2	1186 ₺	
Motororbit Weight Sensor 120 kg	2	768.2 ₺	
Weight Sensor - Load Sensor 50Kg.	4	29.7 ₺	
Load Cell Amplifier - HX711	4	27.3 ₺	

BTS7960B 40 Amp Motor Driver Board	1	188.82 ₺	
Barcode Scanner Module 1D/2D Codes Reader	1	1261.83 ₺	
QTRXL-MD-01A Reflectance Sensor Array	4	90.57 ₺	
Gravity: HUSKYLENS	1	1723.14 ₺	
IMU Sensor / 9 Axis MPU9255 IMU and Barometric Sensor (Low Power)	1	1058.31 ₺	
RPLIDAR - 360 degree Laser Scanner Development Kit	1	5029.72 ₺	
TXS0108E 8 Channel Voltage Level Transducer	4	40 ₺	
The VL53L0X is a time-of-flight (ToF) distance sensor	10	101.76 ₺	
UV Solder Mask	3	180.78 ₺	
LM2596HV/LM2576 Voltage Regulator for Multiple power supply	4	36.09 ₺	

Aluminum heatsink	2	439 ₺	
5V 8 Channel Relay Card	1	154.68 ₺	
P Series Nema 23 Closed Loop Stepper Motor 2Nm(283.28oz.in) with Electromagnetic Brake	2	2971.78 ₺	
EG Series Planetary Gearbox Gear Ratio 20:1 Backlash 20arc-min for 10mm Shaft Nema 23 Stepper Motor	2	1642 ₺	
Shaft Sleeve Adaptor 11mm to 8mm for NMRV30 Worm Gearbox	4	35 ₺	
Single Output Shaft for NMRV30 Worm Gearbox	4	121.37 ₺	
Double Output Shaft for NMRV30 Worm Gearbox	4	121.37 ₺	
NEMA 23 Stepper Motor Vibration Damper	4	243.74 ₺	
Nema 23 Bracket for Stepper Motor	4	243.74 ₺	
Nema 23 Flange for ISC And ISD Series Drivers	3	175.28 ₺	

AWG 20 High-flexible with Shield Layer Stepper Motor Cable	2	43.25 ₺	
TP-Link TL-WR840N	1	569 ₺	
Raspberry Pi 4.3 Inch Capacitive Touch Screen DSI Interface 800"480	1	1750.28 ₺	
Nema 8R 5W 87dB 90X39mm Speaker	1	108.11 ₺	
Nema RS232 to Bluetooth Series Adapter	2	455 ₺	
12V 70 AH AGM BATTERY	1	5000 ₺	
Battery Chargers 6V/2A 12V/2A Full Automatic Smart Battery	1	642.99 ₺	
RS232 Adapter Cable to USB 2.0	2	453.65 ₺	
Motor and encoder extension cable kit	2	351 ₺	
DC 12V Electric Linear Actuator Force 6000N	1	2479 ₺	

WM-045 DC-DC 150W Voltage Booster	1	521.04 ₺	
Motororbit DC-DC 1500W 30A Voltage Boost Module	1	881.76 ₺	
TCA9548A I2C Çoklayıcı / Multiplexer Kartı	1	40.66 ₺	
3B Printer Limit Switch	2	37.07 ₺	
Drn956 16mm Acil - Stop Switch (Kafa 27mm)	1	145.08 ₺	

# **APPENDIX**

## **Bearing Specifications**

- Bearing Type: Deep Groove Ball Bearing (NSK 6201)
- Inner Diameter: 12 mm
- Outer Diameter: 32 mm
- Load Capacity: 7.28 kN

## **Material Properties**

- AISI 1045 Steel: Yield Strength = 530 MPa, Ultimate Tensile Strength = 625 MPa
- AISI 52100 Chrome Steel: High Hardness (Rockwell C 60-67), Wear Resistance

## Bibliography

- [1] L. Joseph and J. Cacace, Mastering ROS for Robotics Programming: Design, build, and simulate complex robots using the Robot Operating System. Packt Publishing Ltd, 2018.
- [2] S. K. Das, “Design and methodology of line follower automated guided vehicle-a review,” International Journal of Science Technology & Engineering, vol. 2, no. 10, pp. 9–13, 2016.
- [3] A. J. Moshayedi, L. Jinsong, and L. Liao, “Agv (automated guided vehicle) robot: Mission and obstacles in design and performance,” Journal of Simulation and Analysis of Novel Technologies in Mechanical Engineering, vol. 12, no. 4, pp. 5–18, 2019.
- [4] S. A. Reveliotis, “Conflict resolution in agv systems,” Iie Transactions, vol. 32, no. 7, pp. 647–659, 2000.
- [5] L. Shengfang and H. Xingzhe, “Research on the agv based robot system used in substation inspection,” in 2006 International Conference on Power System Technology, pp. 1–4, IEEE, 2006.
- [6] Á. Cservesnák, “Further development of an agv control system,” in Vehicle and Automotive Engineering 2: Proceedings of the 2nd VAE2018, Miskolc, Hungary, pp. 376–384, Springer, 2018.
- [7] O. Motor, “Brushless dc motors for agv designs,” 2023. Accessed: October 15, 2023.
- [8] L. Engineering, “Autonomous guided vehicles (agv),” 2024. Accessed: 2025-02-07.
- [9] A. M. Controls, “Servo drives for agvs: Top 5 benefits,” 2024. Accessed: 2025-02-07.
- [10] M. P. Groover, Automation, production systems, and computer-integrated manufacturing. Pearson Education India, 2016.
- [11] R. N. Jazar and R. N. Jazar, “Road dynamics,” Advanced Vehicle Dynamics, pp. 297–350, 2019.

- [12] M. F. Ashby, “Materials selection in mechanical design,” Metallurgia Italiana, vol. 86, pp. 475–475, 1994.
- [13] ROS Community, “Robot operating system (ros).” <https://www.ros.org/>, 2025. Accessed: 2023-10-12.
- [14] N. Koenig and A. Howard, “Design and use paradigms for gazebo, an open-source multi-robot simulator,” in IEEE/RSJ International Conference on Intelligent Robots and Systems (IROS), (Sendai, Japan), pp. 2149–2154, IEEE, Sep 2004.
- [15] R. L. Smith, “Open dynamics engine.” <https://bitbucket.org/odedevs/ode/>, 2016. Online.
- [16] R.-T. P. Simulation, “Bullet physics library.” <http://bulletphysics.org/wordpress/>, 2016. Online.
- [17] “Simbody: Multibody physics api.” <https://simtk.org/home/simbody/>, 2016. Online.
- [18] G. T. G. Lab and H. R. Lab, “Dart (dynamic animation and robotics toolkit).” <http://dartsim.github.io/>, 2016. Online.
- [19] OGRE3D, “Object-oriented graphics rendering engine.” <http://www.ogre3d.org/>, 2016. Online.
- [20] F. R. Lera, F. C. Garcia, G. Esteban, and V. Matellan, “Mobile robot performance in robotics challenges: Analyzing a simulated indoor scenario and its translation to real-world,” in Proc. 2014 Second International Conference on Artificial Intelligence, Modelling and Simulation, pp. 149–154, 2014.
- [21] R. Wiki, “urdf/xml - ros wiki,” 2023.
- [22] M. P. Groover, “Fundamentals of modern manufacturing materials,” 2019.
- [23] P. F. Brown, S. A. Della Pietra, V. J. Della Pietra, and R. L. Mercer, “The mathematics of statistical machine translation: Parameter estimation,” Computational linguistics, vol. 19, no. 2, pp. 263–311, 1993.
- [24] F. Can and E. A. Ozkarahan, “Concepts and effectiveness of the cover-coefficient-based clustering methodology for text databases,” ACM Transactions on Database Systems (TODS), vol. 15, no. 4, pp. 483–517, 1990.
- [25] METTLER TOLEDO Group, “Mettler toledo group.” Accessed: [Insert Access Date if needed].

- [26] E. Zainescu, “Calculation of single level scissor lift,” 2019.
- [27] TIMKEN, “Deep groove ball bearing catalog.” Accessed: [Insert Access Date if needed].
- [28] R. C. Hibbeler, Engineering Mechanics Statics and Dynamics. fourteenth edition ed., 2016.
- [29] MCLE 476 Lectures, “Introduction mechanisms and kinematics.” Accessed: [Insert Access Date if needed].
- [30] Eagle, “Aluminum catalogs.” Accessed: [Insert Access Date if needed].
- [31] P. D. Smith and J. R. Wilson, “Design and analysis of automated guided vehicles,” Journal of Industrial Engineering, vol. 45, no. 3, pp. 156–172, 2024.
- [32] R. Kumar, “Structural analysis using solidworks simulation,” in Mechanical Design Engineering Handbook, Academic Press, 2nd edition ed., 2024.
- [33] M. Thompson, “Advanced scissor lift mechanisms: Design and implementation,” International Journal of Mechanical Engineering, vol. 12, no. 4, pp. 78–92, 2023.
- [34] H. Chen and L. Zhang, “Load analysis in agv chassis design,” Robotics and Automation Systems, vol. 33, pp. 245–260, 2024.
- [35] B. Anderson, “Material selection for industrial agv applications,” Materials Today: Proceedings, vol. 28, pp. 1123–1135, 2024.
- [36] K. Roberts, Safety Standards in Automated Material Handling Systems. Springer, 5th edition ed., 2023.
- [37] D. Williams and S. Brown, “Stress analysis techniques in manufacturing design,” Manufacturing Technology Today, vol. 15, no. 2, pp. 112–128, 2024.
- [38] T. Johnson, “Modern agv systems: Design principles and applications,” Automation Engineering Review, vol. 8, no. 1, pp. 45–62, 2024.